



UNIVERSITY OF
BIRMINGHAM

**ANTENNAS USING LEFT HANDED
TRANSMISSION LINES**

by

Qing Liu

A thesis submitted to
The University of Birmingham
for the degree of
DOCTOR OF PHILOSOPHY

Department of Electrical, Electronic and Computer Engineering
School of Engineering
University of Birmingham
December 2009

UNIVERSITY OF
BIRMINGHAM

University of Birmingham Research Archive

e-theses repository

This unpublished thesis/dissertation is copyright of the author and/or third parties. The intellectual property rights of the author or third parties in respect of this work are as defined by The Copyright Designs and Patents Act 1988 or as modified by any successor legislation.

Any use made of information contained in this thesis/dissertation must be in accordance with that legislation and must be properly acknowledged. Further distribution or reproduction in any format is prohibited without the permission of the copyright holder.

ABSTRACT

The research described in this thesis is concerned with the analysis and design of conventional wire antenna types, dipoles and loops, based on the left-handed transmission line approach. The left handed antennas have a unique feature that the wavelength of the induced current becomes shorter with decreasing frequency. The left handed transmission line concept can be extended to construct reduced-size dipole or loop antennas in the VHF frequency band. The use of higher order modes allows orthogonal polarisation to be obtained, which is thought to be a feature unique to these antennas.

Efficiency is a key parameter of left handed antennas as the heavy left handed loading increases the resistive loss. A study of the efficiency of small dipole antennas loaded with a left-handed transmission line is specially described, and the comparison with conventional inductive loading dipoles. In a low order mode, the efficiency of L-loading dipole is better with low number of unit cell. If the number of cell increases, CL-loading presents comparable and even better performance. In a high mode the meandered left handed dipole gives the best efficiency due to the phase distribution, presenting orthogonal polarization as well. The optimized dipole loaded with parallel plate capacitors and spiral inductors presents the best performance in impedance and efficiency, even better than the conventional inductive loading.

A planar loop antenna using a ladder network of left handed loading is also presented. Various modes can be obtained in the left handed loop antenna. The zero order mode gives rise to omnidirectional patterns in the plane of the loop, with good efficiency. By loading the loop with active components, varactors, a tunable left handed loop antenna with a switchable radiation pattern is implemented. The loop gives an omnidirectional pattern with a null to z axis while working in an $n = 0$ mode and can switch to a pattern with a null at $\phi = 45^\circ$ in the plane of the loop in an $n = 2$ mode.

ACKNOWLEDGEMENTS

First of all, I would like to express my heartfelt gratitude to my supervisor, Prof. Peter Hall, for his support, encouragement and guidance throughout my PhD study. His teachings have improved my personality and my way of doing the research and the way of thinking. This work would not come through without his outstanding supervision and valuable advice.

I would like to thank Toyota Central Research and Development Laboratories for partly supporting this work and to Dr H Iizuka and Dr Lucas Borja for their many contributions.

I would also like to thank all members in the Communications Engineering Research Group for their help and support over the last three years, particularly to Dr Peter Gardner, Dr Kelvin Chan, Dr Yuriy Nechayev, Simon Bai, Dr James Kelly and Wei Zhang who providing me measurement figures for this thesis. Technician support was appreciated from Mr. Alan Yates. We made an artwork board together!

Thanks also go to my friends, Jing Hu, Xu Wang, Michael Hu, Xin Zou, Jie Hao, Peng Bao, Ming Xiao, Yi Qin, and Jin Tang etc. My study life becomes rich and happy with all your friendships.

Always I would like to give my deepest gratitude to my parents for their unconditional support and love. Their support means the most to me. And thanks to my sister, my lovely nephew.

Finally, my utmost gratitude goes to my husband Qi Zhang for his support, encouragement, and love all the time. This thesis is dedicated to him!

LIST OF ACRONYMS

G	Gain
Q	Quality Factor
UWB	Ultra Wide Band
RF	Radio Frequency
RFID	Radio Frequency IDentification
ESA	Electrically Small Antenna
TE	Transverse Electric
TM	Transverse Magnetic
TEM	Transverse ElectroMagnetic
TL	Transmission Line
RH	Right-handed
LH	Left-handed
RHM	RH Material
LHM	LH Material
CRLH	Composite Right/Left Handed
VLf	Very Low Frequency
VHF	Very High Frequency
UHF	Ultra High Frequency
SHF	Super High Frequency
SMT	Surface-Mount Technology
PCB	Printed Circuit Board

SRR	Split-Ring Resonator
BLC	Branch-Line Coupler
LW	Leaky-Wave
L	Inductive
CL	Capacitive-Inductive
HPF	High Pass Filter
LPF	Low Pass Filter
VSWR	Voltage Standing Wave Ratio
CST	Computer Simulation Technologies
FIT	Finite Integration Technique
FDTD	Finite Difference Time Domain
RAM	Radiation Absorbent Material

TABLE OF CONTENTS

INTRODUCTION	1
References	6
CHAPTER I ELECTRICALLY SMALL ANTENNA PROPERTIES AND FUNDAMENTAL LIMITATIONS	8
1.1 Electrically Small Antennas	9
1.1.1 Background of Electrically Small Antennas	9
1.1.2 Applications and Future Trends	11
1.2 Fundamental Limitations in Small Antennas	12
1.2.1 Antenna Fundamental Parameters	13
1.2.2 Effect of Antenna Size on Antenna Performances	17
1.2.2.1 Chu Limit on Antenna Q	20
1.2.2.2. Harrington Limit on Antenna Gain	26
1.2.3 Summary for Fundamental Limits and Size Reduction Ways.....	28
References	31
CHAPTER II METAMATERIALS AND TRANSMISSION LINES	34
2.1 Metamaterial Definition and Development in Electromagnetism.....	35
2.1.1 Metamaterial Definition and Characteristics.....	35
2.1.2 Development in Electromagnetism	37
2.1.3 Metamaterial Applications in Electromagnetism	40
2.2 Transmission Lines and Applications.....	43
2.2.1. Right Handed Transmission Lines	43
2.2.1.1 Transmission Lines.....	43
2.2.1.2. Transmission Line Theory.....	45
2.2.2 Left Handed Transmission Lines	49
2.2.2.1 Homogeneous Models.....	50
2.2.2.2 Metamaterial Implementations.....	55

2.2.3 CRLH TL Microwave Applications	61
2.2.3.1 Guided-Wave Devices.....	61
2.2.3.2 Radiated-Wave Devices	64
2.2.3.3 Refracted-Wave Devices	65
References.....	66
CHAPTER III DIPOLE ANTENNAS USING LEFT HANDED TRANSMISSION LINES	72
3.1 Basic Dipole Antenna Properties	74
3.1.1 Elementary Doublet	74
3.1.2 Short Dipole	75
3.1.3 Half-Wave Dipole Antenna	77
3.2 Reviews on Left Handed Dipole Antennas and Their Implementations	81
3.2.1 Conceptual Model	82
3.2.2 Simulation Performance.....	85
3.2.2.1 Near Field Distributions.....	85
3.2.2.2 Frequency, Phase Constant Relationship	86
3.2.2.3 Current Distributions.....	88
3.2.2.4 Reflection Characteristics	90
3.2.2.5 Loading Contributions	91
3.2.2.6 Bandwidth Property	93
3.2.3 Implementations.....	93
3.2.3.1 Short Dipole with Distributed Elements	93
3.2.3.2 Meandered Dipole with Distributed Elements.....	97
3.3 Dipole Antennas with Left Handed Loading.....	103
3.3.1 Short Dipole with Lumped Elements.....	103
3.3.1.1 Model	103
3.3.1.2 Implementation	107
3.3.2 Meandered Left Handed Dipoles	111

3.3.2.1 Effect of Cell Number on Polarization.....	111
3.3.2.2 3D Meandered Left Handed Dipole.....	115
3.4 Summary	119
References.....	121
CHAPTER IV EFFICIENCY OF ELECTRICALLY SMALL PERIODICALLY LOADED DIPOLE ANTENNAS	124
4.1 Dipole Antennas with Lumped Loading	125
4.1.1 Configuration	125
4.1.1.1 Dipole with Left Handed Loading	125
4.1.1.2 Dipole with Periodic Inductive Loading	127
4.1.2 Simulation Performance.....	127
4.1.2.1 Performance for Size Reduction Dipoles in $lnl = 1$ Mode.....	127
4.1.2.2 Performance of Dipole Antennas with a High Order Mode $lnl = 7$	133
4.1.2.3 Bandwidth Performance of Left Handed Dipoles.	135
4.1.3 Implementation of 4 Cell Left Handed Dipole.....	136
4.2 Optimized Loaded Dipole Antennas	140
4.2.1 Dipole with Optimized Component Configuration.....	140
4.2.1.1 Configuration	142
4.2.1.2 Simulated and Measured Performances	143
4.2.1.3 Comparisons.....	146
4.2.2 Dipole with Non-linear Loading	149
4.3 Summary	151
References.....	153
CHAPTER V LOOP ANTENNAS USING LEFT HANDED TRANSMISSION LINES	157
5.1 Basic Loop Antenna Properties.....	158
5.1.1 Small / large Loop Antennas	158
5.1.2 Particular Loop Antennas.....	159

5.2 Omnidirectional Left Handed Loop Antenna.....	162
5.2.1 Configuration	162
5.2.2 Performances.....	163
5.2.2.1 Simulation Model and Prototype Antenna	163
5.2.2.2 Simulated and Measured Results	166
5.2.3 Summary	173
References.....	174
CHAPTER VI DUAL MODE RECONFIGURABLE LEFT HANDED LOOP	
ANTENNA	177
6.1 Configuration	178
6.2 Performance	181
6.2.1 Simulation results.....	181
6.2.2 Measurement results.....	184
6.3 Summary	187
References.....	188
CHAPTER VII CONCLUSIONS AND FUTURE WORK.....	189
7.1 Conclusions.....	189
7.1.1 Conclusions for Left Handed Dipoles.....	189
7.1.2 Conclusions for Left Handed Loop Antennas	191
7.2 Future Work	193
References.....	195
APPENDIX A TELEGRAPHER'S EQUATIONS	196
A.1. Lossless Transmission Line.....	196
A.2 Lossy Transmission Line.....	197
A.3 Input Impedance of a Transmission Line	198
A.4 Direction of Signal Propagations	199
APPENDIX B ANTENNA PARAMETERS	201

B.1 Return loss	201
B.2 Input Impedance	202
B.3 Radiation Pattern	203
B.4 Directivity and Gain	203
B.5 Polarization.....	204
APPENDIX C CST MICROWAVE STUDIO	205
APPENDIX D ANTENNA MEASUREMENT	208
D.1 Background to Antenna measurement	208
D.2 Antenna Test Range.....	208
D.3 Antenna Range Instrumentation	209
D.4 Typical Applications of Antenna Range Instrumentation.....	210
D.4.1 Near-Field Range	210
D.4.2 Indoor Far-Field Range	212
APPENDIX E WIDEBAND LC BALUN.....	214
References.....	218
PUBLICATIONS	220

INTRODUCTION

Metamaterials are artificially constructed materials that have electromagnetic properties not found in nature. The concept of metamaterials with simultaneously negative permittivity and permeability, more commonly referred to as left-handed materials, was first theorized by the Russian physicist Veselago [1] in 1968. During the past years, left-handed materials made by inserting periodic inclusions [2] with dimensions smaller than the guided wavelength, have attracted considerable attention in view of minimizing antenna size [3], which may lead to the development of new applications.

The unique properties of left-handed materials are promising for a diversity of optical/microwave applications. The split-ring resonator based left-handed structures [4] presented originally were impractical for microwave applications, because of their too lossy and too narrow bandwidth characteristics. The general transmission line approach [5] provides a deeper insight into the physical phenomena of left-handed materials and provides an efficient design tool for left-handed applications. The left-handed transmission line structures with lower loss and wider bandwidth have led to the development of novel microwave devices, such as new types superlenses [6], microwave components [7] and leaky-wave antennas [8].

Transmission lines loaded with reactive components that have left handed wave behavior have been applied to many forms of antennas to investigate the new properties that these antennas have. In some cases new features in the performance arise, such as the ability of a series fed array to scan through broadside [8, 9]. In many other cases, such as size reduction in microstrip patches [10], performance is similar to other antenna configurations.

The research described in this thesis is concerned with the analysis and design of conventional wire antenna types, such as dipoles and loops, based on the left-handed transmission line approach. To the best of the author's knowledge, this is the first time that the concept of left-handed transmission lines has been applied to the development of small wire antennas, extending the degrees of freedom of this sort of structures. Collaborators in this work at Toyota Research Center wish to put these novel designs on their cars. The frequency range for antennas used in vehicles is usually from 100 MHz to 800 MHz and the size of the conventional antennas is about 0.5 to 3 meters as a consequence. Metamaterials could give practically useful size reduction and be used to make a slow-wave and electrically small antennas. The printed circuit board structure allows antennas mounting on glass or roof panel of cars. A left handed antenna with size of 2.5 cm was designed in Toyota lab and could be installed upside down under the real roof of a car as shown in Figure 1 (I would like to thank Dr. H Iizuka, from Toyota, for providing me the car picture.). The work done by Toyota Research Center will be reviewed first in the thesis.

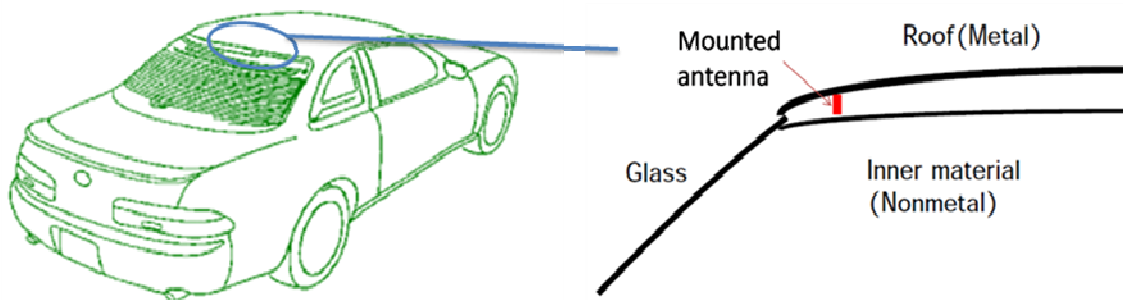


Figure 1. Vehicle with electrically small left handed antenna.

This thesis is divided into seven chapters. The first chapter is literature survey on the properties and fundamental limits of electrically small antennas. There has been much

interest in electrically small antenna technologies recently with increased use of wireless technologies for communications and sensor networks. Electrically small antennas have geometrical dimensions which are small compared to the wavelength. However, there are fundamental limits as to how small the antenna elements can be made. The basic limitations are imposed by the free-space wavelength which the antenna elements must couple to, and the free-space wavelength is not expected to be miniaturized [11]. The approximate fundamental limits given based on Chu [12] and Harrington's theory [13] for the radiation quality factor and gain of an electrically small antenna of a given size has become, by far, the most widely cited. The quality factor and gain approach the limits only if the antenna efficiently utilizes the available volume within the enclosed sphere [14]. Based on these fundamental theories, a large number of downsizing solutions for small antennas can be found in literature. Some of the techniques applied to reduce antenna size are folding configurations, surface etching, shorting walls or pins, or loading high dielectric constant materials [3, 15]. Another typical way for size reduction for antenna design is loading with lumped circuit elements [16] or metamaterial-based antennas.

The literature review about the metamaterials and elementary transmission line theory is covered in Chapter II. Transmission line theory has been a powerful analysis and design tool for conventional (right-handed) and left-handed materials. The fundamental electromagnetic properties of left-handed materials are presented based on a general transmission line approach. Left-handed transmission line implementations and microwave applications are also summarized.

Transmission lines loaded with reactive components that have left handed wave behavior

have been applied to conventional wire antenna design. The fundamental electromagnetic properties and the physical realization of left-handed transmission line loaded dipole antennas presented by our collaborator, Toyota Research Center, are reviewed first in the third chapter. The left handed antennas have a unique feature that the wavelength of the induced current becomes shorter with decreasing frequency. The left handed transmission line concept can be extended to construct reduced-size dipole antennas in the VHF frequency band. Another feature of this left handed behavior is that at higher mode number, the antenna becomes electrically smaller and hence has a well controlled radiation pattern. Based on their results, a short dipole antenna loaded with lumped elements is developed in our lab. Various configurations for left handed dipoles are also studied for their new properties.

Except for the new features, efficiency is low for the left handed dipoles due to the heavy loading. In Chapter IV, an efficiency study is described of straight or meandered dipoles loaded with left-handed transmission line, and the comparison with right handed loaded dipole. The establishment of low loss designs for loaded inductors and capacitors is developed.

Left-handed transmission line concept has also been applied to loop antenna design. A loop antenna using a ladder network with left-handed loading is presented in Chapter V. The left-handed loading loop antenna achieves good performance maintaining a 50Ω impedance matching without a high loss of efficiency.

The resonance frequency of periodically loaded antennas is controlled by the loading

values, independent on the length of the antenna. While loaded with active components, varactors, a reconfigurable left-handed loop antenna is designed and implemented in Chapter VI.

The seventh chapter gives conclusions and future work.

References

- [1] V. Veselago, "The electrodynamics of substances with simultaneously negative values of ϵ and μ ," *Soviet Physics Uspekhi-Ussr*, vol. 10, pp. 509- 514, 1968.
- [2] A. Lai, C. Caloz, and T. Itoh, "Composite Right/Left-Handed Transmission Line Metamaterials," *IEEE Microwave Magazine*, Sep. 2004.
- [3] Jofre, L., Cetiner, B.A., and F. De Flaviis, "Miniature Multi-Element Antenna for Wireles Communications," *IEEE Trans. Antennas Propag.*, vol. 50, pp. 658-669, May, 2002.
- [4] C. R. Simovski, P. A. Belov, and H. Sailing, "Backward wave region and negative material parameters of a structure formed by lattices of wires and split-ring resonators," *IEEE Trans. Antennas Propag.*, vol. 51, pp. 2582—2591, Oct. 2003.
- [5] C. Caloz, H. Okabe, T. Iwai, and T. Itoh, "Transmission line approach of left-handed (LH) materials," presented at Proc. USNC/URSI National Radio Science Meeting, San Antonio, TX, June 2002.
- [6] A. Sanada, C. Caloz, and T. Itoh, "Planar distributed structures with negative refractive properties," *IEEE Trans. Microwave Theory Tech.*, vol. 52, pp. 1252–1263, Apr. 2004.
- [7] I. Lin, C. Caloz, and T. Itoh, "A branch-line coupler with two arbitrary operating frequencies using left-handed transmission lines," presented at IEEE-MTT Int. Symp. Dig., Philadelphia, PA, 2003.
- [8] S. Lim, C. Caloz, and T. Itoh, "Metamaterial-based electronically controlled transmission line structure as a novel leaky-wave antenna with tunable radiation angle and beamwidth," *IEEE Trans. Microwave Theory Tech.*, vol. 52, Dec. 2004.

- [9] L. Liu, C. Caloz, and T. Itoh, "Dominant mode (DM) leaky-wave antenna with backfire-to-endfire scanning capability," *Electron. Lett.*, vol. 38, pp. 1414–1416, 2000.
- [10] M. Schuessler, J. Freese, and R. Jakoby, "Design of compact planar antennas using LH-transmission lines," *IEEE Int. Symp. Microwave Theory and Tech.*, vol. 1, pp. 209-212, Jun. 2004.
- [11] H. A. Wheeler, "The Radian Sphere Around a Small Antenna," *Proceedings of the IRE*, pp. 1325-1331, Aug. 1959.
- [12] L. J. Chu, "Physical limitations on omni-directional antennas," *J. Appl. Phys.*, vol. 19, pp. 1163-1175, Dec.1948.
- [13] R. F. Harrington, "Effect of antenna size on gain, bandwidth and efficiency," *J. Res. Nat. Bur. Stand.*, vol. 64-D, pp. 1-12, Jan./Feb.1960.
- [14] S. R. Best, "A low Q Electrically Small Magnetic (TE Mode) Dipole," *IEEE ANTENNAS AND WIRELESS PROPAGATION LETTERS*, vol. 8, 2009.
- [15] J. R. James, A. J. Schuler, and R. F. Binham, "Reduction of Antenna Dimensions by Dielectric Loading," *Electron. Lett.*, 27th, vol. 10, pp. 263-265, June 1974.
- [16] B. A. Kramer, C. C. Chen, and J. L. Volakis, "Size Reduction of a Low-Profile Spiral Antenna Using Inductive and Dielectric Loading," *IEEE ANTENNAS AND WIRELESS PROPAGATION LETTERS*, vol. 7, 2008.

CHAPTER I ELECTRICALLY SMALL ANTENNA PROPERTIES AND FUNDAMENTAL LIMITATIONS

In almost all areas of electrical engineering, especially in mobile electronic devices and portable computers, the attention has been shifted toward miniaturization. Electromagnetics, and antennas in particular, are no exception. A large emphasis in the last 60 years has been placed toward electrically small antenna technologies with increased use of wireless technologies for communications and sensor networks [1-9], including printed circuit board design. Electrically small antennas have geometrical dimensions which are small compared to the wavelength [2, 5, 7, 8]. However, there are fundamental limits as to how small the antenna elements can be made. The basic limitations are imposed by the free-space wavelength which the antenna elements must couple to, and the free-space wavelength is not expected to be miniaturized [8].

1.1 Electrically Small Antennas

Electrically small antennas are antennas with geometrical dimensions which are small compared to the wavelengths of the electromagnetic fields they radiate. More specifically, the term “electrically small antenna” has become understood to include any antenna which fits inside a sphere of radius $R = 1/k$ where k is the wave number associated with the electromagnetic field [8-10].

1.1.1 Background of Electrically Small Antennas

"Historically, there has been much interest in electrically small antennas. Antennas that are electrically small, efficient, and have significant bandwidth would meet many demands if antenna engineers could reconcile these usually contradictory requirements. [2]" This is especially needed recently with increased uses of wireless technologies for communications and sensor networks.

The first work to address the fundamental limits of electrically small antennas was done by Wheeler in 1947 [9]. Wheeler defined an electrically small antenna as one whose maximum dimension is less than $\lambda/2\pi$. This relation is often expressed as:

$$k a < 1 \quad (1.1)$$

$$k = \frac{2\pi}{\lambda} \text{ (radians/meter)}$$

λ = free space wavelength (meters)

a = radius of sphere enclosing the maximum dimension of the antenna (meters)

This situation described by Wheeler is illustrated in Figure 1-1[9]. The electrically small

antenna of whatever type is in free space and may be enclosed in a sphere of radius a .

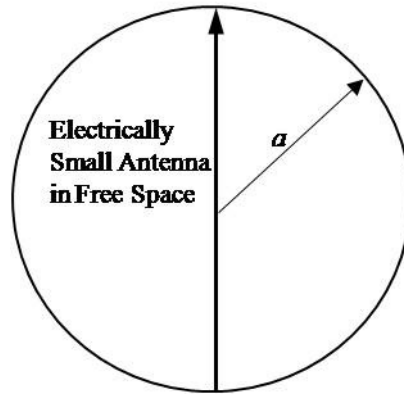


Figure 1-1. Sphere enclosing an electrically small radiating element. [9]

The radiative properties of such electrically small antennas were also investigated by Wheeler [9] who coined the term “radiation power factor.” Later, a very comprehensive theory was presented by Chu [1] in 1948 in which the minimum radiation quality factor Q of an antenna, which fits inside a sphere of a given radius, was derived. This approximate theory was later extended by Harrington [4] in 1960 to include circularly polarized antennas and develop the maximum gain G of an antenna. Collin [11] and later, Fante [12], published an exact theory based on a calculation of the evanescent energy stored round an antenna. More lately, a comprehensive review paper about electrically small antenna properties was published by Hansen [3] in 1981. McLean [6] in 1996 gave a more accurate calculation of the minimum attainable radiation factor Q of general small antennas. The approximate fundamental limits given based on Chu and Harrington’s theory for the radiation quality factor Q and gain G of an antenna of a given size has become, by far, the most widely cited.

1.1.2 Applications and Future Trends

Traditionally, there are many reasons for using electrically small antennas, most of which are physical constraints. For example, big antennas used for LF and HF broadcasts, high speed aircraft or warships are easy to be damaged due to mechanical strength i.e. windage or icing [13]. Electrically small antennas are needed in many applications, like for invisible military ground vehicles, concealed electrical devices of police or security forces, obstacle clearance on road vehicles or trains, and radio tracking of small animals etc. [13]

The growth in the number of wireless systems over the past decade has brought the new requirements for the ever-decreasing size of the RF systems. A modern mobile terminal is not only physically small but also required to operate well across a large number of wireless standards [14]. New mobile communication applications such as RFID and sensing systems enforce the use of devices with an energy efficiency that allows reducing costs and size.

With the development of the new electronic devices and wireless systems the requirements on the antenna performances and modelling become more and more demanding. As we have seen, future wireless communication systems are expected to employ higher carrier frequencies (2 – 6 GHz) and wider bandwidths (10 – 100 MHz, even UWB) than currently deployed systems. Therefore, the trend for future antennas is not only small, internally mounted, but also able to work well across a large bandwidth. In this context intense work is designing efficient, broadband antennas while keeping the size of the antenna as small as possible.

1.2 Fundamental Limitations in Small Antennas

Early in an antenna design cycle it is important to determine if the physical volume specified is, in theory, large enough electrically to allow the design of any antenna which can meet the bandwidth gain requirements specified. From previous designers' experience, there are always various circumstances in antenna designing for different frequency range. For instance, at VLF range, the physical size of the antenna is inevitably small in terms of the operating wavelength and problems of excessive conduction losses and a narrow bandwidth will be faced. However, at microwave frequencies, a higher gain and a broader band have been made possible with a physically small antenna. There seems to be a close relationship between the maximum gain obtainable and the size of the antenna expressed in terms of the operating wavelength, i.e. electrical size. Therefore, over the entire frequency range, there seems to be a practical limit to the performance of a radiating system upon its electrical size. As a matter of fact, bandwidth, losses and electrical dimensions are closely interrelated in electrically small antennas. Classical antennas cannot be made arbitrarily small, while keeping at the same time certain operative parameters.

In general the characteristic expected of an electrically small antenna is low radiation resistance and large reactance and hence it will have very small instantaneous bandwidth with respect to the impedance of normal radio equipment. The physical explanation to understand this and find out the basic performance limitations we can achieve for small antennas are required. In this section, we will discuss the fundamental limits to small antenna performance, like the bandwidth and radiation efficiency of an electrically small antenna of a given size and operating frequencies. Some efficient size reduction ways for antenna design will also be presented.

1.2.1 Antenna Fundamental Parameters

An antenna system, functioning as a transmitter or a receiver, provides a practical means of transmitting or receiving a signal which appears in the form of r - f energy at the terminals, from a point to a distant point or points in space. The performance of such an antenna system is judged by the quality of transmission, and is described in common practice in terms of the bandwidth of its input impedance and its power gain.

The bandwidth [15] of an antenna is defined as “the range of frequencies within which the performance of the antenna, with respect to some characteristic, conforms to a specific standard.” The bandwidth can be considered to be the range of frequencies, on either side of a centre frequency (usually the resonance frequency), where the antenna characteristics (such as input impedance, pattern etc.) are within an acceptable range.

For broadband antennas, the Octaval bandwidth B_o is usually introduced, which is expressed as the ratio of the upper-to-lower frequencies of acceptable operation and shown in equation (1.2).[16]

$$B_o \equiv f_H / f_L \quad (1.2)$$

For example, a 10:1 bandwidth indicates that the upper frequency is 10 times greater than the lower.

For narrowband antennas, the bandwidth is expressed as a percentage of the frequency difference (upper minus lower) over the centre frequency of the bandwidth as shown in equation (1.3) and it's called fractional bandwidth B_f . [16]

$$B_f \equiv \Delta f / f_c \equiv (f_H - f_L) / f_c < 200\% \quad (1.3)$$

For example, a 5% bandwidth indicates that the frequency difference of acceptable operation is 5% of the centre frequency of the bandwidth. The relationship between the two kinds of bandwidth is [16]:

$$B_f = 2(B_o - 1)/(B_o + 1) \quad (1.4)$$

Losses in the antenna can be characterized by the radiation efficiency, η which is defined as “ the ratio of total radiated power to the net power accepted by the antenna from the connected feed line [7] ”. The efficiency of a practical electrically small antenna is determined by the amount of losses in the conductors, dielectrics and other materials out of which the antenna is constructed compared with the radiation loss. This can be expressed as equation 1.5 [3].

$$\eta_a = \frac{R_r}{R_r + R_m} \quad (1.5)$$

η_a = efficiency of ESA

R_r = Radiation Resistance (Ω)

R_m = Material Loss Resistance (Ω)

Antenna gain is a useful measure describing the performance of an antenna, which is closely related to the directivity and efficiency. It is defined as “ the ratio of the radiation intensity of an antenna in a given direction to the intensity that would be produced by a hypothetical ideal isotropic antenna that radiates equally in all directions and has no

losses” [15]. Since the radiation intensity from a lossless isotropic antenna equals the power into the antenna divided by a solid angle of 4π steradians, we can write the following equation (1.6) [15]:

$$Gain = 4\pi \left(\frac{\text{Radiation Intensity}}{\text{Antenna Input Power}} \right) = 4\pi \left(\frac{U(\theta, \phi)}{P_{in}} \right) \text{ Dimensionless Units} \quad (1.6)$$

where $U(\theta, \phi)$ represent the radiation intensity and is a function of spherical coordinate angles θ and ϕ . In most cases we deal with relative gain, which is defined as “the ratio of the power gain in a given direction to the power gain of a reference antenna in its referenced direction.” [15]

The quality factor or Q factor is another important parameter for antenna system. It’s a dimensionless parameter that compares the frequency at which a system oscillates to the rate at which it dissipates its energy. [17]

A higher Q indicates a lower rate of energy dissipation relative to the oscillation frequency, so the oscillations die out more slowly. The concept originated in electronic engineering, as a measure of the 'quality' desired in a good tuned circuit or other resonator. Generally Q is defined to be

$$Q = \omega \times \frac{\text{Energy Stored}}{\text{Power Loss}} \quad (1.7 \text{ a})$$

or, more intuitively,

$$Q = 2\pi \times \frac{\text{Energy Stored}}{\text{Energy dissipated per cycle}} \quad (1.7 \text{ b})$$

where ω is defined to be the angular frequency of the circuit (system), and the energy stored and power loss are properties of a system under consideration.

The radiation Q of a simple antenna is not obviously defined since; in general, such an antenna is not self-resonant. Strictly speaking, the Q of a system is defined to be 2π times the ratio of the maximum energy stored to the total energy lost per period [6]. For an antenna, the following definition for radiation Q is generally accepted [6],

$$Q = \begin{cases} \frac{2\omega W_e}{P_{rad}} & W_e > W_m \\ \frac{2\omega W_m}{P_{rad}} & W_m > W_e \end{cases} \quad (1.8)$$

where W_e is the time-average, non-propagating, stored electric energy, W_m is the time-average, non-propagating, stored magnetic energy, ω denotes radian frequency, and P_{rad} denotes radiated power. The basis for this definition is that it is implicitly assumed that the antenna will be resonated with an appropriate lossless circuit element to affect a purely real input impedance at a specific design frequency. Thus, the definition of the radiation Q of an antenna is similar to the definition of Q for a practical circuit element, which stores predominantly one form of energy while exhibiting some losses.

1.2.2 Effect of Antenna Size on Antenna Performances

With the miniaturization of components prevailing in almost all parts of electronics today, it is important to recognize the limits upon size reduction of antenna elements. These are related to the basic fact that the element's purpose is to couple to a free space wavelength, which has not yet been miniaturized.

It is well known that an electrically small dipole antenna is an inefficient radiator, because it has a very small radiation resistance, while simultaneously having a very large capacitive reactance [7]. Consequently, to obtain a high overall efficiency, considerable effort must be expended on a matching network that produces an impedance that is conjugately matched to the dipole's impedance; i.e., it forces the total reactance to zero by introducing a very large inductive reactance. Because of the very large reactance values involved, these matched resonant systems generally have very narrow bandwidths, imperfect efficiencies, and high tolerance requirements for their fabrication. Consequently the potential trade-off is very narrow bandwidth and poor efficiency because a large reactance matching network has to be involved. The detailed and numerical investigation for electrically small antennas was started by Wheeler.

In 1947, Wheeler firstly introduced fundamental limitations of small antennas. The small antenna in his paper is considered to be one whose maximum dimension is less than the "radianlength". The radianlength is $1/2\pi$ wavelength. The practical efficiency of a small antenna is limited by the "radiation power factor" of the antenna as compared with the power factor and bandwidth of the antenna tuning [9].

In Wheeler's paper [9], he defines two small antenna types, one being a capacitor (electric radiator) and the other an inductor (magnetic radiator) for formula deduction. Their maximum dimensions are smaller than the radianlength of operation and their shapes are cylindrical. By expressing the formulas in fundamental forms, the inherent similarity of the electric and magnetic radiators becomes apparent, as well as the limitation on both types. Wheeler introduced the radiation power factor concept to characterize small antennas. He assumed that any small reactive antenna could be reduced to an equivalent first-order network when operating at low frequencies. Such a network would be either a serial RC network or a parallel RL one depending on whether electric or magnetic stored reactive energy predominates at low frequencies. The fundamental limitation on the bandwidth and the practical efficiency of a small antenna is the radiation power factor, p defined as equation (1.9) [9].

$$p = \frac{1}{6\pi} \frac{k_s V}{l^3} \quad (1.9)$$

where, k_s is shape factor of the capacitor or inductor, V is antenna volume and l is the radianlength. The p is always much less than unity because of the small size. It has the same form for both kinds of antennas and its value depends only on the ratio of the antenna volume to the radian cube.

Wheeler also gives a simple circuit to achieve the fundamental properties of small antennas and their behaviour. The circuit is composed of a generator or load coupled with an antenna of either kind (C or L) through its tuner shown as Figure 1-2 [9].

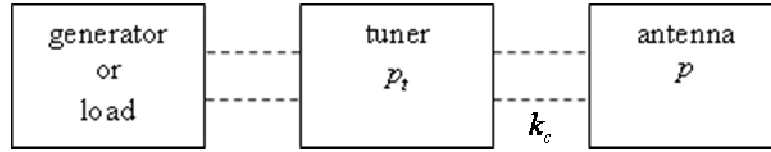


Figure 1-2. Tuned coupling of antenna with generator or load. [9]

Efficient operation of a small antenna requires tuning to the operation frequency by a tuner circuit which offers little additional dissipation. It is assumed that the tuner is coupled with the generator or load to deliver the maximum power. The more general expression of radiation efficiency of antenna circuit e is given in his paper as equation (1.10) [9]. This gives an indication of the relative importance of all factors.

$$e = \frac{k_c^2 p}{k_c^2 p + p_t} \quad (1.10)$$

where, k_c is coupling coefficient between the tuner and the antenna, p is radiation power factor of antenna, and p_t is the power factor of the tuner including all dissipation in the tuner and antenna. In general, the efficiency of the antenna circuit is increased by increasing the coefficient of coupling between the tuner and the antenna, and by decreasing the power factor of the tuner.

For a smaller antenna, the radiation power factor is less than unity and limits the radiation efficiency. Furthermore, the radiation resistance decreases rapidly relative to the other resistance in the coupling circuit. The resulting reduction in coupling efficiency is another principal limitation of the smaller antenna. Put another way, a smaller antenna with the same reactance and radiation resistance must be tuned in more narrow width to deliver its available power. Greater bandwidth may be obtained by increasing the coupling with

generator or load, developing the tuner into a wide-band circuit, or increasing the power factor of the tuner [9]. Therefore, the broader bandwidth for a small antenna must be at the expense of total efficiency.

After Wheeler introduced the properties of electrically small antennas (ESA) and the term “radiation power factor”, some comprehensive theories for ESA property analysis and design technology have been established. A basic approach was taken by Chu [1] and subsequently by Harrington [4].

1.2.2.1 Chu Limit on Antenna Q

In 1948, Chu [1] presented the physical limitations of omni-directional small antennas with the use of the spherical wave functions. Electrically small antennas are analyzed via spherical mode theory, with the antenna enclosed in a virtual smallest possible sphere of a given radius. The minimum radiation quality factor Q of an antenna was derived, which varies inversely as the cube of sphere radius in radian wavelengths when the radius is much less than the latter. This limits the achievable bandwidth.

Any radiation pattern can be written as the sum of spherical modes. So the antenna, of whatever type, is enclosed in a virtual sphere. The radiated power can be calculated from the propagating modes within the sphere. All modes contribute to the reactive power. Based on Chu’s work, each mode n has a Q_n based on the ratio of stored energy to radiated energy, and the Q_n rises rapidly when ka drops below the mode number n . Here k is wave number and defined as $2\pi/\lambda$, and a is the spherical radius. Thus for roughly $ka < 1$, higher

modes ($n > 1$) become evanescent (below cutoff). In Figure 1-3, Q_n of the TM_n waves is plotted against $2\pi a / \lambda$.

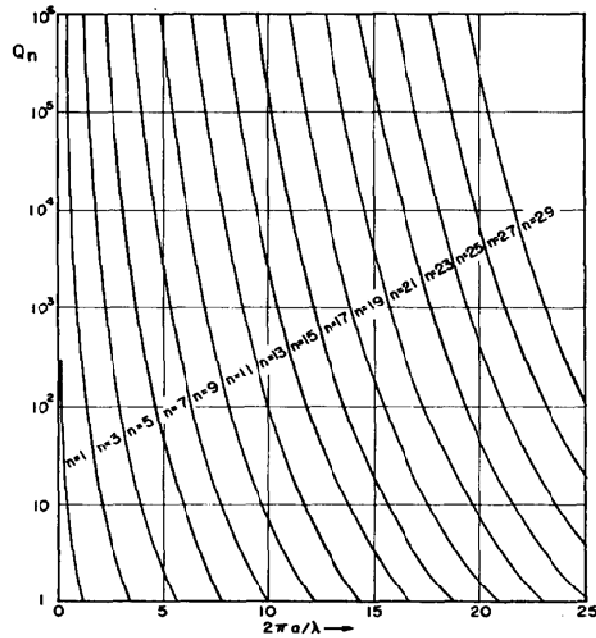


Figure 1-3. Q_n of the equivalent circuit of TM_n or TE_n wave. [1]

When the sphere is sufficiently large to support several propagating modes, this approach is of little value as the modal coefficients are difficult to calculate. For small antennas with only one mode, the radiated power arises primarily from that fundamental mode. For very small antennas, the utility of the Chu work becomes apparent. All modes are then evanescent and the Q becomes large, as the evanescent modes contribute little real power. Note that for $ka \ll 1$, Q varies inversely as the cube of sphere radius in radian wavelengths, which can be expressed as equation 1.11[1]:

$$Q = \frac{1}{(ka)^3} \quad (1.11)$$

The importance of the Chu result is that it relates the lowest achievable Q to the maximum dimension of an electrically small antenna, and this result is independent of the hypothesis that the antenna is constructed within a virtual sphere, except in determining whether a pure TE or pure TM mode, or both, is excited.

The foregoing derivation assumed a lossless antenna, except for radiation resistance. If the antenna is lossy the effect is to insert a loss resistance in series with the radiation resistance. The efficiency affects Q apparently. Figure 1-4 plots single mode Q for various efficiencies. [3] (When both a TM mode and a TE mode are excited, the value of Q is halved.)

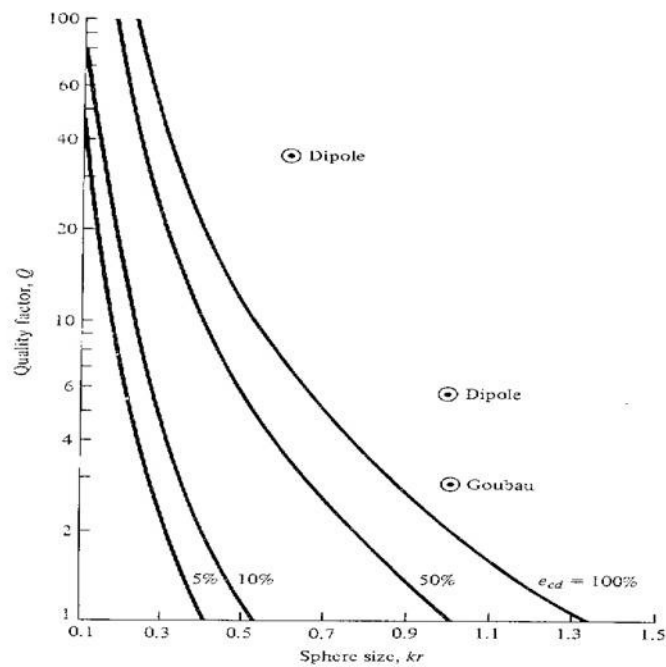


Figure 1-4. Chu-Harrington fundamental limitations for single-mode antenna for various efficiencies. [3]

Bandwidth is derived from Q by assuming that the antenna equivalent is a resonant circuit with fixed values and lossless. Then the fractional bandwidth B_f which is defined as the normalized spread between the half-power frequencies is [3]:

$$B_f = \frac{1}{Q} \quad (1.12)$$

For $Q \gg 1$ the relationship is meaningful as the fixed resonant circuit is a good approximation to the antenna. But for $Q < 2$, the representation is no longer accurate. However, the curves are still useful for low Q even though imprecise, [3].

An octave bandwidth requires relatively small Q and large antenna size. For example $Q = \sqrt{2}$, with no losses, requires a minimum antenna length of 0.365λ . [3] Since most small antennas are loops or dipoles, which do not use the spherical volume efficiently, a practical octave antenna is significantly large, often larger than $\lambda / 2$. It has been concluded that improving bandwidth for an electrically small antenna is only possible by fully utilizing the volume in establishing a TM and TE mode, or by reducing efficiency. The latter is verified by the ELF SQUID [18] which can be extremely small in wavelengths and possess a sizeable bandwidth but has an efficiency which is extremely low.

In 1987 the monograph ‘Small Antennas’ by Fujimoto, Henderson, Hirasawa and James summarized the approaches used to design electrically small antennas [19]. They also surveyed refinements concerning the theoretical limits of electrically small antennas. It has been established that for an electrically small antenna, contained within a given volume, the antenna has an inherent minimum value of Q . This places a limit on the attainable

impedance bandwidth of an electrically small antenna. The higher is the antenna Q the smaller will be the impedance bandwidth.

In 1996, Mclean [6] derived an exact method for the calculation of the minimum radiation Q of a general antenna which is considered electrically small size. In Chu's theory, the calculation of the radiation Q is not straight forward since energy is a nonlinear quantity. Chu derives an equivalent second-order series RLC circuit and calculates the Q form this equivalent circuit. Mclean noted that this is a significant approximation, although a larger radiation Q would still imply a narrower maximum achievable bandwidth. The restriction on bandwidth for an electrically small linearly polarized antenna is actually somewhat more restrictive than is implied by Chu's approximate theory. In Mclean's paper, an exact calculation of the minimum radiation Q has been given by circuit theory based on spherical mode solution. The minimum Q for an electrically small linear antenna in free space with single TE or TM mode is expressed as [6]:

$$\text{for } kr < 1, \quad Q_L = \frac{1}{k^3 a^3} + \frac{1}{ka} \quad (1.13)$$

$$\text{for } kr \ll 1, \quad Q_L = \frac{1}{k^3 a^3} \quad (1.14)$$

The minimum Q for an ESA which is circularly polarised with single TE and TM mode is [6]:

$$\text{for } kr < 1, \quad Q_{cp} = \frac{1}{2} \left(\frac{1}{k^3 a^3} + \frac{2}{ka} \right) \quad (1.15)$$

$$\text{for } kr \ll 1, \quad Q_{cp} = \frac{1}{2k^3 a^3} \quad (1.16).$$

Equations (1.13-1.16) assume a perfect lossless matching network, where a is the radius of the smallest sphere that encloses the antenna and k is the wave number at the operating wavelength λ ($k = 2\pi / \lambda$).

In Figure 1-5 is a graph of the minimum radiation Q associated with the TM_{01} or TE_{01} spherical mode for a linearly polarized antenna in free space. The exact curve was derived by Mclean [6] and should be used in any estimates of minimum Q , which is compared with the approximate curve derived by Chu [1].

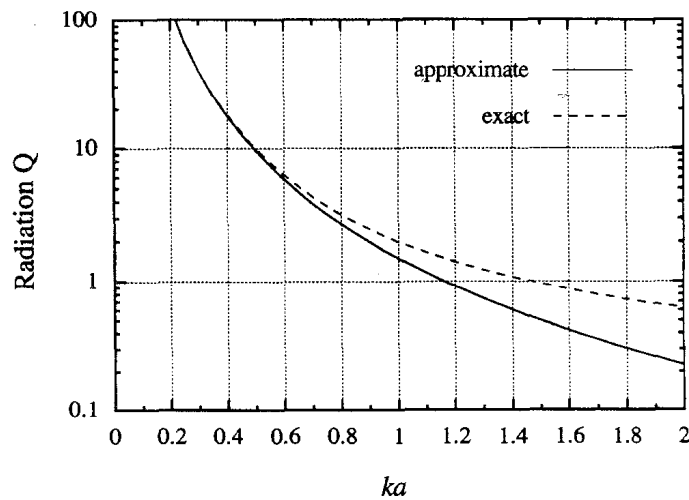


Figure 1-5. Radiation Q of an ESA (linearly polarized) vs. ka . The exact curve was derived by Mclean [6]; the approximate curve was derived by Chu [1].

The above expressions of the limit Q have been formulated considering lossless antennas. Taking into account losses (characterized by η), another fundamental relationship [20] between the radius a of an electrically small antenna, its maximum fractional bandwidth, B_f , and its radiation efficiency, can be written as in following equation:

$$B_f \cdot \eta = (ka)^3 \quad (1.17)$$

The minimum Q relationship was originally derived for the case of an ESA in free space. In any practical environment an electrically small antenna could be near some type of ground plane or other structure. In 2002 Sten et al. [21] evaluated the limits on the fundamental Q of an ESA near a ground plane. The radiation Q is found to depend on the radius (relative to wavelength) of the smallest sphere that encloses the antenna and its image. These relationships provide useful guidelines on theoretical limits to the developments of an actual ESA with a desired impedance bandwidth.

1.2.2.2. Harrington Limit on Antenna Gain

Schelkunoff [22] and LaPaz [23] have computed that there is no mathematical limit to the directivity gain of an antenna of given size. It indicates that an arbitrarily high gain can be obtained with an arbitrarily small antenna, provided the source distribution can be physically arranged. However, Stratton [24] in 1941 demonstrated the impracticality of supergain antennas. Physically, if high current amplitude on the antenna can be realized, high energy is stored in the system, and a large power dissipation, thus giving a low transmission efficiency.

The gain limitation of electrically small antennas was firstly analyzed via spherical mode theory by Chu in 1948. To obtain the optimum performance, various criteria are used. The complete antenna structure including transmission lines and the oscillator can be enclosed inside a geometrical spherical surface of radius a . The current or source distribution inside the sphere is assumed to require the minimum amount of energy stored inside the sphere so

that one has a pure resistive input impedance at a single frequency. Also, the conduction loss will be neglected for simplicity. The quantity Q then is defined at the input terminals:

$$Q = \frac{2\omega \text{ times the mean electric energy stored beyond the input terminals}}{\text{power dissipated in radiation}} \quad (1.18).$$

Based on Chu's work, it is found that an antenna of which the maximum dimension is $2a$ has the potentiality of a broad bandwidth provided that the gain is equal to or less than $4a/\lambda$. To obtain a gain higher than this value, the Q of the antenna increased at an astronomical rate. It is the physical limitation, which limits the gain of all the practical antennas to the approximate value $4a/\lambda$.

Chu's approximate theory was later extended by Harrington to include circularly polarized antennas. In 1960, Harrington [4] gave a theoretical analysis to the effect of antenna size on parameters such as gain, bandwidth, and efficiency. The maximum obtainable gain G of an electrically small antenna of radius r was derived in the radiation zone as following equation:

$$G = (kr)^2 + 2(kr) \quad (1.19)$$

where the radius r of an antenna system is the radius of the smallest sphere that can contain it, k is wave number, assuming a perfect lossless matching network. Figure 1-6 plots the maximum Harrington gain against kr .

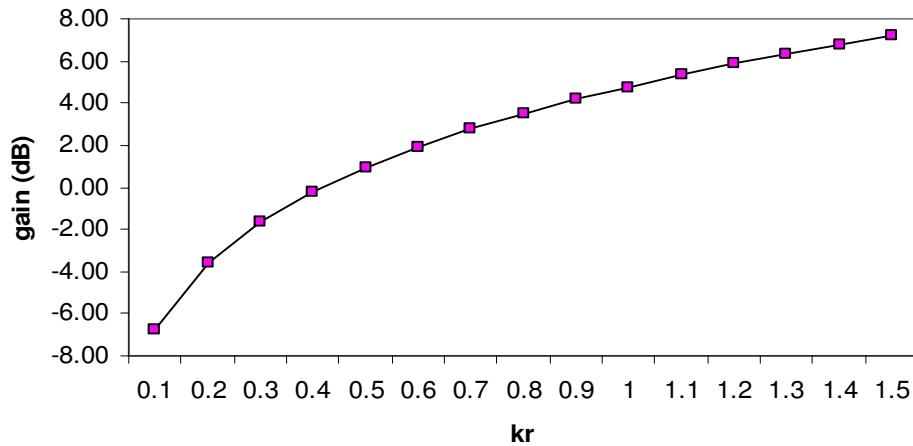


Figure 1-6. Harrington maximum gain versus kr [4].

1.2.3 Summary for Fundamental Limits and Size Reduction Ways

Using spherical mode theory and assuming fundamental mode only in small antennas, Chu's theory defines the limit for the radiation quality factor and, hence bandwidth, of an electrically small antenna which can be enclosed within a sphere of a given effective radius [1]. For linearly polarized lossless antennas the Chu limit can be expressed by equation (1.20). The Harrington limit gives information about the highest achievable gain [4] and summarised by equation (1.21). In both equations, k is the wave number associated with the electromagnetic field and r is the enclosed sphere radius. The quality factor and gain approach the limits only if the antenna efficiently utilizes the available volume within that radiation sphere.

$$\frac{1}{B} = Q = \frac{1}{(kr)^3} + \frac{1}{kr} \quad (1.20)$$

$$G = (kr)^2 + 2kr \quad (1.21)$$

Although in the fundamental limits, the size reduction technique is not specified, the results are representative of what will happen when typical methods are used. For instance, based on the equation (1.21), the highest gain for an electrically small dipole antenna working at 500 MHz is 1.2 dBi for a length of 100mm, which is $0.17 \lambda_0$ and $kr = 0.52$ where λ_0 is free space wavelength. The gain is reduced to -3.3 dBi with antenna length of 40mm, which is $0.07 \lambda_0$ and $kr = 0.22$. Since the potential impact is large, there is difficulty in obtaining good electrical performance (bandwidth, gain) antennas while reducing size. In recent years, there has been a resurgence of interest in electrically small antenna technologies as the development of mobile communications. A large number of downsizing solutions for small antennas can be found in literature. Some of the techniques applied to reduce antenna size are folding configurations, surface etching, shorting walls or pins, or loading high dielectric constant materials [2, 5, 25-28].

Jofre etc. summarized the existing downsizing techniques for planar antennas in wireless communications in 2002 [20]. In his paper, the following basic design guidelines have been derived:

- A multilayered structure to obtain a double resonant behaviour;
- Slit etching as a way of increasing the electrical path while maintaining physical size;
- Short-circuiting walls to utilize the half-size reduction factor;
- Dielectric loading, especially in packaged applications, for further size reduction at the cost of lower efficiency.

Evolution towards miniaturization of communication devices, leads to a significant

reduction of the antenna electrical and physical sizes. Electrical size reduction has a negative impact in bandwidth and radiation efficiency, therefore, the small antenna designer must find a good compromise between size and antenna performance. Some of the currently studied and used small antennas are like internally mounted antennas in terminal design [29], dual-polarized antenna for dual-feed patch in multiband operation [30], and a lot of effort has been concentrated on studying fractal structures. Euclidean-shaped antennas are very far from reaching their limit performance. Poor behaviour is due to the inefficient way that these shapes fill up the volume that encloses them. Recent work [31] by Gonzalez-Arbesu etc. demonstrated how fractal antennas are not more effective than other geometries with the same wire diameter, total wire length, total wire length and occupied area, as in Figure 1-7. The antenna efficiency and radiation quality factor Q approach fundamental limits as iteration increases.

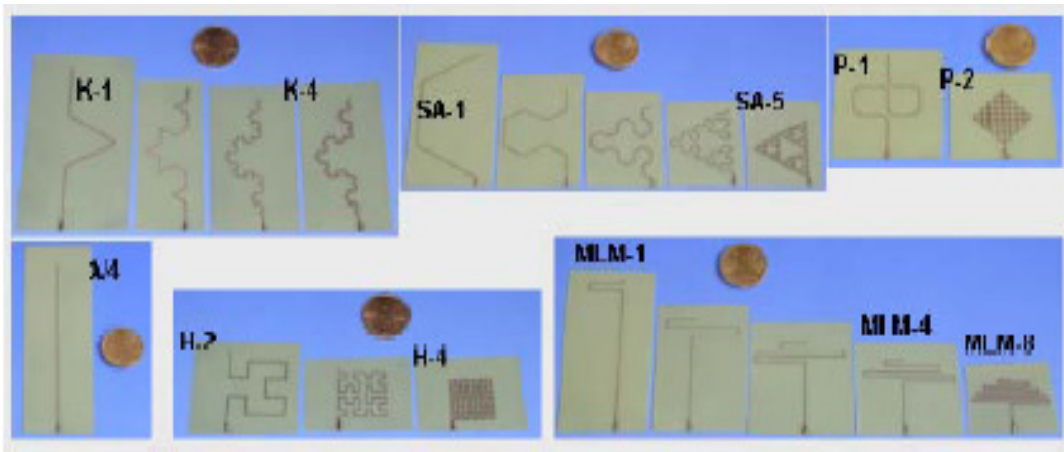


Figure 1-7. Different fractal monopoles, (U. Politècnica de Catalunya) [31]

Another typical way for size reduction for antenna design is loading with lumped circuit elements [2, 5, 25-28] or metamaterial-based antennas. These technologies will be studied in detail in the next chapters.

References

- [1] L. J. Chu, "Physical limitations on omni-directional antennas," *J. Appl. Phys.*, vol. 19, pp. 1163-1175, Dec.1948.
- [2] R. W. Ziolkowski and A. Erentok, "Metamaterial-Based Efficient Electrically Small Antennas," *IEEE Trans. Antennas Propag.*, vol. 54, pp. 2113-2130, July 2006.
- [3] R. C. Hansen, "Fundamental limitations in antennas," *Proc. IEEE*, vol. 69, pp. 170-182, Feb.1981.
- [4] R. F. Harrington, "Effect of antenna size on gain, bandwidth and efficiency," *J. Res. Nat. Bur. Stand.*, vol. 64-D, pp. 1-12, Jan./Feb.1960.
- [5] J. R. James, A. J. Schuler, and R. F. Binham, "Reduction of Antenna Dimensions by Dielectric Loading," *Electron. Lett.*, 27th, vol. 10, pp. 263-265, June 1974.
- [6] J. S. Mclean, "A Re-Examination of the Fundamental limits on the Radiation Q of Electrically Small Antennas," *IEEE Transactions on Antennas and Propagation*, vol. 44, pp. 672-675, May 1996.
- [7] G. S. Smith, "Efficiency of electrically small antennas combined with matching networks," *IEEE Trans. Antennas Propag.*, vol. AP-40, pp. 369-373, May 1977.
- [8] H. A. Wheeler, "The Radian Sphere Around a Small Antenna," *Proceedings of the IRE*, pp. 1325-1331, Aug. 1959.
- [9] H. A. Wheeler, "Fundamental limitations of small antennas," *Proc. I.R.E.*, vol. 35, pp. 1479-1484, Dec.1947.
- [10] H. A. Wheeler, "Small antennas," *IEEE Trans. Antennas Propag.*, vol. AP-23, pp. 462-1169, July 1975.
- [11] R. E. Collin and S. Rothschild, "Evaluation of antenna Q," *IEEE Trans. Antennas Propag.*, vol. AP-12, pp. 23-27, Jan.1964.

- [12] R. L. Fante, "Quality factor of general ideal antennas," *IEEE Trans. Antennas Propag.*, vol. AP-17, pp. 151-155, Mar. 1969.
- [13] R. A. Burberry, "Electrically Small Antenna: A Review," *Electrically Small Antennas, IEE Colloquium*, pp. 1/1 - 1/5, 23 Oct 1990.
- [14] R. Serrano, S. Blanch, and L. Jofre, "small antenna fundamental and technologies: future trends," presented at Antennas and Propagation, EuCAP 2006, Nice, France, Nov. 2006.
- [15] C. A. Balanis, *Antenna Theory, Analysis, and Design*. New York: Wiley, 1982.
- [16] J. J. H. Wang, "Fundamental Bandwidth Limitation for Small Antennas on a Platform," *2006 IEEE International Workshop on Antenna Technology Small Antennas and Novel Metamaterials*, pp. 281 - 284, Mar. 2006.
- [17] R. C. Johnson and H. Jasik, *Antenna Engineering Handbook, Chapt. 6*: McGraw Hill Book.
- [18] S. A. Wolf and etc, "Superconducting extremely low frequency (ELF) magnetic filed sensors for submarine communications," *IEEE Trans. Commun.*, vol. COM-22, pp. 549-554, 1974.
- [19] K. Fujimoto, A. Henderson, K. Hirasawa, and J. R. James, *Small Antennas*: John Wiley & Sons Inc, 1987.
- [20] Jofre, L., Cetiner, B. A., and F. De Flaviis, "Miniature Multi-Element Antenna for Wireless Communications," *IEEE Trans. Antennas Propag.*, vol. 50, pp. 658-669, May, 2002.
- [21] J. C. E. Sten, A. Hujanen, and P. K. Koivisto, "Quality Factor of an Electrically Small Antenna Radiating Close to a Conducting Plane," *IEEE Transactions on Antennas and Propagation*, vol. 49, pp. 829-837, May 2002.

- [22] S. A. Schelkunoff, *Bell System Tech.*, vol. 22, pp. 80-107, 1943.
- [23] L. LaPaz and G. A. Miller, presented at Proc. I.R.E, 1943.
- [24] J. A. Stratton, *Electromagnetic Theory*. New York: McGraw-Hill Book Company, Inc. Chap.7, p.392, 1941.
- [25] J. R. James and R. M. Burrows, "Resonance Properties of Dielectric-loaded Short Unipoles," *Electron. Lett.*, 12th, vol. 9, pp. 300-302, July 1973.
- [26] J. R. James and A. Henderson, "Electrically short monopole antennas with dielectric or ferrite coatings," *PROC. IEE*, vol. 125, pp. 793-803, Sept. 1978.
- [27] K.-L. Wong and Y.-F. Lin, "Small broadband rectangular microstrip antenna with chip-resistor loading," *Electron. Lett.*, vol. 33, pp. 1593-1594, Sept. 1997.
- [28] B. A. Kramer, C. C. Chen, and J. L. Volakis, "Size Reduction of a Low-Profile Spiral Antenna Using Inductive and Dielectric Loading," *IEEE ANTENNAS AND WIRELESS PROPAGATION LETTERS*, vol. 7, 2008.
- [29] Suárez-Pejenaute, E., Baggen, R., and M. Martínez-Vázquez, "Integrated Antennas on LTCC Substrate for Bluetooth Applications," *Journées Internationales de Nice sur les Antennes*, 2002.
- [30] Zürcher, J. F., Mosig, J.R., Skrivervik, A.K., Xu, Q., and S. Vaccaro, "Multi-frequency, multi-polarization N-port printed planar antennas," *Microw. Engin. Europe*, pp. 29-33, June 2000.
- [31] Gonzalez-Arbesu, J.M., Blanch, S., and J. Romeu, "Are space-filling curves efficient small antennas?" *Antennas & Wireless Propag. Lett.*, vol. 2, pp. 147-150, 2003.

CHAPTER II METAMATERIALS AND TRANSMISSION LINES

Transmission lines are essential components in modern wireless systems, being used to connect antennas to transmitters and receivers, for impedance matching in mixers and amplifiers, or as resonant elements in oscillators and filters.[1] When the electrical wavelengths are shorter than or comparable to the physical dimensions of a network, the length becomes important and transmission line theory should be applied instead of standard circuit analysis. Thus high-frequency transmission lines can be defined as transmission lines that are designed to carry electromagnetic waves whose wavelengths are shorter than or comparable to the length of the line. An electrical transmission line is a distributed-parameter network, where voltages and currents can vary in magnitude and phase over the length of the line, and it can be analyzed by general transmission line model and equations. The fundamental electromagnetic properties of right-handed, left-handed or composite right/left hand transmission lines and the physical realization of left-handed materials are reviewed in this chapter based on a general transmission line approach. The general transmission line approach provides insight into the physical phenomena of left-handed materials and provides an efficient design tool for left-handed applications.

2.1 Metamaterial Definition and Development in Electromagnetism

2.1.1 Metamaterial Definition and Characteristics

A metamaterial is a material which obtains its properties from its structure rather than directly from its chemical composition. To distinguish metamaterials from other composite materials, the metamaterial label is usually used for a material which has unusual properties, not available in nature. Like electromagnetic properties, especially a material engineered to have features of a size less than that of the wavelength of the electromagnetic radiation it interacts with, [2].

The main reason researchers have investigated metamaterials is the possibility to create a structure with a negative refractive index, since this property is not found in any naturally occurring material [3]. Although the optical properties of a conventional material are fully specified by the parameters permittivity ϵ and permeability μ , in practice the refractive index N is often used. N may be determined from [4]:

$$N = \pm\sqrt{\epsilon \cdot \mu} \quad (2.1).$$

Almost all transparent materials, such as glass or water, have positive values for both permittivity ϵ and permeability μ . However, many metals (such as gold and silver) have negative ϵ at visible wavelengths. A material having either ϵ or μ negative (but not both) is opaque to electromagnetic radiation [4]. For both above materials, the positive square root is used for N by convention. However, some artificial metamaterials have $\epsilon < 0$ and $\mu < 0$; because the product $\epsilon\mu$ is positive, N is also real. Under such circumstances, it is necessary to take the negative square root for N [4]. The foregoing considerations are simplistic for

actual materials, which must have complex-valued ϵ and μ . The real parts of both ϵ and μ do not have to be negative for a passive material to display negative refraction. [5]

Electromagnetics researchers often use the term 'left-handed metamaterial', quite narrowly, for materials which exhibit negative refraction. A comparison of refraction in a left-handed metamaterial to that in a normal material is shown in Figure 2-1. [2]

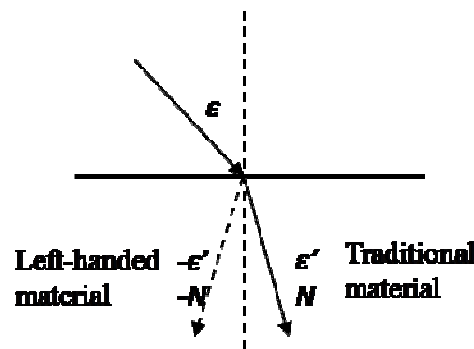


Figure 2-1. Refraction in a left-handed metamaterial. [2]

Metamaterials with negative refractive index N have numerous unusual properties as following, [6]. Snell's law ($N_1 \sin \theta_1 = N_2 \sin \theta_2$) still applies, but as N_2 is negative, the rays will be refracted on the same side of the normal on entering the material. The Doppler shift is reversed: that is, a light source moving toward an observer appears to reduce its frequency. Cherenkov radiation (radiation produced by a fast-moving particle as it travels through a medium) points the other way. The time-averaged Poynting vector is antiparallel to phase velocity. This means that unlike a normal right-handed material, the wave fronts are moving in the opposite direction to the flow of energy [7]. For plane waves propagating in such metamaterials, the electric field, magnetic field and wave vector follow a left-hand rule, thus giving rise to the name left-handed metamaterials [6]. The effect of negative

refraction is analogous to wave propagation in a left-handed transmission line, and such structures have been used to verify some of the effects and particular importance in electromagnetism which will be described later.

2.1.2 Development in Electromagnetism

W. E. Kock developed the first metamaterials in the late 1940s with metal-lens antennas [8] and metallic delay lenses [9].

The terminology 'left-handed' was originally introduced theoretically by the pioneer Victor Veselago in 1967 [6]. In his paper, Veselago speculated on the possible existence of Left-handed materials and anticipated their unique electromagnetic properties such as the reversal of Snell's Law, the Doppler effect, and the Vavilov-Cerenkov effect. Veselago showed that the electric field, magnetic field, and wavevector of an electromagnetic wave in an LHM form an LH triad. As a result, LHMs support electromagnetic waves whose phase velocity is antiparallel to group velocity, known as backward waves [7]. Consequently, while energy still travels away from the source, so as to satisfy causality, wavefronts travel backward toward the source in an LHM, a phenomenon which is associated with negative index of refraction.[10]

J. B. Pendry was the first to theorize a practical way to make a left-handed metamaterial [11-13]. 'Left-handed' in this context means a material in which the 'right-hand rule' is not obeyed, allowing an electromagnetic wave to convey energy (have a group velocity) in the opposite direction to its phase velocity. Pendry's initial idea was that metallic wires aligned along propagation direction could provide a metamaterial with negative permittivity ($\epsilon < 0$).

Note however that natural materials (such as ferroelectrics) were already known to exist with negative permittivity: the challenge was to construct a material which also showed negative permeability ($\mu < 0$). In 1999, Pendry demonstrated that an open ring ('C' shape) with axis along the propagation direction could provide a negative permeability [11]. In the same paper, he showed that a periodic array of wires and rings could give rise to a negative refractive index. A related negative permeability particle, which was also proposed by Professor Pendry, is the Swiss roll [11]. Swiss roll is a type of optical metamaterial that has negative refractive index. It is named for its resemblance to the confectionery Swiss roll: it consists of concentric cylinders of insulated metal. The analogy is as follows: Natural materials are made of atoms, which are dipoles. These dipoles modify the light velocity by a factor n (the refractive index). The ring and wire units play the role of atomic dipoles: the wire acts as a ferroelectric atom, while the ring acts as an inductor L and the open section as a capacitor C . The ring as a whole therefore acts as a LC circuit. When the electromagnetic field passes through the ring, an induced current is created and the generated field is perpendicular to the magnetic field of the light. The magnetic resonance results in a negative permeability; the index is negative as well [11]. Perfect lens concept made by negative refraction then was suggested by Pendry [12]. A 'Superlens' can be realized in the microwave band in the form of a thin slab of silver with current technology. The unique properties of metamaterials were verified by full-wave analysis in Caloz et al. (2001) [14-16]. Caloz provided a full-wave demonstration of fundamental electromagnetic properties of LHMs using the finite-element method in LHM-loaded rectangular waveguide structure [13]. The propagation of electromagnetic waves in double negative media has also been investigated by Ziolkowski with the double negative slab solution [14]. Both analytical and numerical investigations are promising for a diversity of

optical/microwave applications, such as new types of beam steerers, modulators, band-pass filters, superlenses, microwave components and antennas.

In 2002, other groups such as University of California at San Diego (UCSD) and Massachusetts Institute of Technology (MIT) start to do experimental verification of LH materials. The group in UCSD first reviewed the topic [17, 18]. They highlighted the direct relationship of the LH triad (E, H, k) obtained from Maxwell equations when ε and μ are simultaneously negative and they are the most general because they apply also to one-dimensional (1-D) backward-wave structures that may be used in novel components and antennas applications. The UCSD's LHM consisted of copper split-ring resonators (SRRs) and thin copper wires, providing negative permeability and negative permittivity, respectively [15]. By constructing a wedge-shaped structure with their SRR-based LHM, the group at UCSD demonstrated the concept of a negative index of refraction. A group at MIT repeated this experiment, confirming UCSD's findings [16]. Following these experimental verifications, several researchers have further studied the characteristics and applications of SRR-based LHMs [21-23]. However, the LH resonant structures such as SRRs devised up to 2002 were impractical for microwave applications because they had a too narrow bandwidth and were quite lossy. And alternative theories are desirable to gain a deeper insight into their behaviour.

Several researchers soon realized that a transmission line approach towards left-handed materials was possible [17, 18]. The idea of using the TL theory to describe and design LH material was first introduced at approximately the same time mainly by the group at the University of California, Los Angeles (UCLA) and by the group of the University of

Toronto, where several novel metamaterials concepts have been developed and verified independently. The concepts in LH materials of negative permeability, negative permittivity and a negative index of refraction have been demonstrated [19, 20]. Eleftheriades et al. (2002) [18], and Caloz et al. (2002) [17] provided a method to realize left-handed metamaterials using artificial lumped-element loaded transmission lines in microstrip technology. The TL approach of LHMs, presented in their article, has led to non-resonant structures with lower loss and wider bandwidth. In particular, metamaterials with right-handed and left-handed properties known as composite right/left-handed metamaterials [21] have led to the development of several novel microwave devices [22].

2.1.3 Metamaterial Applications in Electromagnetism

Metamaterials are of particular importance in electromagnetism. In order for its structure to affect electromagnetic waves, a metamaterial must have structural features smaller than the wavelength of the electromagnetic radiation it interacts with. For instance, if a metamaterial is to behave as a homogeneous material accurately described by an effective refractive index, the feature sizes must be much smaller than the wavelength. For visible light, which has wavelengths of less than one micrometre typically, the structures are generally half or less than half this size; i.e., less than 280 nanometres. For microwave radiation, the structures need only be on the order of one decimetre [23]. Microwave frequency metamaterials are almost always artificial, constructed as arrays of current-conducting elements (such as loops of wire) which have suitable inductive and capacitive characteristics [2].

a. Superlens

The materials can have a negative refractive index, which allows them to focus near field light thus creating a perfect or "super"-lens. The first Superlens with a negative refractive index provided resolution three times better than the diffraction limit and was demonstrated at microwave frequencies at the University of Toronto by Grbic and Eleftheriades.[24]

b. Cloaking devices

Metamaterials have been proposed as a mechanism for building a cloaking device. These mechanisms typically involve surrounding the object to be cloaked with a shell which affects the passage of light near it [25].

In October 2006, a US-British team of scientists created a metamaterial which made an object invisible to microwave radiation.[26] Since light is just another form of electromagnetic radiation, this was considered the first step towards a cloaking device for visible light, though more advanced nano-engineering techniques would be needed due to visible light's short wavelengths.[23, 25] On April 2, 2007, two Purdue University engineers announced a theoretical design for an optical cloaking device based on the 2006 British concept. The design deploys an array of tiny needles projecting from a central spoke that would render an object within the cloak invisible in a wavelength of 632.8 nanometres, [25]. Duke University and Imperial College London are currently researching this use of metamaterials and have managed to cloak an object in the microwave spectrum using special concentric rings; the microwaves were barely affected by the presence of the cloaked object.[27] In early 2007, a metamaterial with a negative index of refraction for visible light wavelengths was announced by a joint team of researchers at the Ames

Laboratory of the United States Department of Energy and at Karlsruhe University in Germany. The material had an index of -0.6 at 780 nanometres.[23]

c. Agile antennas

Metamaterials have been also proposed for designing agile antennas.[28] Research at the National Institute of Standards and Technology in US has demonstrated that thin films made of metamaterials can greatly reduce the size of resonating circuits that generate microwaves, potentially enabling even smaller cell phones and other microwave devices.[29]

2.2 Transmission Lines and Applications

The unique properties of left handed materials have allowed novel applications, concepts, and devices to be developed. In this research work, transmission line theory for conventional RH transmission lines will be summarized first. The fundamental electromagnetic properties of LHMs and the physical realization of these materials are then investigated based on a general transmission line approach. The general TL approach provides insight into the physical phenomena of LHMs and provides an efficient design tool for LH applications.

2.2.1. Right Handed Transmission Lines

2.2.1.1 Transmission Lines

Ordinary transmission lines are considered right handed due to the relationship between electric field, magnetic field and wave vectors which obeys right handed rule. A transmission line is the material medium or structure that forms all or part of a path from one place to another for directing the transmission of energy, such as electromagnetic waves or acoustic waves, as well as electric power transmission [19]. How well this is done depends on the special physical and electrical characteristics (impedance and resistance) of the transmission line. Components of transmission lines include wires, coaxial cables, dielectric slabs, optical fibers, electric power lines, and waveguides. Practical types of electrical transmission line include coaxial cable, microstrip line, strip lines, and balanced lines etc which are described in the following [30].

A coaxial cable consisting of an electrically conductive wire surrounded by a layer of insulating material, a layer of shielding material, and an outer layer of insulating material, usually plastic or rubber. The purpose of the shielding layer is to reduce external electrical interference [31]. Coaxial lines confine the electromagnetic wave to the area inside the cable, between the center conductor and the shield. In radio-frequency applications up to a few gigahertz, the wave propagates in the transverse electric and magnetic mode only, which means that the electric and magnetic fields are both perpendicular to the direction of propagation (the electric field is radial, and the magnetic field is circumferential). However at frequencies, for which the wavelength (in the dielectric) is significantly shorter than the circumference of the cable, transverse electric and transverse magnetic waveguide modes can also propagate. When more than one mode can exist, bends and other irregularities in the cable geometry can cause power to be transferred from one mode to another [30]. Coaxial cables are most commonly used for transmission of high-frequency audio, video, computer network and other signals [31].

Microstrip line is fabricated using printed circuit board (PCB) technology, and is used to convey microwave-frequency signals. Microstrip can be made by having a strip of copper on one side of a printed circuit board or a dielectric layer (known as the substrate), while the other side is a continuous ground plane. The width of the strip, the thickness of the insulating layer and the dielectric constant of the insulating layer determine the characteristic impedance [32].

A strip line uses a flat strip of metal on a surface layer. The insulating material of the dielectric forms a substrate. The top strip is usually sandwiched between two parallel

ground planes. The width of the strip, the thickness of the substrate and the relative permittivity of the substrate determine the characteristic impedance of the strip line[30].

The foregoing transmission lines are unbalanced lines. Balanced lines are often operated with differential signals. A balanced transmission line consists of two conductors of the same type, and equal impedance to ground and other circuits [30].

2.2.1.2. Transmission Line Theory

In many electric circuits, the signal voltage on the wire at a given time is almost the same at all points at lower frequencies. Thus the length of the wires connecting the components can for the most part be ignored. However, when the signal includes high frequency components whose wavelengths are comparable to or less than the length of the wire, the voltage changes in a time interval comparable to the time it takes for the signal to travel down the wire. In this case the length becomes important and the wire must be treated as a transmission line [1]. A common rule based on previous experience is that the cable or wire should be treated as a transmission line if the length is greater than 1/10 of the wavelength. At this length the phase delay and the interference of any reflections on the line become important and can lead to unpredictable behavior in systems which should be carefully analyzed using transmission line theory [33].

For the purposes of analysis, an electrical transmission line can be modeled as a two-port network (also called a quadrupole network), shown in Figure 2-2:



Figure 2-2. Transmission line model: a two-port network.

If the transmission line is uniform along its length, then its behavior is largely described by a single parameter called the characteristic impedance, symbol Z_0 , which is the ratio of the complex voltage of a given wave to the complex current of the same wave at any point on the line [30]. Typical values of Z_0 are 50 or 75 ohms for a coaxial cable used in radio transmission.

If both the load impedance and the source impedance are equal to Z_0 , the transmission line is matched in both ports. Under such circumstances, the maximum power transfers from the source to the transmission line and down to the load, and has no reflection back to the source. In the simplest case, the two ports A and B are assumed to be interchangeable (i.e. matching in two ports), and the network is assumed to be linear (i.e. the complex voltage across either port is proportional to the complex current flowing into the same port when there are no reflections) [30].

Some of the power may be lost when sent down a transmission line. Resistive or ohmic loss is caused by conductor resistance. At high frequencies, dielectric loss becomes significant because the insulating material inside the transmission line absorbs energy from the alternating electric field and converts it to heat [34]. The total loss of power in a transmission line is often specified in decibels per metre (dB/m), and usually depends on

the frequency of the signal. The manufacturer often supplies a chart showing the loss in dB/m at a range of frequencies. A loss of 3 dB corresponds to a halving of the power.

More parameters and equations are needed to represent and investigate the characteristics of the transmission lines for practical case. The transmission line model was first developed by Oliver Heaviside [35], and is based on Maxwell's Equations. The theory applies to high-frequency transmission lines but is also important for designing high-voltage transmission lines. The transmission line model demonstrates that the electromagnetic waves can be reflected on the transmission line, and that wave patterns can appear along the line.

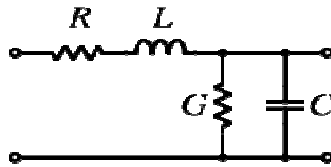


Figure 2-3. Infinitesimal circuit model of a transmission line.

In a more practical approach, the model represents the transmission line as an infinite series of two-port elementary components, each representing an infinitesimally short segment of the transmission line [35]. The model consists of an infinite series of the elements shown in Figure 2-3, and the values of the components are specified per unit length. R , L , C , and G may also be functions of frequency and are defined as [35]:

- The distributed resistance R of the conductors is represented by a series resistor (expressed in ohms per unit length).

- The distributed inductance L (due to the magnetic field around the wires, self-inductance, etc.) is represented by a series inductor (expressed in Henries per unit length).
- The capacitance C between the two conductors is represented by a shunt capacitor C (expressed in Farads per unit length).
- The conductance G of the dielectric material separating the two conductors is represented by a conductance G shunted between the signal wire and the return wire (expressed in Siemens per unit length).

These above quantities are known as the primary line constants, from which the secondary line constants, these being the propagation constant, attenuation constant and phase constant, are derived. The propagation constant, symbol γ , for a given system is defined by "the ratio of the amplitude at the source of the wave to the amplitude at some distance x ", [36] expressed as

$$\frac{A_0}{A_x} = e^{\gamma x} \quad (2.2).$$

Since the propagation constant, γ is a complex quantity we can write;

$$\gamma = \alpha + j\beta \quad (2.3)$$

where; α , the real part, is called the attenuation constant;

β , the imaginary part, is called the phase constant.

For example in a copper transmission line, the propagation constant can be calculated from the primary line constants by means of the relationship;

$$\gamma = \sqrt{ZY} \quad (2.4)$$

where; $Z = R + j\omega L$, the series impedance of the line per meter and,

$Y = G + j\omega C$ the shunt admittance of the line per meter.

Based on these primary and secondary line coefficients, the voltage and current on an electrical transmission line with distance and time can be described. These are introduced in the Appendix A- Telegrapher's Equations.

2.2.2 Left Handed Transmission Lines

Transmission lines with left handed properties are a subset of the wider topic of metamaterials. LH materials have first been studied and verified based on SRRs structures. However, since resonant structures are lossy and narrow-banded, a TL approach of LHMs has been developed. The idea of using the transmission line theory to describe and design LH material was first introduced in 2002 by Caloz group [22] etc.

Transmission line theory has long been a powerful analysis and design tool for conventional (i.e., RH) materials. The fundamental electromagnetic properties of LH materials will be presented in the following based on a general TL approach. In fact, a purely left-handed TL is not physical and can never be realized because of the parasitic effects. Metamaterials with left-handed properties have inevitable right-handed properties, known as composite right/left hand metamaterials. LHMs are considered to be a special simplified model of CRLH structures. By modelling a CRLH metamaterial as an equivalent TL, TL theory can be used to analyze and design CRLH metamaterials.

2.2.2.1 Homogeneous Models

To gain immediate insight into CRLH metamaterial fundamental characteristics, a homogeneous (continuous and invariant along the direction of propagation) TL model was firstly examined by Caloz etc in 2004[10]. For simplicity, the TL is assumed to be lossless.

The homogeneous models of a purely RH, purely LH, and CRLH lossless transmission lines are shown in Figure 2-4 (a), (b), and (c), respectively [10]. For a purely RH lossless TL, its model is developed from conventional infinitesimal circuit model (Figure2-3), where L'_R is a per-unit length series inductance and C'_R is a per-unit length shunt capacitance. The purely LH model is obtained by interchanging the inductance/capacitance and inverting the series/parallel arrangements in the equivalent circuit of the RH-TL, where C'_L presents a per-unit length series capacitance and L'_L presents a per-unit length shunt inductance. LH-TL is obviously of high-pass nature, in contrast to that of the RH-TL, which is of low-pass nature. In effect, parasitic capacitance due to development of voltage gradients and unavoidable parasitic inductance due to current flow along the metallization will be added to LH TL and result in CRLH TL structure [10].

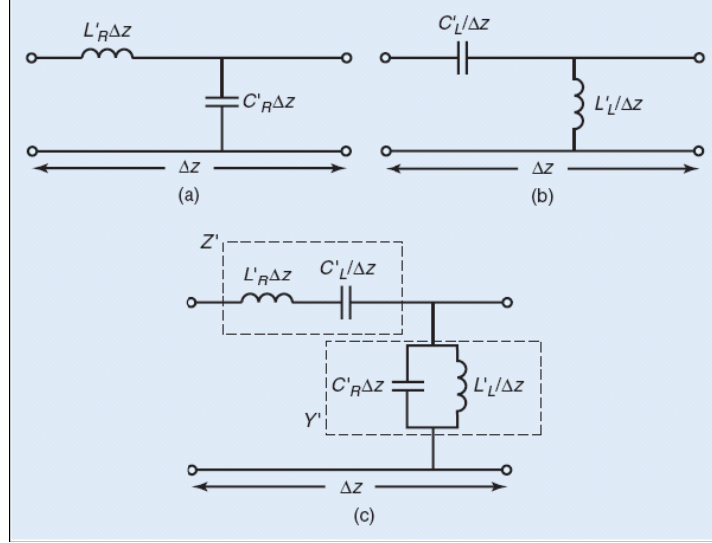


Figure 2-4. Equivalent circuit model. (a) Homogeneous RH TL. (b) Homogeneous LH TL. (c) Homogeneous CRLH TL.[10]

The propagation constant of a TL is given $\gamma = \alpha + j\beta = \sqrt{Z'Y'}$, where Z' and Y' are, respectively, the per-unit length impedance and per-unit length admittance. In the special case of the CRLH TL, Z' and Y' are defined as [10]

$$Z'(\omega) = j(\omega L'_R - \frac{1}{\omega C'_L}) \quad (2.5)$$

$$Y'(\omega) = j(\omega C'_R - \frac{1}{\omega L'_L}) \quad (2.6).$$

After calculation, the dispersion relation for a homogenous CRLH TL is [10]

$$\beta(\omega) = s(\omega) \sqrt{\omega^2 L'_R C'_R + \frac{1}{\omega^2 L'_L C'_L} - (\frac{L'_R}{L'_L} + \frac{C'_R}{C'_L})} \quad (2.7)$$

where [10]

$$s(\omega) = \begin{cases} -1 & \text{if } \omega < \omega_{\Gamma 1} = \min(\frac{1}{\sqrt{L'_R C'_L}}, \frac{1}{\sqrt{L'_L C'_R}}) \\ 0 & \text{if } \omega_{\Gamma 1} < \omega < \omega_{\Gamma 2} \\ +1 & \text{if } \omega > \omega_{\Gamma 2} = \max(\frac{1}{\sqrt{L'_R C'_L}}, \frac{1}{\sqrt{L'_L C'_R}}) \end{cases} \quad (2.8).$$

Figure 2-5 (a), (b), and (c) shows the ω - β or dispersion diagram of a purely RH TL, purely LH TL, and CRLH TL, respectively. The group velocity ($v_g = \partial\omega/\partial\beta$) and phase velocity ($v_p = \omega/\beta$) of these TLs can be inferred from the dispersion diagram. For a purely RH TL, it is shown that v_g and v_p are parallel ($v_g v_p > 0$). However for a purely LH TL, the negative sign in $\beta(\omega)$ indicates a negative phase velocity and v_g and v_p are antiparallel ($v_g v_p < 0$). In addition, the CRLH TL's dispersion diagram shows that, it has both LH ($v_g v_p < 0$) and RH ($v_g v_p > 0$) region. Also note that the stop-band occurs in the frequency range where γ is purely real for a CRLH TL.

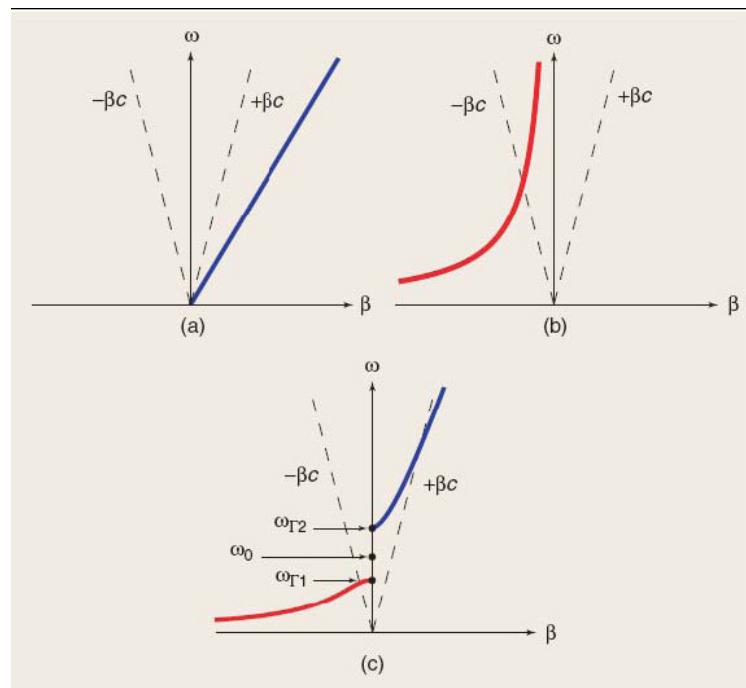


Figure 2-5. Dispersion diagrams for the TLs of Figure 2-4. (a) Homogeneous RH TL. (b) Homogeneous LH TL. (c) Homogeneous CRLH TL (unbalanced).[10]

A CRLH-TL contributes LH property at lower frequencies and RH at higher frequencies with a transition frequency ω_0 . It has been developed that under balanced condition (2.9), when the series and shunt resonances are equal [10],

$$L'_R C'_L = L'_L C'_R, \quad (2.9)$$

the propagation constant in (2.7) reduces to the simpler expression [10]

$$\beta = \beta_R + \beta_L = \omega \sqrt{L'_R C'_R} - \frac{1}{\omega \sqrt{L'_L C'_L}} \quad (2.10)$$

where the phase constant distinctly splits up into the RH phase constant β_R and the LH phase constant β_L . Thus, there is a seamless transition from LH to RH for the balanced case occurring at the transition frequency [10]:

$$\omega_0 = \frac{1}{\sqrt[4]{L'_R C'_R L'_L C'_L}} \quad (2.11)$$

and in the balanced case, ω_0 balanced $\frac{1}{\sqrt{L'_R C'_L}} = \frac{1}{\sqrt{L'_L C'_R}}$.

A balanced form of a CRLH TL is shown in Figure 2-6. The simplified equivalent circuit is the series combination of a RH and a LH TLs. Also, the balanced CRLH TL's dispersion curve does not have a stop-band. In addition, at ω_0 the phase shift ($\phi = -\beta d$) for a TL of length d is zero ($\beta = 0$). Phase advance ($\phi > 0$) occurs in the LH frequency range ($\omega < \omega_0$, $\beta < 0$), and phase delay ($\phi < 0$) occurs in the RH frequency range ($\omega > \omega_0$, $\beta > 0$) [10].

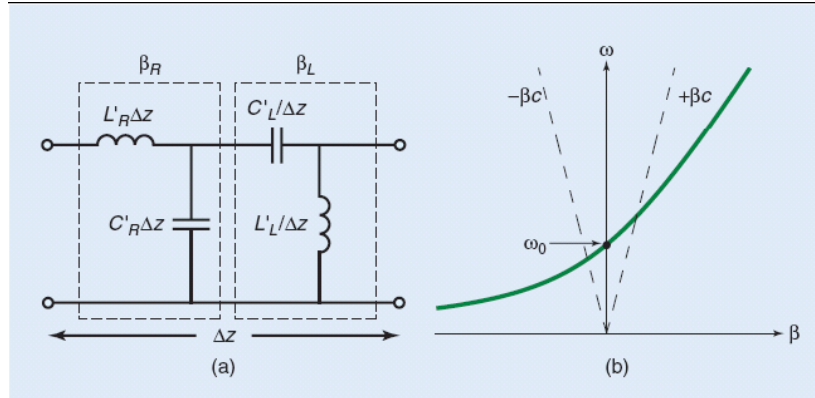


Figure 2-6. Balanced form of Figure 2-4(c). (a) Simplified equivalent circuit model.

(b) Dispersion diagram showing seamless LH to RH transition. [10]

The characteristic impedance of a TL is given by $Z_0 = \sqrt{Z'/Y'}$. For the CRLH TL, the characteristic impedance is [10]

$$Z_0 = Z_L \sqrt{\frac{L'_R C'_L \omega^2 - 1}{L'_L C'_R \omega^2 - 1}} \quad (2.12 \text{ a})$$

(in the balanced case, $Z_0 = Z_L = Z_R$)

$$Z_L = \sqrt{\frac{L'_L}{C'_L}} \quad (2.12 \text{ b})$$

$$Z_R = \sqrt{\frac{L'_R}{C'_R}} \quad (2.12 \text{ c})$$

where Z_L and Z_R are the purely LH and RH impedances, respectively. The characteristic impedance for the unbalanced case is frequency dependent, (2.12a) however, the balanced case is frequency independent and, therefore, can be matched over a wide bandwidth.

In Caloz's work [10], the permeability and permittivity of a TL material have been related to the impedance and admittance of its equivalent TL model.

$$\mu = \frac{Z'}{j\omega} = L'_R - \frac{1}{\omega^2 C'_L}, \quad (2.13 \text{ a})$$

$$\varepsilon = \frac{Y'}{j\omega} = C'_R - \frac{1}{\omega^2 L'_L}. \quad (2.13 \text{ b})$$

Equation (2.13 a, and b) verified that for balanced case the permeability and permittivity are negative in LH region, where $\omega < \omega_0$.

The index of refraction ($n = c\beta/\omega$) for the balanced and unbalanced CRLH TL is displayed in Figure 2-7 [10]. This figure shows that the CRLH TL has a negative index of refraction in its LH range and a positive index of refraction in its RH range.

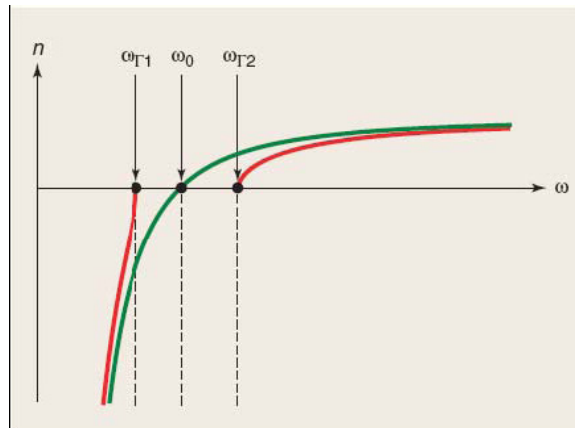


Figure 2-7. Typical index of refraction plots for the balanced (green) and unbalanced (red) CRLH TL. [10]

2.2.2.2 Metamaterial Implementations

a. LC Network

Metamaterials (CRLH) can be represented, for simplicity, by an equivalent homogeneous TL in an LC network implementation [10] as shown in Figure 2-8. An effectively homogeneous CRLH TL of length d can be constructed by cascading the band-pass LC

unit cell of Figure 2-8 (a) in either a non-periodic or periodic fashion. Usually periodicity is preferred for computational and fabrication convenience of the CRLH TL [19]. The LC unit cell's physical dimensions depend on the practical implementation of the inductors and capacitors and the technology used (e.g., microstrip, coplanar waveguide, surface mount components, etc.)

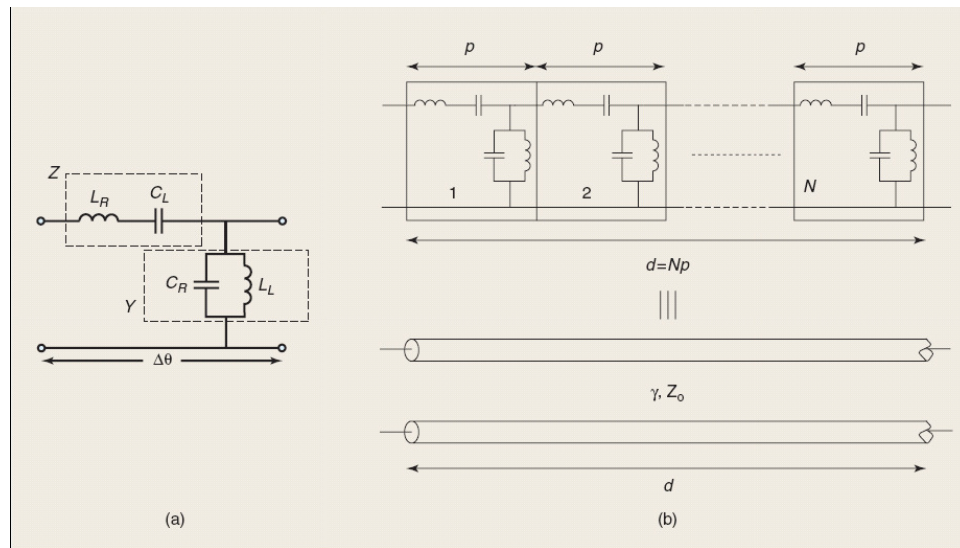


Figure 2-8. LC-based CRLH TL. (a) Unit cell. (b) LC periodic network equivalent to a homogeneous CRLH TL of length d for $p = \Delta z \rightarrow 0$. [10]

By applying periodic boundary conditions related to the Bloch-Floquet theorem to the LC unit cell [19], the LC dispersion relation

$$\beta(\omega) = \frac{1}{p} \cos^{-1} \left(1 + \frac{ZY}{2} \right) \quad (2.14)$$

is obtained, where p is unit cell length, and the series impedance (Z) and shunt admittance (Y) of the LC unit cell are given by

$$Z(\omega) = j(\omega L_R - \frac{1}{\omega C_L}) \quad (2.15),$$

$$Y(\omega) = j(\omega C_R - \frac{1}{\omega L_L}) \quad (2.16).$$

For unit cell length $p = \Delta z \rightarrow 0$, $\cos(\beta p) \approx 1 - \frac{(\beta p)^2}{2}$ and equation (2.14) becomes (2.7).

The 1-D CRLH TL can be extended to a 2-D CRLH TL [19, 37] by using the modified unit cell of Figure 2-8 (a). Similar to the design of a 1-D CRLH TL, 2-D CRLH TL can be constructed by repeating the 2-D unit cell of Figure 2-9 along two directions (x, y).

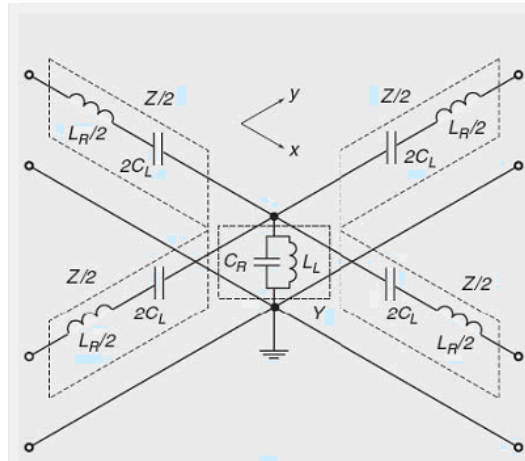


Figure 2-9. Unit cell for LC-based 2D CRLH TL. [10]

b. Physical Implementations

The physical implementation for above LC network approach for 1- or 2-D CRLH TL requires physical components that can generate capacitances (C_R and C_L) and inductances (L_R and L_L). Currently, surface-mount technology (SMT) chip components or distributed components have been used to realize the LC network. Distributed components can be implemented via microstrip, stripline, coplanar waveguide, or another technology. SMT-based CRLH structures are generally easier and quicker to implement. However, SMT

components are only available in discrete values and are limited to low frequencies (3–6GHz, depending on their values) [10]. Distributed components can be used for higher frequency application except that they need to be designed and fabricated.

An example of a distributed component based 1-D CRLH TL is shown in Figure 2-10. [19]. This structure is implemented on microstrip with interdigital capacitors and stub inductors shorted to the ground plane. The unit cell of the structure shown in the inset is equivalent to the circuit model of Figure 2-8 (a). The interdigital capacitors and stub inductors provide both LH and RH contributions. In particular, the RH capacitance is derived from the capacitance between the trace and ground plane, and the RH inductance is caused by the magnetic flux generated by the current flow in the digits of the interdigital capacitor.

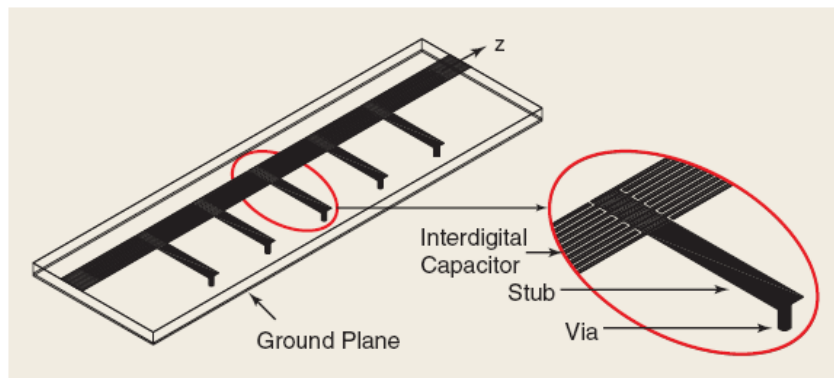


Figure 2-10. A 1-D microstrip CRLH TL consisting of interdigital capacitors and shorted stub inductors. [19].

A balanced, 24 unit-cell microstrip CRLH TL based on Figure 2-10 is displayed in Figure 2-11(a). The entire circuit was implemented on Rogers RT / Duroid 5880 with dielectric constant $\epsilon_r = 2.2$ and thickness $h = 1.57$ mm. Parameter extraction was based on the unit

cell of Figure 2-11 (b) with $p = 6.1$ mm, $l_c = 5.0$ mm, $w_c = 2.4$ mm, $l_s = 8.0$ mm, $w_s = 1.0$ mm, and five pairs of digits with widths of 0.15 and 0.1 mm spacing. The extracted LH and RH parameters were $L_L = 3.38$ nH, $C_L = 0.68$ pF, $L_R = 2.45$ nH, and $C_R = 0.50$ pF.

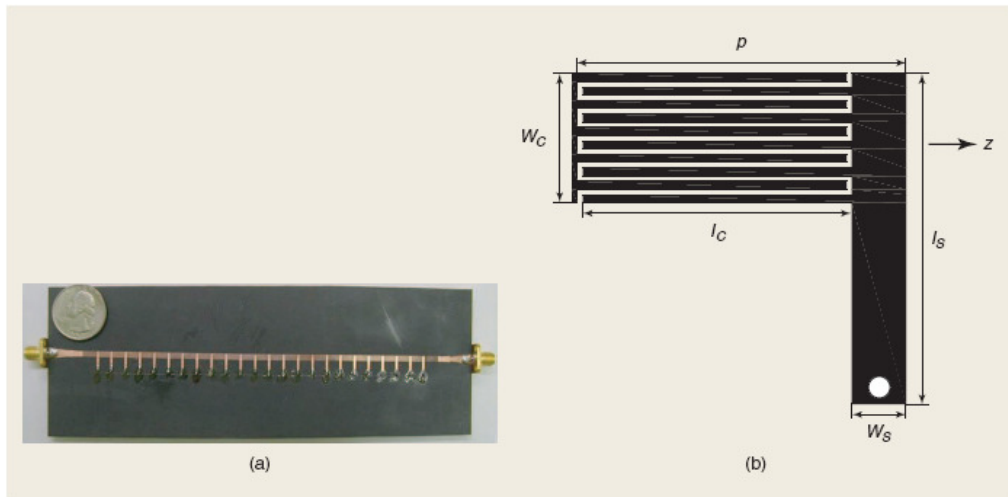


Figure 2-11. 24 unit-cell microstrip CRLH TL based on Figure 2-10. (a) Photograph of prototype. (b) Unit cell used for parameter extraction [19].

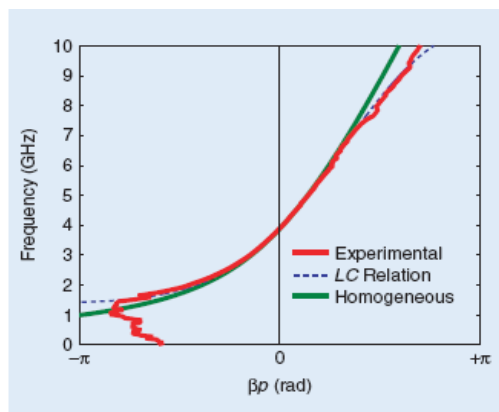


Figure 2-12. Experimental dispersion diagram compared with the homogeneous TL relation (2.7) and LC network relation (2.14) for the 24-cell CRLH TL of Figure 2-11(a) [19].

The experimental dispersion diagram [19] is compared with the homogeneous TL relation (2.23) and LC network relation (2.30) in Figure 2-12.

The physical way to implement 2-D CRLH TL structures is by periodic repetition of the capacitively enhanced mushroom structure of Figure 2-13(a), which was presented by Sanade etc in 2004 [38]. The mushroom structure was first proposed by Sievenpiper et al. [39] for the realization of high-impedance surfaces. Sanade's group at UCLA demonstrated that Sievenpiper's mushroom structure is, in essence, a CRLH structure, capable of exhibiting a negative index of refraction [38]. The mushroom structure of Figure 2-13(a) is equivalent to the 2-D circuit model of Figure 2-9. The capacitance couplings between adjacent top patches contribute to the LH capacitance, and the vias shorted the top patches to the ground plane contribute to the LH inductance. The caps are added to enhance the weak capacitance couplings between adjacent patches. The RH inductance is provided by the magnetic flux caused by the flow of current on the top patches, while the RH capacitance is caused by the parallel-plate structure between the patches and the ground plane. The open 2-D CRLH mushroom structure of Figure 2-13(b) can be implemented with microstrip. [38]

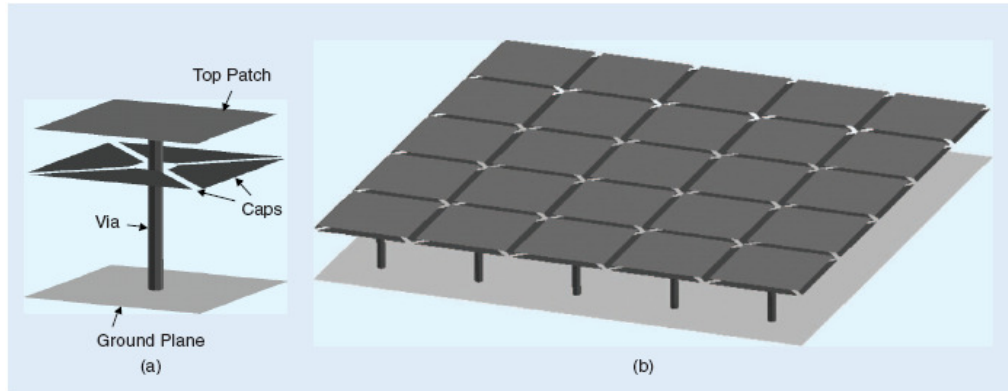


Figure 2-13. Open 2-D CRLH mushroom structure. (a) Unit cell [38]. (b) 2-D CRLH structure formed by periodic repetition of the unit cell. The caps are floating (not connected to the vias) patches located at a short distance from the connected patch to enhance CL contribution [38].

2.2.3 CRLH TL Microwave Applications

The unique properties of metamaterials, verified by full-wave analysis in, are promising for a diversity of optical/microwave applications. There are guided-, radiated-, and refracted-wave microwave devices based on the TL approach of CRLH metamaterials [10].

2.2.3.1 Guided-Wave Devices

The CRLH TL has an additional degree of freedom compared to the RH TL in the non-linear phase response. A novel Branch-line coupler (BLC) with an arbitrary second operating frequency [40] by replacing the conventional RH TLs with CRLH TLs was proposed by UCLA. By changing the dc offset and phase slope, the CRLH TL's phase-response curve can intercept a desired pair of phases at any arbitrary pair of frequencies for dual-band operation.

Figure 2-14(a) shows a CRLH-based BLC with operational frequencies at $f_1 = 930$ MHz and $f_2 = 1.780$ MHz and corresponding phase delays of 90° and 270° , respectively. [40] The CRLH TLs were implemented with SMT chip components. The magnitude response of the CRLH-based BLC is also shown in Figure 2-14(b). $|S_{21}|$ and $|S_{31}|$ of -3 dB are achieved at both operational frequencies.

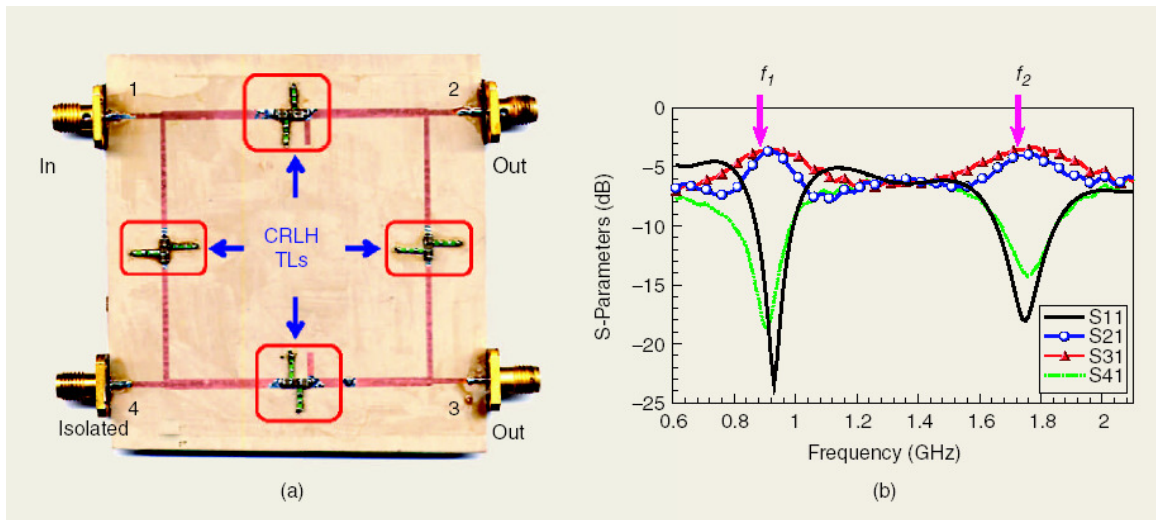


Figure 2-14. Dual-band branch-line coupler. (a) Photograph of completed dual-band BLC with CRLH TLs. [40] (b) Measured S-parameters [40].

In general, this CRLH dual-band concept can be applied to any microwave component, such as phase shifters, matching networks, baluns, etc [41].

A novel CRLH coupled-line directional coupler with arbitrary coupling level and broad bandwidth was designed [42]. By operating the CRLH line in its LH region, backward coupling is achieved, which can offer much tight coupling level than conventional broadband coupler.

The CRLH structure can support a β of zero at a non-zero frequency. This unique feature can be used to implement a novel zeroth order resonator [43] which is depicted in Figure 2-15(a). The resonator consists of two series interdigital capacitors and one shunt stub inductor open-ended by capacitive slits with parameters shown in Figure 2-15(b). At $\beta=0$ there is no phase shift across the resonator since phase shift is determined by $\phi = -\beta d = 0$. In addition, it can be shown that the resonance is independent of the length of the structure but depends only on the reactive loadings.

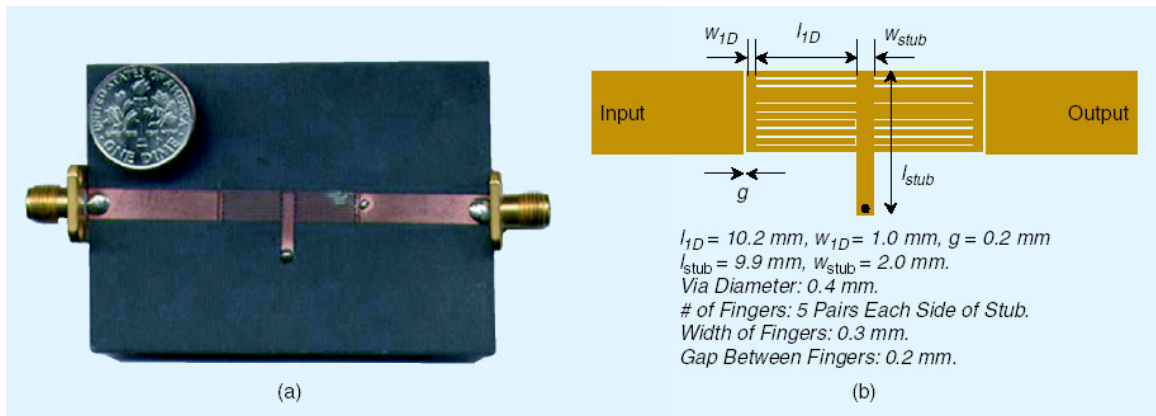


Figure 2-15. One-cell zeroth order resonator. (a) Photograph of prototype [43]. (b) Layout with parameters shown [43].

With the use of CRLH metamaterials, size reduction and bandwidth enhancement of conventional microwave components can be achieved for a variety of other guided-wave applications. For instance, a novel compact enhanced-bandwidth hybrid ring using a left-handed (LH) transmission line was presented in [44]. The proposed hybrid shows a 54% bandwidth enhancement and 67% size reduction compared to the conventional hybrid at 2GHz.

2.2.3.2 Radiated-Wave Devices

The ZOR discussed above can be used to construct a electrically small ZOR antenna in [45]. The balanced CRLH TL of Figure 2-11(a) can be used as an efficient, frequency-scanned leaky-wave (LW) antenna when optimally matched to the air impedance [46]. A CRLH LW antenna has two distinct advantages over conventional LW antennas. First, a CRLH LW antenna can operate at its fundamental mode, because this mode contains a radiation (or fast-wave) region ($|\beta| < k_0$, where k_0 is the free-space propagation constant) in addition to a guided (or slow-wave) region ($|\beta| > k_0$), as shown in Figure 2-16(a). In contrast, RH structures have to be operated at higher order modes in order to radiate and, consequently, require a more complex and less-efficient feeding structure, because the fundamental mode of RH structures are always guided ($|\beta| > k_0$). Second, a CRLH LW antenna is capable of continuous scanning from backward (backfire) to forward (endfire) angles since β can be positive or negative, unlike conventional LW antennas. By operating the CRLH LW antenna below or above its transition frequency ω_0 , forward and backward scanning is achieved. Also at ω_0 , the antenna is able to radiate broadside because $v_g \neq 0$ at $\beta=0$ for the balanced CRLH TL. Figure 2-16 (b) depicts the scanning operation of the CRLH LW antenna.

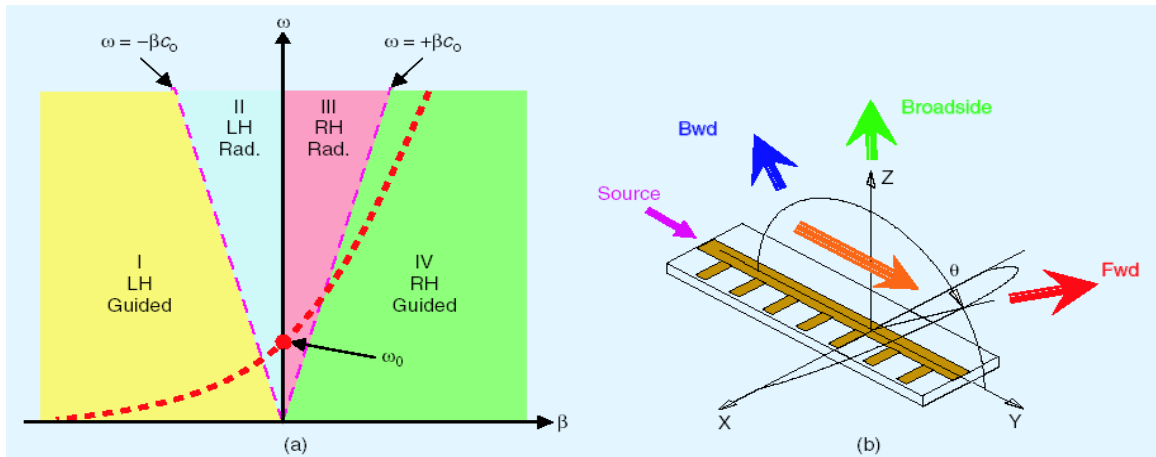


Figure 2-16. CRLH LW Antenna. (a) Typical dispersion diagram showing guided and radiation regions. [46] (b) Scanning operation. [46]

The scanning angle of above CRLH LW antenna is determined by its operating frequency. By replacing the capacitor included in the CRLH unit cell with varactor diodes, a frequency-independent LW antenna capable of continuous scanning and beamwidth control was realized [47]. By controlling the bias voltage of varactor diodes, the capacitance of the cell is changed. As a result, the propagation constant of the CRLH unit cell becomes electronically controlled, which is a unique property of LH material. The CRLH LW antennas are even capable of 2-D scanning by using an open mushroom structure similar to Figure 2-13 (a) [48].

2.2.3.3 Refracted-Wave Devices

The CRLH structure's negative index of refraction could be utilized to create a planar, distributed flat lens, which showed the negative lens effects, and was characterized by a first focus in the LH medium and a second focus in the output RH medium [38].

References

- [1] D. M. Pozar, *Microwave and RF Design of Wireless Systems*. New York, USA: John Wiley & Sons, Inc., 2000.
- [2] A. Sihvola, "Metamaterials in electromagnetics," *Metamaterials*, vol. 1, pp. 2-11, 2007.
- [3] E. Shamonina and L. Solymar, "Metamaterials: How the subject started," *Metamaterials*, vol. 1, pp. 12-18, 2007.
- [4] R. M. Walser, *Introduction to Complex Mediums for Optics and Electromagnetics*. Bellingham, WA, USA: SPIE Press, Nov. 2003.
- [5] R. A. Depine and A. Lakhtakia, "A new condition to identify isotropic dielectric-magnetic materials displaying negative phase velocity," *Microwave and Optical Technology Letters*, vol. 41, pp. 315-316, 2004.
- [6] V. Veselago, "The electrodynamics of substances with simultaneously negative values of ϵ and μ ," *Soviet Physics Uspekhi-Ussr*, vol. 10, pp. 509- 514, 1968.
- [7] S. Ramo, J. R. Whinnery, and T. V. Duzer, *Fields and Waves in Communication Electronics*, 2nd ed. New York: Wiley, 1984.
- [8] "Metal-lens antennas," *IRE Proc.*, pp. 828-836, 34 November 1946.
- [9] "Metallic delay lenses," *Bell. Sys. Tech. Jour.*, pp. 58-82, 27, January 1948.
- [10] A. Lai, C. Caloz, and T. Itoh, "Composite Right/Left-Handed Transmission Line Metamaterials," *IEEE Microwave Magazine*, Sep. 2004.
- [11] J. B. Pendry, A. J. Holden, D. J. Robbins, and W. J. Stewart, "Magnetism from conductors and enhanced nonlinear phenomena," *IEEE Transactions on Microwave Theory and Techniques*, vol. 47, pp. 2075-2084, 1999.

- [12] J. B. Pendry, "Negative refraction makes a perfect lens," *Phys. Rev. Lett.*, vol. 85, pp. 3966—3969, Oct. 2000.
- [13] C. Caloz, C.-C. Chang, and T. Itoh, "Full-wave verification of the fundamental properties of left-handed materials in waveguide configurations," *J. Appl. Phys.*, vol. 1, pp. 5483-5486, Dec. 2001.
- [14] R. W. Ziolkowski and E. Heyman, "Wave propagation in media having negative permittivity and permeability," *Physical Review E*, vol. 64, pp. -, 2001.
- [15] R. A. Shelby, D. R. Smith, and S. Schultz, "Experimental verification of a negative index of refraction," *Science*, vol. 292, pp. 77-79, 2001.
- [16] A. A. Houck, J. B. Brock, and I. Chuang, "Experimental observations of a left-handed material that obeys Snells Law," *Phys. Rev. Lett.*, vol. 90, pp. 137-401, Apr. 2003.
- [17] C. Caloz, H. Okabe, T. Iwai, and T. Itoh, "Transmission line approach of left-handed (LH) materials," presented at Proc. USNC/URSI National Radio Science Meeting, San Antonio, TX, June 2002.
- [18] G. V. Eleftheriades, O. Siddiqui, and A. K. Iyer, "Transmission line models for negative refractive index media and associated implementations without excess resonators," *IEEE Microwave Wireless Compon. Lett.*, vol. 13, pp. 51-53, Feb. 2003.
- [19] C. Caloz and T. Itoh, *Electromagnetic Metamaterials: Transmission Line Theory and Microwave Applications*. New York: Wiley, 2004.
- [20] C. Caloz and T. Itoh, "Novel microwave devices and structures based on the transmission line approach of meta-materials," presented at IEEE MTT-S Int. Symp., Philadelphia, PA, June 2003.

- [21] A. Lai, C. Caloz, and T. Itoh, "Composite Right/Left-Handed Transmission Line Metamaterials," *IEEE microwave magazine*, Sep. 2004.
- [22] C. Caloz and T. Itoh, "Application of the transmission line theory of left-handed (LH) materials to the realization of a microstrip 'LH line'," *IEEE Antennas and Propagation Society International Symposium*, vol. 2, pp. 412-415, 2002.
- [23] "Metamaterials found to work for visible light,"
http://www.eurekalert.org/pub_releases/2007-01/dl-mft010407.php.
- [24] A. Grbic and G. V. Eleftheriades, "Overcoming the diffraction limit with a planar left-handed transmission-line lens," in *Physical Review Letters*, vol. 92, March 19, 2004.
- [25] "Engineers see progress in creating 'invisibility cloak'," at www.purdue.edu.
- [26] "Experts test cloaking technology," BBC News (2006-10-19) Retrieved on 2008-08-05.
- [27] "News Releases," in *Feature Stories and Profiles about Duke University's Pratt School of Engineering*.
- [28] H. Boutayeb, T. A. Denidini, K. Mahdjoubi, A.-C. Tarot, A.-R. Sebak, and L. Talbi, "Analysis and design of a cylindrical EBG-Based directive antenna," *IEEE Transaction on antennas and propagation*, vol. 54, Jan. 2006.
- [29] "'Metafilms' Can Shrink Radio, Radar Devices," in *Newswise*,
<http://newswise.com/articles/view/538769/>, Retrieved on September 14, 2008.
- [30] R. Ludwig and P. Bretchko, "RF Circuit Design: Theory and Applications," Pearson Education Inc. Prentice Hall, 2000.
- [31] *The American Heritage Science Dictionary*: Houghton Mifflin Company, 2005.

- [32] J. R. James and P. S. Hall, *Handbook of Microstrip antennas*. London: IEE - Peter Peregrinus, Ltd. (IEE Electromagnetic Waves Series. Volume 28), 1989.
- [33] Ulaby and F.T., *Fundamentals of Applied Electromagnetics*, Media ed: Prentice Hall, 2004.
- [34] H. S. Nalwa, *Low and High Dielectric Constant Materials and Their Applications*: Academic Press, May 1999.
- [35] Heaviside and Oliver, "Electromagnetic Theory," *American Mathematical Society*, 1970.
- [36] E. Weber and F. Nebeker, "The Evolution of Electrical Engineering," presented at IEEE Press, Piscataway, New Jersey USA, 1994.
- [37] G. V. Eleftheriades, A. K. Iyer, and P. C. Kremer, "Planar negative refractive index media using periodically L-C loaded transmission lines," *IEEE Trans. on Microwave Theory and Techniques*, vol. 50, pp. 2702-2712, 2002.
- [38] A. Sanada, C. Caloz, and T. Itoh, "Planar distributed structures with negative refractive properties," *IEEE Trans. Microwave Theory Tech.*, vol. 52, pp. 1252–1263, Apr. 2004.
- [39] D. Sievenpiper, L. Zhang, F. J. Broas, N. G. Alexopoulos, and E. Yablonovitch, "High-impedance electromagnetic surfaces with a forbidden frequency band," *IEEE Trans. Microwave Theory Tech.*, vol. 47, pp. 2059–2074, Nov. 1999.
- [40] I. Lin, C. Caloz, and T. Itoh, "A branch-line coupler with two arbitrary operating frequencies using left-handed transmission lines," presented at IEEE-MTT Int. Symp. Dig., Philadelphia, PA, 2003.

-
- [41] I. Lin, M. DeVincentis, C. Caloz, and T. Itoh, "Arbitrary dual-band components using composite right/left-handed transmission lines," *IEEE Trans. Microwave Theory Tech.*, vol. 52, pp. 1142–1149, Apr. 2004.
- [42] C. Caloz and T. Itoh, "A novel mixed conventional microstrip and composite right/left-handed backward-wave directional coupler with broadband and tight coupling characteristics," *IEEE Microwave Wireless Compon. Lett.*, vol. 14, pp. 31–33, Jan. 2004.
- [43] A. Sanada, C. Caloz, and T. Itoh, "Zeroth order resonance in composite right/left-handed transmission line resonators," presented at Proc. Asia-Pacific Microwave Conf., Seoul, Korea, 2003.
- [44] H. Okabe, C. Caloz, and T. Itoh, "A compact enhanced-bandwidth hybrid ring using an artificial lumped-element left-handed transmission-line section," *IEEE Trans. Microwave Theory Tech.*, vol. 52, pp. 1142–1149, Apr. 2004.
- [45] A. Sanada, M. Kimura, I. Awai, H. Kubo, C. Caloz, and T. Itoh, "A planar zeroth order resonator antenna using left-handed transmission line," presented at European Microwave Conf., Amsterdam, Netherlands, 2004.
- [46] L. Liu, C. Caloz, and T. Itoh, "Dominant mode (DM) leaky-wave antenna with backfire-to-endfire scanning capability," *Electron. Lett.*, vol. 38, pp. 1414–1416, 2000.
- [47] S. Lim, C. Caloz, and T. Itoh, "Metamaterial-based electronically controlled transmission line structure as a novel leaky-wave antenna with tunable radiation angle and beamwidth," *IEEE Trans. Microwave Theory Tech.*, vol. 52, Dec. 2004.

- [48] C. Allen, C. Caloz, and T. Itoh, "Leaky-waves in a metamaterial based two-dimensional structure for a conical beam antenna application," presented at IEEE-MTT Int. Symp., Fort Worth TX, 2004.

CHAPTER III DIPOLE ANTENNAS USING LEFT HANDED TRANSMISSION LINES

The unique properties of left-handed metamaterials are promising for a diversity of optical/microwave applications. However, the SRR-based left-handed structures presented originally were impractical for microwave applications, because of their high loss and narrow bandwidth characteristics. The idea of using the transmission line theory to describe and design left-handed material was first introduced at approximately the same time by three different groups [1-4], where several novel metamaterials concepts have been developed and verified independently. In particular, left-handed metamaterials using artificial lumped-element loaded transmission lines have been implemented in microstrip technology [5]. The unique properties of these non-resonant structures with lower loss and wider bandwidth have led to the development of novel microwave devices, such as new types superlenses [6], microwave components [7, 8] and leaky-wave antennas [9]. Nonetheless, the left-handed transmission lines approach has never been focused on the analysis and design of conventional linear antennas, like dipole or loop antennas.

A different antenna understanding based on a general transmission line approach is presented in the following chapters. Moreover, the fundamental electromagnetic properties and the physical realization of these left-handed transmission line loaded antennas are studied and developed. To the best of the author's knowledge, this is the first time that this concept is applied to the development of small antennas, extending the degrees of freedom of this sort of structures.

Collaborators in this work at Toyota Research Center wish to design novel antennas with metamaterials for their cars. The first design of a left handed dipole antenna by Dr. Hideo Iizuka (from Toyota Reserach Center) and Prof. Peter Hall (from Birmingham University) [10, 11] could give size reduction and be applied on the vehicles for receiving radio and TV signals, whose frequency range is from 100 MHz to 800 Mhz. The printed circuit board structure allows mounting on glass or roof panel of the cars.

In this chapter, the conceptual model and the fundamental electromagnetic properties of the left handed dipole antennas which are worked by Dr. Hideo Iizuka and Prof. Peter Hall etc [10-12] will be reviewed first, including the implementations. Based on their conceptual model, a lumped element loaded left handed dipole antenna is developed and measured to verify the theory. Also various configurations have been studied for the left handed dipoles to extend the design degrees of freedom.

3.1 Basic Dipole Antenna Properties

First, basic dipole antenna development and properties are reviewed in this section. A dipole antenna, developed by Heinrich Rudolph Hertz around 1886 [13], is a basic type of antenna consisting of two pieces, with a centre-fed driven element for transmitting or receiving radio frequency energy. These antennas are the simplest practical antennas from a theoretical point of view; the antenna can be made by a simple wire and the current amplitude on such an antenna decreases uniformly from maximum at the centre to zero at two ends.

3.1.1 Elementary Doublet

In order to understand the dipole antenna's properties, the elementary doublet is analyzed. An elementary doublet is a small length of conductor δl (compared with the wavelength λ) traversed by an alternating current:[14]

$$I = I_0 e^{j\omega t} \quad (3.1)$$

In reality, any real antenna can be divided by multiple segments of this small length of conductor, whose far electrical field can be calculated as: [14]

$$E_\theta = \frac{-jI_0 \sin \theta}{2\epsilon_0 c r} \frac{\delta l}{\lambda} e^{j(\omega t - kr)} \quad (3.2)$$

where, E_θ is the far electric field of the electromagnetic wave radiated in the θ direction; c is the speed of light in vacuum; ϵ_0 is the permittivity of vacuum; r is the distance from the doublet to the point where the electrical field E_θ is evaluated; k is the wave number

($k = 2\pi/\lambda$). The exponent of e accounts for the phase change of the electrical field with time and the distance to the dipole. The far electric field E_θ of the electromagnetic wave is coplanar with the doublet and perpendicular with the line joining the dipole to the point where the field is evaluated [15].

3.1.2 Short Dipole

A short dipole is a physically feasible dipole formed by two conductors with a total length L ($L \ll \lambda$) as shown in Figure 3-1. The two conducting wires are fed at the centre of the dipole, where the current is maximal and it decreases linearly to be zero at the ends of the wires. Note that the direction of the current in both the dipole arms is the same to the right in both or to the left in both. [15]

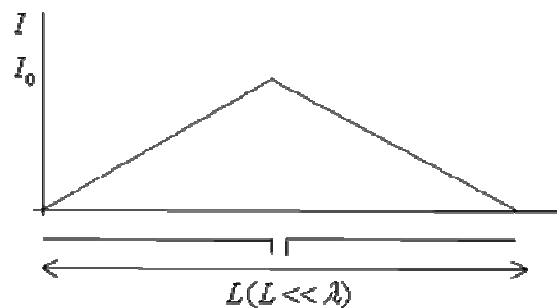


Figure 3-1. Short dipole current distribution.

The radiation pattern of a short dipole is shown in Figure 3-2, where the dipole is positioned vertically. The section of radiation pattern is circular torus shaped (shown in the left image of Figure 3-2) with zero inner diameter. Radiation is maximal in the plane perpendicular to the dipole and is zero in the direction of wires, that is, the current

direction. The perspective view is shown in the right of Figure 3-2 where dipole is vertical in the torus centre.

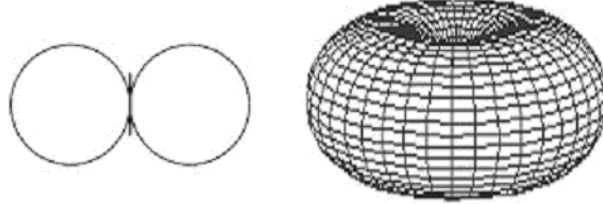


Figure 3-2. Short dipole antenna radiation pattern [15].

Substituting the length in (3.2), the far field E_θ of the electromagnetic wave radiated by this dipole is:

$$E_\theta = \frac{-jI_0 \sin \theta L}{4\epsilon_0 cr} \frac{L}{\lambda} e^{j(\omega t - kr)} \quad (3.3)$$

Then we can compute the total emitted power and the resistive part of the series impedance of this dipole due to the radiated field, known as the radiation resistance [16]:

$$R_{series} = \frac{\pi}{6} Z_0 \left(\frac{L}{\lambda}\right)^2 \quad (\text{for } L \ll \lambda) \quad (3.4)$$

where Z_0 is the impedance of free space. Assuming a common approximation of $Z_0 = 120\pi$

ohms, $R_{series} = 20\pi^2 \left(\frac{L}{\lambda}\right)^2$ ohms.

Antenna gain is defined as "the ratio of surface power radiated by the antenna to the power density radiated by a hypothetical isotropic antenna [16]":

$$G = \frac{\left(\frac{P}{S}\right)_{ant}}{\left(\frac{P}{S}\right)_{iso}} \quad (3.5)$$

The surface power carried by an electromagnetic wave is: $(\frac{P}{S})_{ant} = \frac{1}{2} c \epsilon_0 E_\theta^2 \cong \frac{1}{120\pi} E_\theta^2$. The

surface power radiated by an isotropic antenna with the same power is: $(\frac{P}{S})_{iso} = \frac{1}{2} \frac{R_{series} I_0^2}{4\pi r^2}$.

Replacing values for the case of a short dipole, final result is: $G = \frac{\pi(\frac{L}{\lambda})^2}{\epsilon_0 c \frac{2\pi}{3\epsilon_0 c} (\frac{L}{\lambda})^2} = 1.5 =$

1.76 dBi. dBi simply means decibels gain as referenced to an isotropic antenna [15].

3.1.3 Half-Wave Dipole Antenna

Dipoles that are much smaller than the wavelength of the signal are called Hertzian, short, or infinitesimal dipoles. They are usually inefficient due to a very low radiation resistance and a high reactance, but they are often the only available antennas at very long wavelengths. Dipoles whose length is half the wavelength of the signal are called half-wave dipoles, and are more efficient. In general radio engineering, the term dipole usually means a half-wave dipole. Typically a half-wave dipole antenna is formed by two quarter wavelength conductors or elements placed back to back for a total length of $\lambda/2$ as shown in Figure 3-3 [15]. A standing wave on an element of a length of $\lambda/4$ yields the greatest voltage differential, as one end of the element is at a node of the wave while the other is at an antinode. The larger the differential voltage is, the greater the current flows through the dipole.

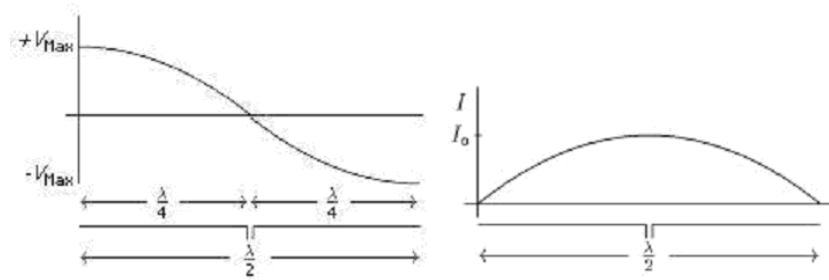


Figure 3-3. Half-wave dipole voltage, current distribution [15].

Assuming a sinusoidal distribution, the current caused by this voltage differential is given by [17]:

$$I = I_0 e^{j\alpha x} \cos kl \quad (3.6).$$

The far field E_θ of the electromagnetic wave radiated by the dipole is somewhat complex [17]:

$$E_\theta = \frac{-jI_0}{2\pi\epsilon_0 cr} \frac{\cos(\frac{\pi}{2} \cos \theta)}{\sin \theta} e^{j(\alpha x - kr)} \quad (3.7).$$

But the fraction $\frac{\cos(\frac{\pi}{2} \cos \theta)}{\sin \theta}$ is close to $\sin \theta$. The half-wave dipole resistance can be

approximately calculated by: $R_{\frac{\lambda}{2}} = 60 \text{Cin}(2\pi) = 120 \int_0^{\frac{\pi}{2}} \frac{\cos(\frac{\pi}{2} \cos \theta)^2}{\sin \theta} d\theta \cong 73.13 \Omega$; The

maximum theoretical gain of a half-wave dipole antenna

$$\text{is: } G_{\frac{\lambda}{2}} = \frac{60^2}{30R_{\frac{\lambda}{2}}} \approx \frac{120}{73.13} \approx 1.64 \approx 2.15 \text{dBi}. [15]$$

The resistance is not enough to characterize the dipole impedance, as there is also an imaginary part. Due to the difference in the velocity of wave propagation in wire as opposed to the same wave in free space, resistance and impedance multiply the dipole wavelength by about 95% are most commonly used in practice. The impedance of a dipole antenna for lengths going from 0.4λ to 0.6λ is drawn in Figure 3-4. The blue line represents imaginary part (reactance), which is a function of dipole's length. For a half-wave dipole, it is equal to $j42.5$. To reduce the imaginary part of the dipole impedance to zero, the length of the antenna is reduced to 0.47λ to 0.48λ for the first resonance. The maximum theoretical gain of a dipole increases from 2.15 dBi to 2.55 dBi for lengths going from 0.5λ to λ , and increases highly to 8.51 dBi for the length of 8λ [18].

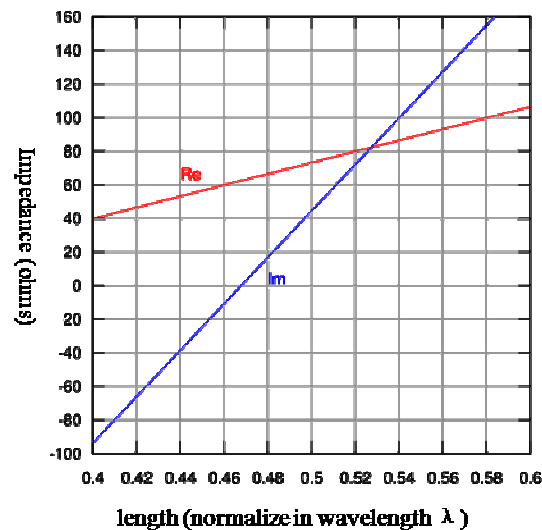


Figure 3-4. Dipole impedance versus 0.4 to 0.6 wavelengths. [18]

In practice, a resonant dipole, having an input impedance that is purely resistive and lies between 30 and 80 ohms, could provide a good match to commercially available 50 ohms coaxial cables as well as commercial transmitters and receivers, most of which have 50

ohm output and input impedances. The input impedance of a dipole antenna also depends on its electrical length. When the antenna is approximately an odd multiple of a half wavelength long, the input impedance is resistive and lies between 50 and 200 ohms. For antennas that are an even number of half wavelengths long, the input impedance is resistive and extremely high, between 1000 and 50,000 ohms. [19]

Ideally, a half-wave dipole should be fed with a balanced line matching the theoretical 73 ohm impedance of the antenna. A folded dipole uses a 300 ohm balanced feeder line. Practically, a dipole is often fed with a coaxial cable. A dipole is a balanced device (the same voltage referred to common ground on both terminal), but coax is unbalanced. If a dipole antenna is fed with a direct coax, currents flows on the coax cable radiate in addition to the antenna itself, and the radiation pattern may be asymmetrically distorted [20]. A balun could be used to remedy this. Several types of baluns are commonly used to transmit on a dipole: current baluns, coax baluns and sleeve baluns [20].

3.2 Reviews on Left Handed Dipole Antennas and Their Implementations

A purely left-handed transmission line can be represented as the combination of a series capacitance and a shunt inductance (dual case of the right-handed transmission line), previously introduced in the Chapter II. In reality, a purely left-handed structure is not possible because of unavoidable right-handed parasitic series inductance and shunt capacitance effects (parasitic capacitance is due to development of voltage gradients, and unavoidable parasitic inductance is due to current flow along the metallization). Therefore, a composite right/left-handed structure represents the most general form of a structure with left-handed attributes.

The fundamental physical characteristics of such composite right/left-handed transmission line can be derived from elementary transmission line theory also summarized in Chapter II. For a balanced composite right/left-handed transmission line, at low frequencies, it is dominantly left-handed with a hyperbolic dispersive phase constant β , equation (3.8), while at high frequencies; it is dominantly right-handed, with a linear non dispersive phase constant β , equation (3.9). The transition frequency ω_0 between the left-handed and right-handed ranges is given by equation (3.10) where zero phase constant β and infinite wavelength λ are achieved.

$$\beta_L = - \frac{1}{\omega \sqrt{L_L C_L}} \quad (3.8)$$

$$\beta_R = \omega \sqrt{L_R C_R} \quad (3.9)$$

$$\omega_0 = \frac{1}{\sqrt[4]{L_L C_L L_R C_R}} \quad (3.10)$$

A CRLH medium can be practically realized by periodically or non-periodically inserting series capacitors and shunt inductors along a conventional transmission line with average lattice constant or distance much smaller than wavelength, thus an electromagnetic wave does not “see” discontinuities because the guided wavelength is much larger than them. Transmission Line theory is used to analyze the design of composite right/left-handed structures [5].

Based on the LH transmission line configuration and similar to conventional dipole antenna design, a novel small dipole antenna loading with left-handed transmission lines has been proposed [10, 11]. The antenna is composed of a ladder network periodic structure of unit cells having series capacitors and shunt inductors. The antenna achieves size reduction in the left handed region depending on the loading, and the resonance number n is based on the conventional resonant mode numbering. The concept and radiation properties are investigated numerically, and verified by measurements.

3.2.1 Conceptual Model

The conceptual model of the dipole antenna using a left-handed transmission line is shown in Figure 3-5, [10,11,12]. The transmission line can be considered as a folded dipole with open circuit ends. The loading is performed by inserting series capacitors and shunt inductances in a number of unit cells. The components can be either lumped or distributed elements. The antenna has a ladder network periodic structure of any number of cell; 4 unit cells are shown in the figure. The unit cell has a shunt inductor L_L and two series capacitors C_L . The inductors L_L and capacitors C_L operate as a left-handed transmission line. The resonant frequency and input impedance are controlled by their values, independent on the

length of the antenna. The currents I_1 and I_2 on wires along the z axis are defined to have the same direction in Figure 3-5. The capacitors C_L are put on one side of the ladder network, which also has the feed point. This leads to a difference of the amplitude of currents I_1 and I_2 on the vertical wires. Because the out-of-phase currents as presented later have different amplitudes, they do not completely cancel in the far field, and as a result radiate [12]. This radiation mechanism of the left-handed dipole antenna is very different from those of previous left-handed antennas based on microstrip lines. Thus, the proposed antenna allows for size reduction while maintaining impedance matching by the adjustment of L_L and C_L .

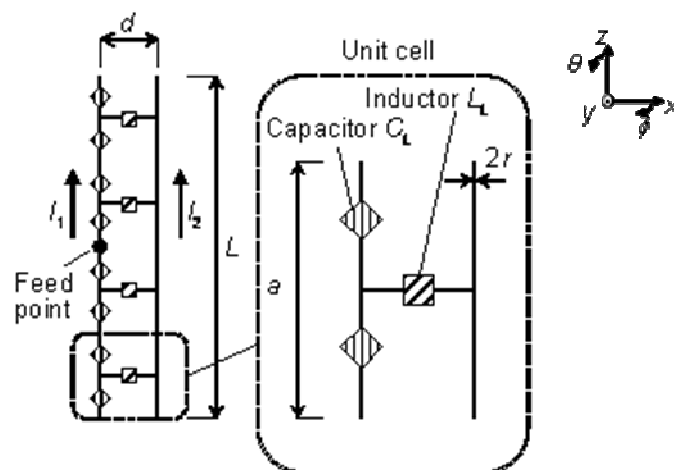


Figure 3-5. Conceptual model of a left-handed dipole antenna. [12]

The left handed antennas have a unique feature that the wavelength of the induced current becomes shorter with decreasing frequency. The standing wave on the dipole is formed in the same way as in a conventional dipole by the interference between oppositely directed current waves. The fact that, in the antenna with left handed loading the direction of the

phase velocity is opposite to that of the group velocity, does not appear to change this mechanism, but just produces a different resonant frequency behaviour with mode number. Increasing mode number occurs at decreasing frequency and the mode number n in the left-handed region is defined by negative numbers. The number, n , of resonances depends on the number of unit cells N . A dipole antenna usually achieves its resonances at odd modes and anti-resonances at even modes. For example, in a dipole antenna with $N = 4$, the resonance numbering is $n = -3, -2, -1$ in the left-handed frequency region or $n = 1, 2, 3$ in the right-handed frequency region as shown in Figure 3-6, each relating to a current distribution with the same number of peaks in the current distribution along the dipole.

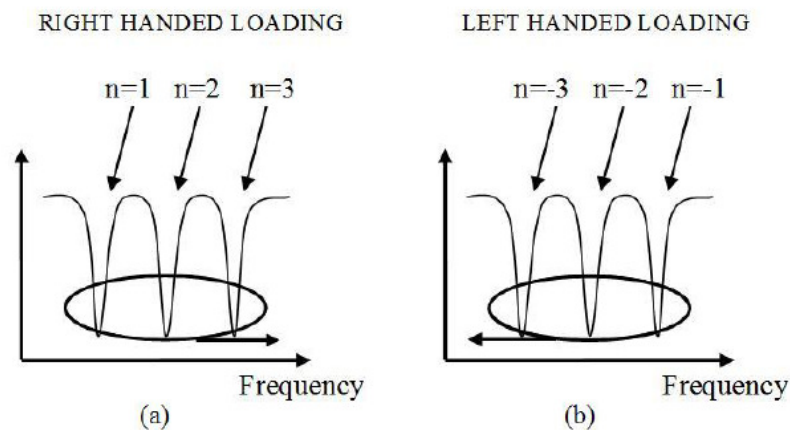


Figure 3-6 (a) right- handed and (b) left-handed region resonance numbering.

Antennas loaded with left-handed transmission lines allow operation with higher order mode current distributions and small size, whereas conventional antennas operating in a higher order mode are usually larger than a wavelength.

3.2.2 Simulation Performance

Various parameters are used to analyze the performance of an antenna and are introduced in Appendix B. Simulations use the commercial simulator “FEKO”, [21], which is based on the method of moments. Table 3-1 gives the parameters. Lossless LC lumped elements and wires are assumed.

Table 3-1 Parameters of the conceptual left-handed dipole antenna. [12]

Length L of antenna	100 mm
Length a of unit cell	25 mm
Distance d of wires	10 mm
Radius r of wire	0.44 mm
Number N of unit cells	4
Capacitance of C_L	0.45 pF
Inductance of L_L	140 nH
Length of LC elements	1 mm

3.2.2.1 Near Field Distributions

Equation (3.11) gives the relationship between the resonance number n , the length L of the antenna, and the wavelength λ_a of the current on the antenna

$$L = |n| \frac{\lambda_a}{2} \quad (3.11).$$

The resonance number, n , is negative, based on the conventional resonant mode numbering. Figure 3-7 shows near field distributions in the zx plane at $n = -3, -2$ and -1 , where three,

two and one standing wave peaks, respectively, can be seen although less clearly. This reduced wavelength, λ_a , with decreasing frequency is a unique feature of the left-handed operation. It can also be seen that the field contours are widely spread at $n = -1$, indicating strong radiation, whilst at $n = -3$, out of phase currents on the three standing wave peaks reduce radiation.

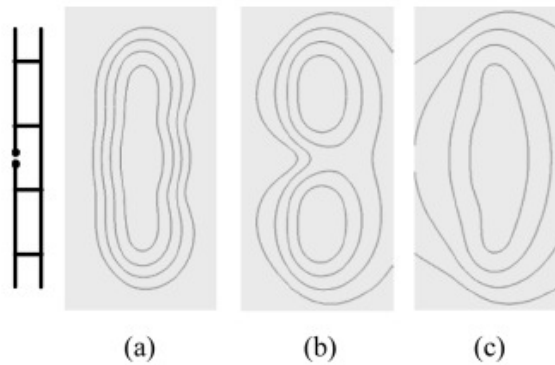


Figure 3-7. Simulated near field distributions of dipoles loaded by left-handed ladder networks. (zx plane; Fields are normalized by the maximum value at each frequency; Contour ranges from -20 to 0 dB with the step of 5 dB.)

(a) 318 MHz, $n = -3$, (b) 369 MHz, $n = -2$, and (c) 466 MHz, $n = -1$. [11]

3.2.2.2 Frequency, Phase Constant Relationship

In 5GHz frequency ranges, all antenna resonances and anti-resonances can be obtained from reflection coefficient phase characteristics, where phases are zero. Left handed modes $n = -3, -2, -1$ and right handed modes $n = 1, 2, 3$ can be identified from their near field distributions, each relating to a current distribution with the same number of peaks along the dipole. Figure 3-8 (a) and (b) shows the relationship between the frequency, phase constant, β , and wavelength, λ_a . It can be seen, in Figure 3-8 (a), that the operating frequency in the left-handed region is lower than that in the right-handed region. An $n = -1$

mode is suitable for small antenna operation, although the antenna could also work in an $n = 0$ mode with appropriate CL values and shorted terminals at both ends. However the operating frequency in the $n = 0$ mode will be higher than that in the $n = -1$ mode. Wavelength, λ_a , and phase constant, β , has (3.12), and the results of Figure 3-8 (a) are presented as a relationship between wavelength, λ_a , and frequency in Figure 3-8 (b).

$$\lambda_a = \frac{2\pi}{|\beta|} \quad (3.12)$$

An opposite relationship between the frequency and wavelength, λ_a , is clearly observed in the left-handed and right-handed regions. It can be seen that the wavelength λ_a becomes shorter with decreasing frequency, which is one of the unique features of a left-handed material.

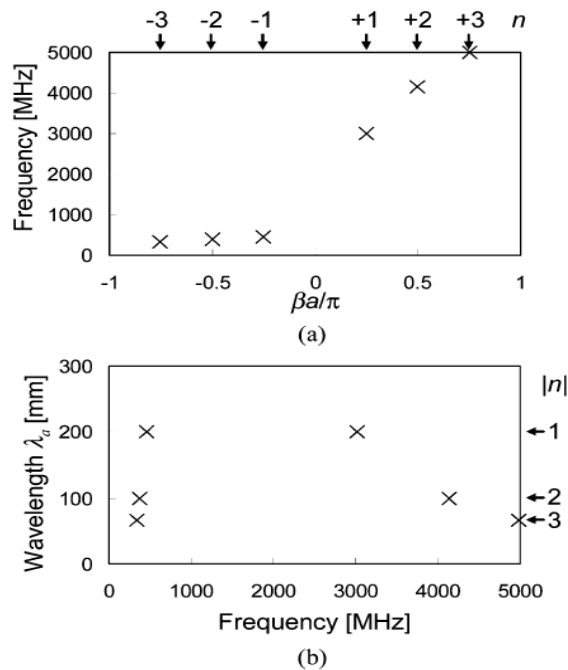


Figure 3-8. Simulated relationship between the frequency, phase constant β , and wavelength λ_a for right- and left-hand regions.

(a) Frequency versus phase constant β (b) wavelength λ_a versus frequency.[11]

3.2.2.3 Current Distributions

Figure 3-9 (a) and (b) show current distributions on wires along the z axis at 466 MHz. A voltage of 1V was applied at the feed point. Currents I_1 and I_2 have different amplitude levels in Figure 3-9 (a). There are discontinuities at ± 12.5 mm and ± 37.5 mm in I_1 and I_2 due to currents flowing on interconnecting wires having inductors L_L . Since the currents in the x direction are out-of-phase at the symmetrical positions for the feed point, cross polarization remains low level. The currents I_1 and I_2 are seen to be out-of-phase in Figure 3-9 (b). The radiation mechanism of the antenna is considered here. In the case of the distance d being much smaller than a free space wavelength, λ_0 , no phase difference of the two paths is assumed in the far field radiated from the currents I_1 and I_2 . Then the radiation source becomes the summation of I_1 and I_2 . The magnitude of I_1+I_2 is the difference of their magnitudes, $|I_2|-|I_1|$, as they are out-of-phase. The interesting point is that I_1+I_2 becomes a near cosine amplitude distribution with flat phase, and consequently radiation occurs. If the capacitors C_L were put on both wires, both currents I_1 and I_2 would have the same amplitude and be out-of-phase, and the radiation would be negligibly small. In this case, the structure would only be working as a transmission line.

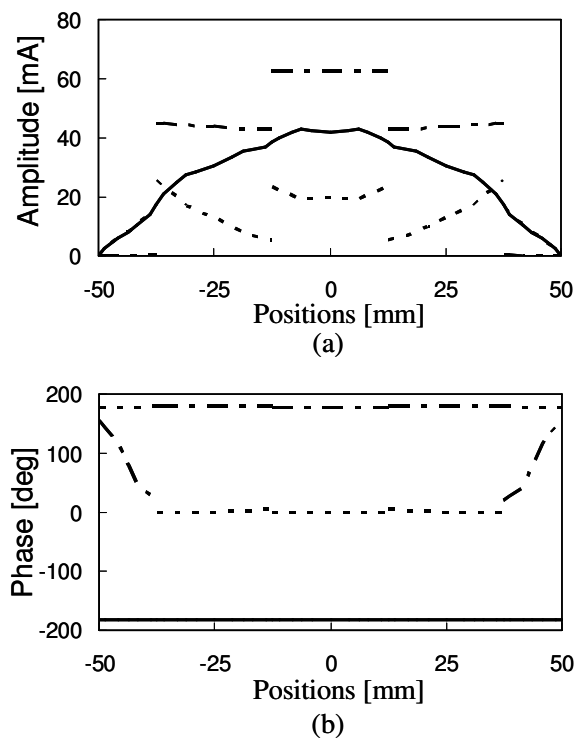


Figure 3-9. Current distributions of the conceptual left-handed dipole antenna along z axis at 466 MHz, $n = -1$. (----: I_1 , - - -: I_2 , —: $I_1 + I_2$). (a) Amplitude and (b) phase. [12]

Current distributions from $n = -1$ to -3 are seen here. $I_1 + I_2$ is presented in Figure 3-10 (a), (b) since it is related to radiation. The vertical axis in Figure 3-10 (a) is relative amplitude normalized by the maximum value at each frequency, which is 43 mA at 466 MHz, 0.6 mA at 369 MHz, and 3584 mA at 318 MHz, respectively. The currents of $(1/2) \lambda_a$, λ_a , and $(3/2) \lambda_a$ are observed at 466 MHz, 369 MHz, and 318 MHz. In the case of $n = -2$, $|I_1 + I_2|$ becomes small at the position of 0 mm, and impedance has an open circuit at the feed point. There are phase changes of 180 degrees at ± 12.5 mm for $n = -3$ giving very small radiation.

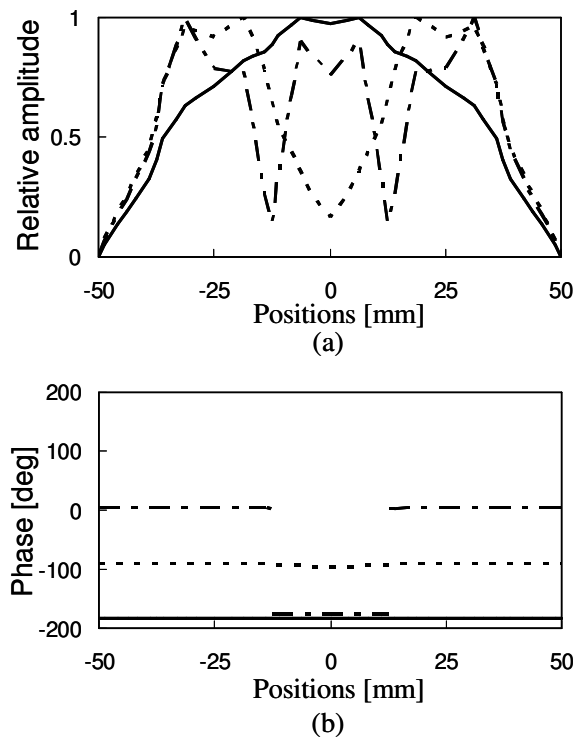


Figure 3-10. Summation of currents I_1 and I_2 of the conceptual left-handed dipole antenna along the z axis. (—: 466 MHz, $n = -1$, ----: 369 MHz, $n = -2$, -.-: 318 MHz, $n = -3$). (a) Amplitude normalized by the maximum value at each frequency. The magnitude $|I_1+I_2|$ is the difference of their magnitudes $|I_2|-|I_1|$. (b) Phase. [12]

3.2.2.4 Reflection Characteristics

Reflection characteristics are shown in Figure 3-11 (a) and (b). One resonance for $n = -1$ was observed in the amplitude characteristic with respect to 50Ω in Figure 3-11 (a). An input impedance with a real part close to 50Ω was achieved at $n = -1$ by the values of L_L and C_L , specified in Table 3-1. Bandwidth of $|S_{11}| < -10$ dB is 0.43 %. Three resonances were observed in phase characteristic in Figure 3-11 (b). In the case of $n = -2, -3$, no resonance of $|S_{11}|$ was observed due to mismatching at the feed point, which was expected as the current distributions in Figure 3-10 (a), (b).

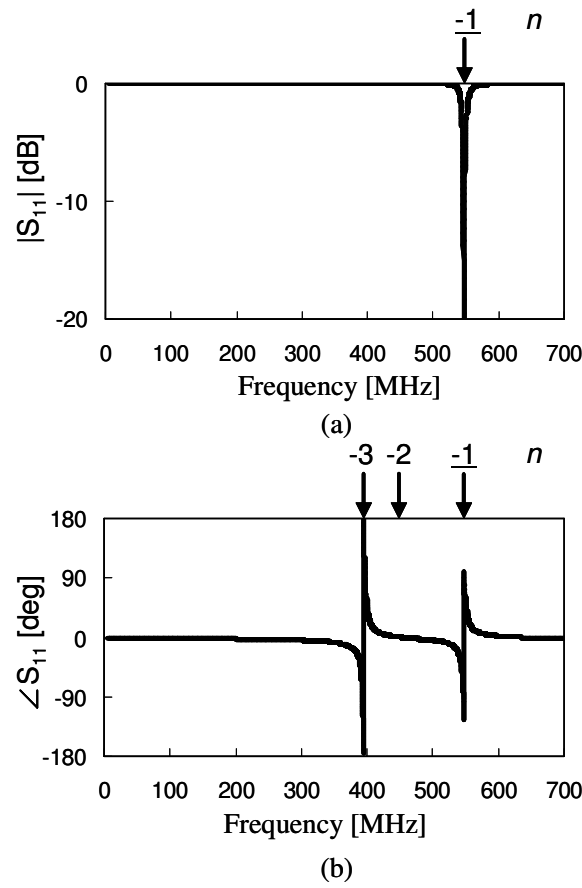


Figure 3-11 Reflection characteristics of the conceptual left-handed dipole antenna.

(a) Amplitude with respect to 50Ω and (b) phase. [12]

3.2.2.5 Loading Contributions

The contributions of inductor L_L and capacitor C_L to the resonant frequency and input impedance for $n = -1$ are next analyzed. Figure 3-12 (a) shows the resonant frequency for variation of values of the inductor L_L and capacitor C_L . L_L and C_L were normalized in the horizontal axis to 140 nH and 0.45 pF, respectively. It can be seen that resonant frequency decreases with increasing L_L and C_L . As shown in Figure 3-12 (b), the input impedance also decreases with increasing L_L and C_L . For a simple design, it is important that L_L and C_L have different variations of resonant frequency and input impedance and this is

explained as follows. L_L contributes to larger variation of resonant frequency rather than C_L . On the other hand, changes in C_L give larger variation of input impedance rather than L_L . Thus, the desired resonant frequency and input impedance can be obtained with the adjustment of L_L and C_L . When the operating frequency needs to be set lower while maintaining the same input impedance, an increase of L_L and the decrease of C_L would provide the desired frequency.

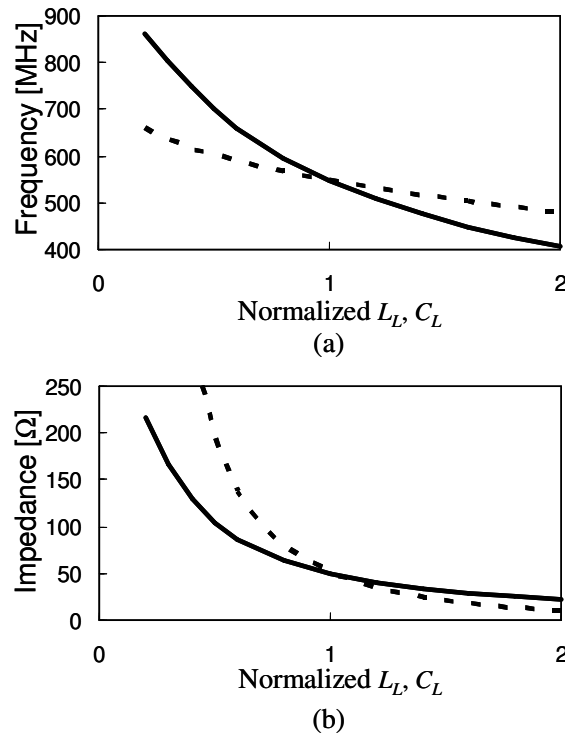


Figure 3-12. Resonant frequency and input impedance of the conceptual left-handed dipole antenna for $n = -1$ with variation of inductor L_L and capacitor C_L . L_L and C_L are normalized by 140 nH and 0.45 pF, respectively. (a) Resonant frequency and (b) input impedance. (—: L_L , ----: C_L) [12]

3.2.2.6 Bandwidth Property

The bandwidth for $|S_{11}| < -10$ dB is plotted as a function of the normalized length L/λ_0 in Figure 3-13. The operating frequency, which was related to λ_0 , was varied for the model of Figure 3-5, while maintaining input impedance close to 50Ω with the adjustment of L_L and C_L . Other parameters of the model of Figure 3-5 are the same as those shown in Table 3-1. It can be seen that bandwidth narrows steeply from 2.1 % to 0.1 % with decreasing the normalized length L/λ_0 from 0.27 to 0.12, in a way that is similar to an ordinary right-handed dipole antenna.

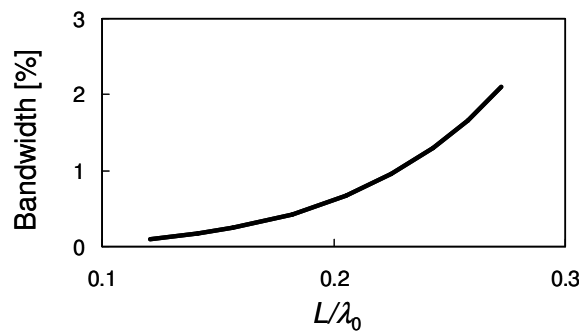


Figure 3-13. Bandwidth for $|S_{11}| < -10$ dB v.s. the length L/λ_0 . Input impedance is adjusted to be close to 50Ω . [12]

3.2.3 Implementations

3.2.3.1 Short Dipole with Distributed Elements

The loading in the left-handed dipole can be realized by distributed elements for ease of fabrication and avoidance of large loss in lumped elements. Figure 3-14 shows the printed straight left-handed dipole antenna, which was designed by Dr. Hideo Iizuka etc [12]. The antenna was implemented on Teflon substrate with the thickness of 0.6 mm and

permittivity of 2.6. The length L of the antenna, the length a of unit cell, the distance d of lines, and number N of unit cells are the same as those of the model of Figure 3-5. Inductors L_L and capacitors C_L are used by meander inductors and interdigitated capacitors. Conductivity of 5.8×10^7 S/m for copper with the thickness of 0.04 mm and loss tangent of 0.0015 for dielectric substrate with the thickness of 0.6 mm were used. The designed parameters for the distributed elements are as follows. The width of outer conductors in the z axis is 1.75mm. The widths of lines and their gaps are 0.4 mm and 0.1 mm for the meander inductor, and 0.4 mm and 0.05 mm for the interdigitated capacitors.

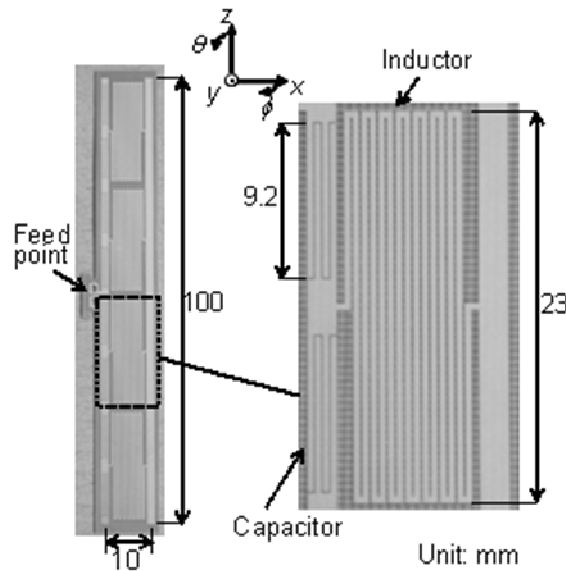


Figure 3-14. Configuration of the printed straight left-handed dipole antenna. [12]

The prototype antenna is shown in Figure 3-15. A wideband LC balun is used to feed the dipole and can give impedance transformation. The balun consists of a high pass filter, a low pass filter and a T-junction [22]. The balun for the short dipole in Figure 3-14 has impedance of $Z_b = 50 \Omega$ for the balanced port and $Z_u = 50 \Omega$ for the unbalanced port. The balun has parameters of $C_{H1} = 18$ pF, $C_{H2} = 6$ pF, $L_{H1} = 18$ nH, $L_{L1} = 3.9$ nH, $L_{L2} = 15$ nH,

and $C_{L1} = 4$ pF. The configuration of the balun is shown in Figure 3-16. The frequency bandwidth of the balun for $|S_{11}| < -10$ dB starts at 330MHz and ends at 700MHz. The detailed design process and calculation equations are presented in Appendix E.

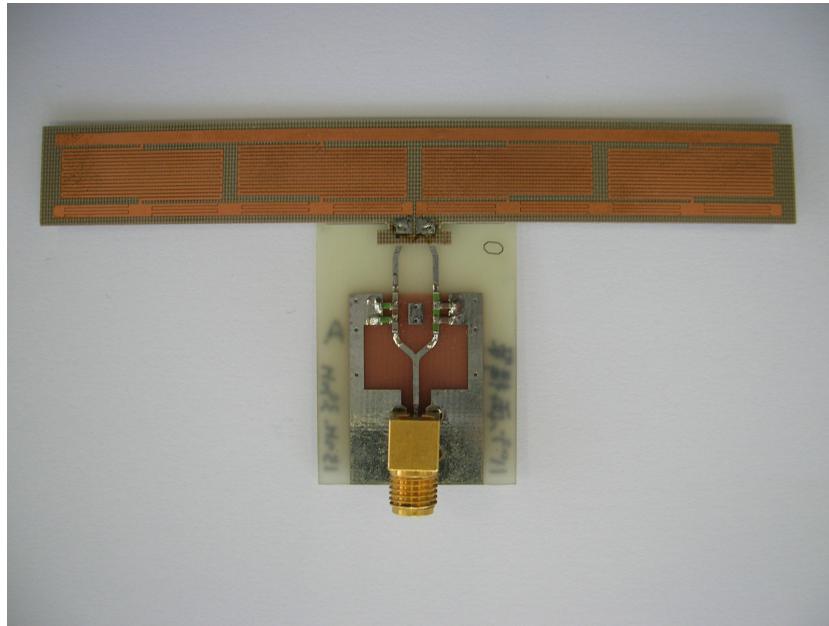


Figure 3-15. The prototype of the distributed left-handed dipole.

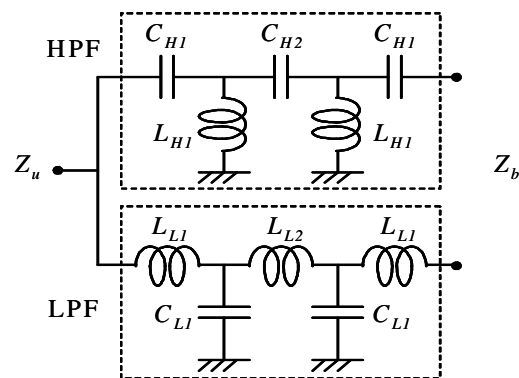


Figure 3-16. Configuration of balun. [12]

Reflection characteristic was measured through the balun. This measurement is represented by the thick line in Figure 3-17. An input impedance with a real part close to 50Ω was achieved at 547 MHz in an $n = -1$ mode. Bandwidth for $|S_{11}| < -10$ dB was 1.7 %. Agreement between simulation and measurement was encouraging, although there are frequency shifts of 15 MHz for $n = -1$ and 30 MHz for $n = -3$. Also, one more dip is observed below 300 MHz due to the limit frequency bandwidth of the balun, from 330 MHz to 700 MHz.

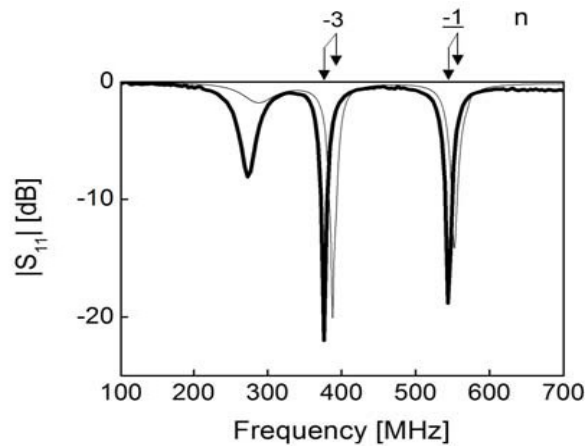


Figure 3-17. Measured and simulated reflection characteristics of printed straight left-handed dipole antenna. (Measurement: thick line, Simulation: thin line) [12].

Figure 3-18 shows measured radiation pattern in the yz plane at 547 MHz. A figure of 8 radiation pattern was obtained as expected from the current distributions of Figure 3-9 (a), (b). The simulated efficiency of the printed antenna is 27%. Simulated gain is -1 dB at 562 MHz for $n = -1$ mode. Measured gain was -3.9 dBi including 0.4 dB loss of the balun. Cross polarization was lower than -13 dB. In the case of $n = -3$, measured gain was -24.3 dBi at 379 MHz.

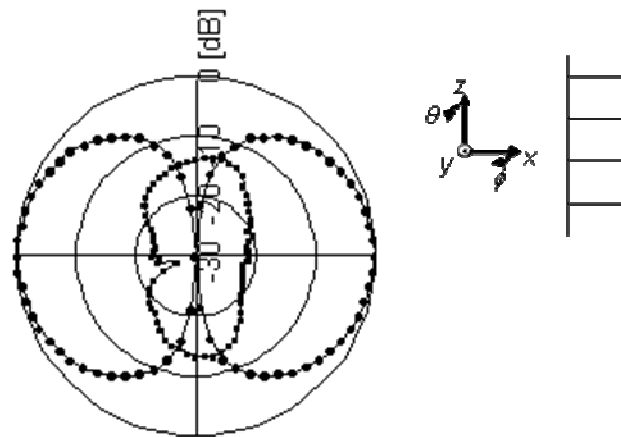


Figure 3-18. Measured radiation pattern of the printed straight left-handed dipole antenna in the yz plane at 547 MHz, $n = -1$. (\bullet —: E_θ , \blacksquare —: E_ϕ). [12]

3.2.3.2 Meandered Dipole with Distributed Elements

A printed meandered left-handed dipole antenna for orthogonal polarization has been implemented in Toyota Research Centre by Dr. H Iizuka etc [23]. The fundamental structure of the ladder network is the same as the straight left handed dipole antenna shown in Figure 3-5. The new configuration has a ladder network periodic structure of any number of unit cells with a meander arrangement.

Figure 3-19 shows the printed meandered left-handed dipole antenna with a distributed realization of meandered inductors and interdigital capacitors. The meander structure has 18 unit cells and enables opposite polarization to be obtained compared to a right-handed dipole. The antenna dimensions are 20 mm by 180 mm. The total path length along the meandered centre line is 360 mm. The width of the line sections is 1.35 mm and the widths of lines and their gaps are 0.3 mm and 0.1 mm for the meander inductor, and 0.3 mm and 0.05 mm for the interdigitated capacitors.

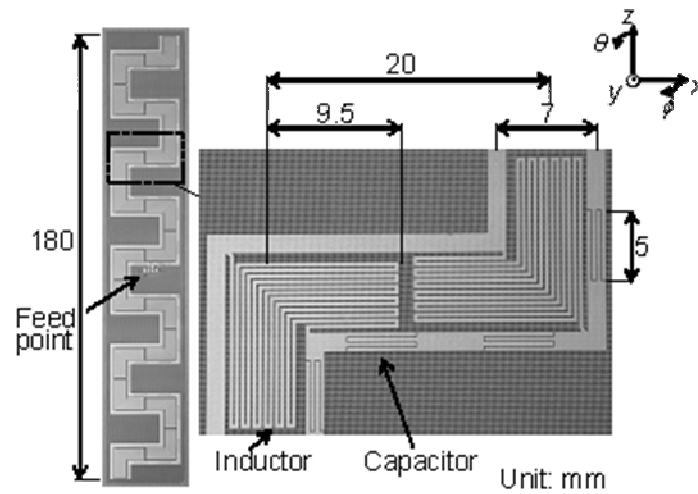


Figure 3-19. Photograph of the printed meandered left-handed dipole antenna. [23]

Figure 3-20 shows measured reflection characteristic through a balun. The frequency range was limited from 400 MHz to 1000 MHz due to the limited bandwidth of the balun. Resonances above this frequency range are expected. Odd numbered resonances only are indicated for clarity. The balun for the meandered dipole has the same configuration in Figure 3-16 as that used on the straight dipole, but it has different parameters. The parameters are $C_{H1} = 8$ pF, $C_{H2} = 3$ pF, $L_{H1} = 33$ nH, $L_{L1} = 8.2$ nH, $L_{L2} = 27$ nH, and $C_{L1} = 2$ pF. The balun transforms the impedance from $Z_b = 200 \Omega$ to $Z_u = 50 \Omega$ so that matching can be achieved in an $n = -9$ mode (the balun design process is described in Appendix E). The measured resonant frequency is 643 MHz. The minimum resonance number is $n = -17$ and resonances numbers from -17 to 5 are observed. Simulation result including the loss is also shown and agrees with the measurement, although resonant frequencies in simulation are approximately 30 MHz higher than those in measurement. Another unique feature of an antenna constructed with left-handed materials is that the resonant frequencies occur as a nonlinear function of frequency, which can be also seen in Figure 3-20, where the spacing

of the resonant frequencies between resonance numbers, $n-1$ and n , becomes narrower with decreasing frequency. In right-handed materials, the resonant frequencies are generally a linear function of frequency. The resonant behaviour is summarized in Figure 3-21 as a relationship between wavelength λ_a and frequency. Circles represent the measurement results, while crosses the simulation results. The difference of approximately 30 MHz between measurement and simulation results becomes clearer. The unique features of a left-handed material, mentioned above, are clearly observed. [23]

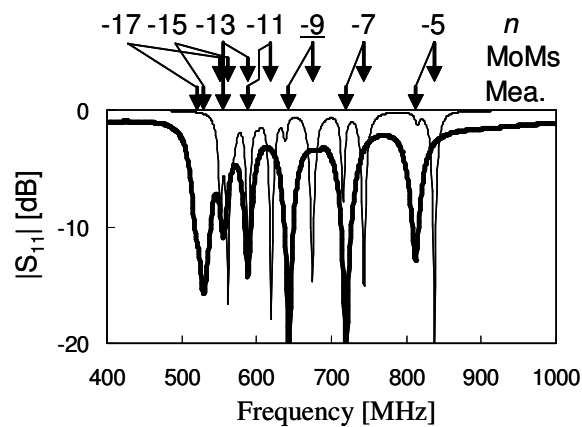


Figure 3-20. Measured reflection characteristic of the printed meandered left-handed dipole antenna through a balun. Simulated one including loss of the conductors and dielectric is also presented for comparison. (—: Mea., - - -: MoMs) [23]

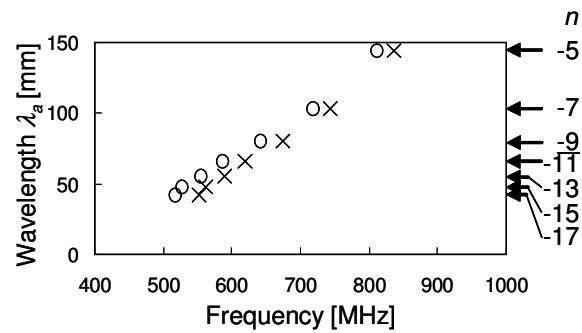


Figure 3-21. Relationship of the printed meandered left-handed dipole antenna between wavelength λ_a and frequency. (○: Mea., ×: MoMs) [23]

The radiation pattern was measured in the xy plane at 643 MHz and is presented in Figure 3-22. The shape of radiation pattern is a figure of eight, as expected for an electrically small dipole. However now the E_ϕ component becomes dominant compared to the straight dipole pattern in Figure 3-18. In other words the dipole is polarized orthogonal to its length. This change of polarization can be understood as follows. The induced current distribution on the dipole antenna is a standing wave pattern, which has $|n|$ half wavelengths, λ_a , when working in an $n = -9$ mode. That is confirmed from the near field distribution of the simulation model, shown in Figure 3-23. This current distribution results in the currents induced on the line sections along the x axis (or horizontal in Figure 3-19) being in-phase and along the z axis (or vertical) being out-of-phase. In addition the peaks of the standing wave occur on the horizontal sections and the nulls on the vertical sections. Thus, radiation from the vertical currents cancel, while those from the horizontal sections reinforce and form an array of 9 small horizontal dipole antenna sources, with the spacing of 20 mm. These sources will have a radiated field polarized in the E_ϕ direction. Measured gain was -11.7 dBi. Loss of 0.3 dB for the balun was included. Cross polarization is lower than -6.8 dB.

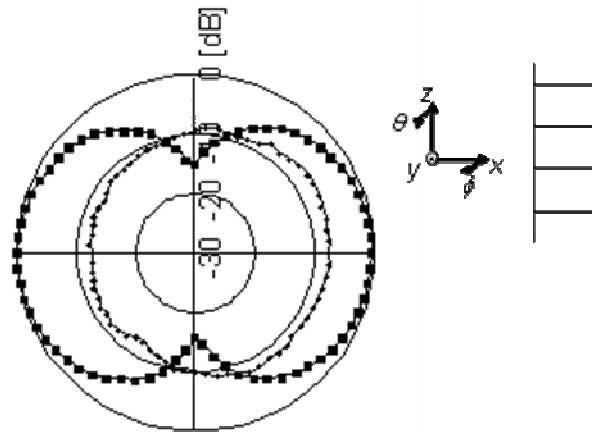


Figure 3-22. Measured radiation pattern of the printed meandered left-handed dipole antenna in the xy plane at 643 MHz, $n = -9$. (\bullet : E_θ , \blacksquare : E_ϕ). [23]

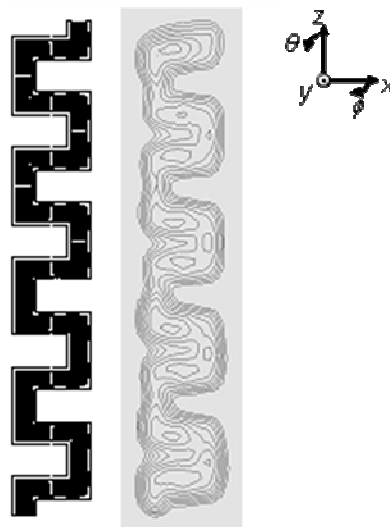


Figure 3-23. Near field distribution of the simulation model at 674 MHz, $n = -9$. The fields are normalized by the maximum value and are represented in the range from 0 dB to -12 dB with the step of 1.5 dB. [12]

A printed meandered right-handed dipole antenna was constructed for comparison. The right-handed dipole had the same dimensions as the meander line of the left-handed one,

along the centre of the ladder network and operates in an $n = +1$ mode. The standing wave in this case has only one peak, in the middle of the dipole. Thus, the currents induced on line sections along the x and z directions become out-of-phase and in-phase, respectively, which is opposite to the left-handed dipole. This right-handed dipole had a resonant frequency of 484 MHz and a dominant polarization in the E_θ (or vertical direction) direction. It is clear that if this dipole was shortened to operate at 643 MHz, it would also have its dominant polarization in the E_θ direction. This comparison confirmed that the meandered left-handed dipole antenna has orthogonal polarization to an equivalent right-handed one.

3.3 Dipole Antennas with Left Handed Loading

Based on previous left handed conceptual model (Figure 3-5), a short dipole antenna loaded with lumped elements is developed and implemented in our lab. Information about antenna measurement is introduced in Appendix D.

3.3.1 Short Dipole with Lumped Elements

3.3.1.1 Model

In this project, simulation work plays an essential role regarding the evaluation the antenna behaviour and characteristics. The main commercial software tool employed in this work is CST Microwave Studio[®], which is the product of CST-Computer Simulation Technology [24]. The software package will be introduced in Appendix C, as well as the fundamental theory behind them.

The performance of the left handed dipole antenna is investigated numerically using the commercial simulator CST. A model including loss is created in CST as shown in Figure 3-24. Conductivity of $5.8e7$ S/m for copper forms the parallel line and interconnecting wires. Lumped elements are assumed with loss resistors as indicated in the manufacturers datasheets.

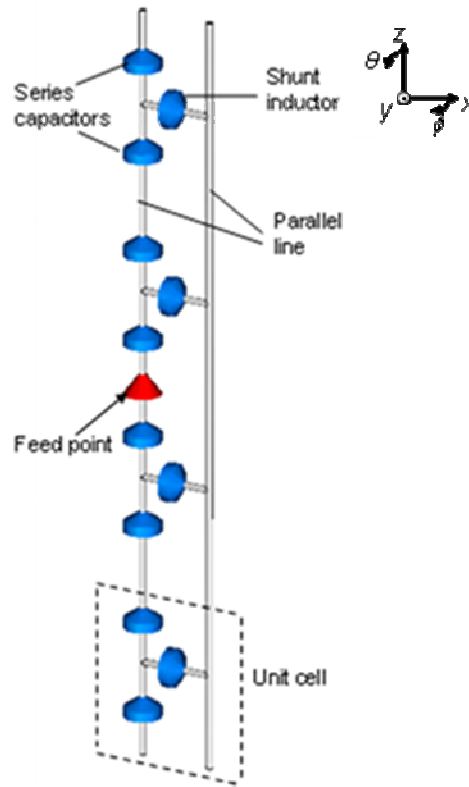


Figure 3-24. Simulation model of the left handed dipole in CST.

In the left handed dipole model, values of series capacitors C_L and shunt inductors L_L for left handed components decide the resonant frequency and input impedance. Based on equation (2.14-2.16) introduced in chapter II, the following dispersion relation β [25] is applied for the design.

$$\beta = \frac{1}{a} \cos^{-1} \left\{ 1 - \frac{1}{2} \left[\frac{1}{\omega^2 L_L C_L} + \omega^2 L_R C_R - \left(\frac{L_R}{L_L} + \frac{C_R}{C_L} \right) \right] \right\} \quad (3.13)$$

where ω is angular frequency. C_R and L_R are inherent capacitance and inductance of a parallel line per section length of a . Since the antenna is composed of a parallel wire, there are unavoidable parasitic right handed components of series inductors L_R and shunt

capacitors C_R . C_R and L_R values per section length a for a parallel wire can be calculated using following equations [26], in which d is the distance between two wires.

$$L_R = \frac{\mu}{\pi} \cdot \ln[(d/2a) + \sqrt{(d/2a)^2 - 1}] \quad (3.14)$$

$$C_R = \frac{\pi\epsilon}{\ln[(d/2a) + \sqrt{(d/2a)^2 - 1}]} \quad (3.15)$$

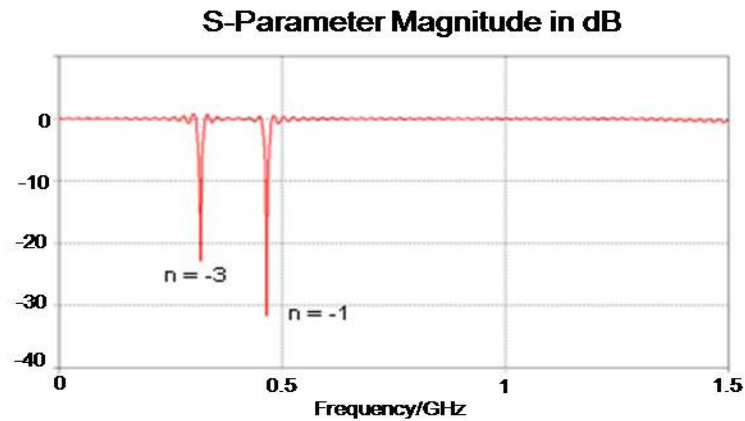
Based on equations (3.13-3.15), the parameters of the simulation model, shown in Table 3-2, were specified so that the antenna would have a length of 100 mm, which is 0.16 times free-space wavelengths, λ_0 , at 466 MHz, and have an 50 Ω impedance.

Table 3-2 Parameters of the Simulation model.

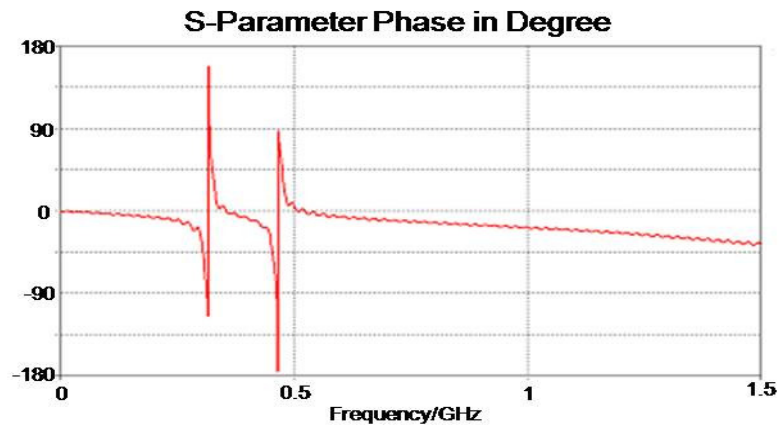
Length L of antenna	100 mm
Length a of unit cell	25 mm
Distance d of wires	10 mm
Radius r of wire	0.44 mm
Number N of unit cells	4
Capacitance of C_L	0.85 pF
Inductance of L_L	100 nH
Length of LC elements	1 mm

Reflection characteristics are shown in Figure 3-25(a), (b). Two resonance for $n = -1$ and $n = -3$ was observed in the amplitude characteristic with respect to 50 Ω in Figure 3-25(a). An input impedance with a real part close to 50 Ω was achieved at $n = -1$ by the values of

L_L and C_L , specified in Table 3-2. Bandwidth of $|S_{11}| < -10$ dB is 1.2 %. Three resonances were observed in phase characteristic in Figure 3-25 (b). In the case of $n = -2$, no resonance of $|S_{11}|$ was observed due to mismatching at the feed point.



(a)



(b)

Figure 3-25. Reflection characteristics of the conceptual left-handed dipole antenna. (a) Amplitude with respect to 50Ω and (b) phase.

Figure 3-26 shows the simulated radiation pattern in the yz planes at 466 MHz for $n = -1$. A figure of 8 radiation pattern was obtained for E_θ . Cross polarization, E_ϕ caused by currents

on the cross wires along the x axis, is -15.5 dB. The radiation efficiency is 23% at 466 MHz.

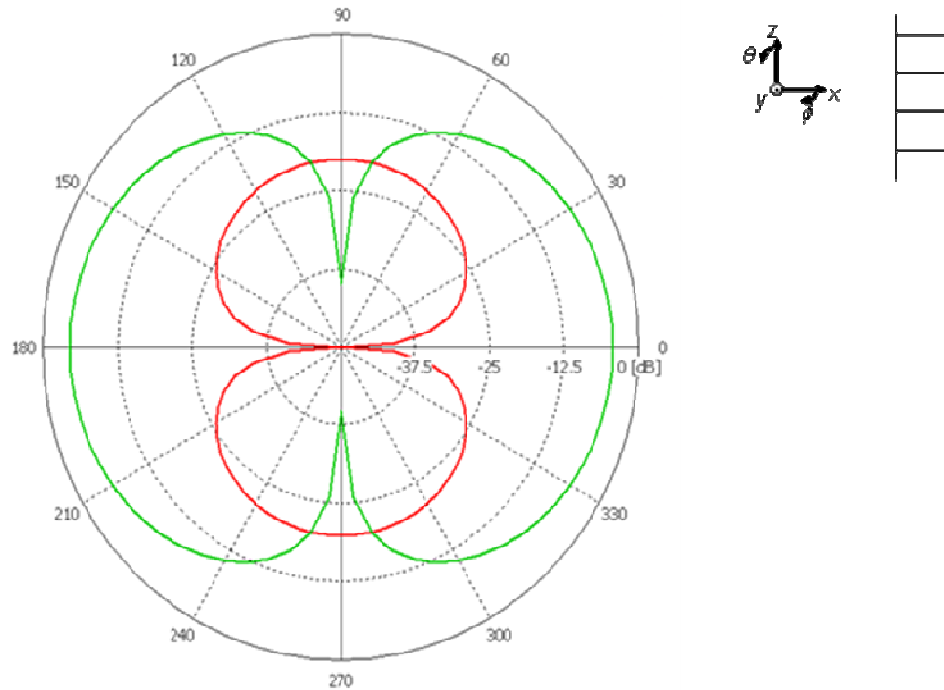


Figure 3-26. Simulated radiation pattern of left-handed dipole. (yz plane, freq.=466MHz, $n = -1$, Green line: E_θ , Red line: E_ϕ . Dipole details as Table 3-2.)

3.3.1.2 Implementation

The printed left handed dipole antenna loaded with lumped elements is shown in Figure 3-27. The antenna was implemented on FR4 substrate with the thickness of 0.8 mm and permittivity of 4.4. The parameters of the antenna are the same as Table 3-2 except that the values of loaded lumped elements are adjusted to $L_L = 140$ nH and $C_L = 0.45$ pF for obtaining good input impedance. A T-junction balun is used to feed the dipole and its configuration is the same as Figure 3-16.

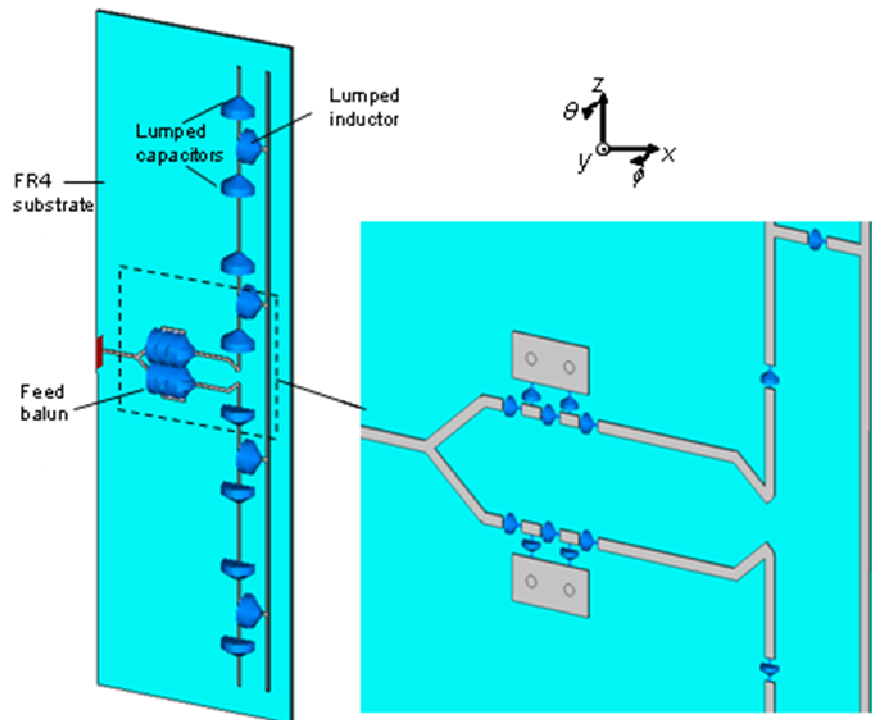


Figure 3-27. Configuration of a lumped left-handed dipole.

The prototype of the lumped left-handed antenna is designed and constructed for measurements as shown in Figure 3-28.

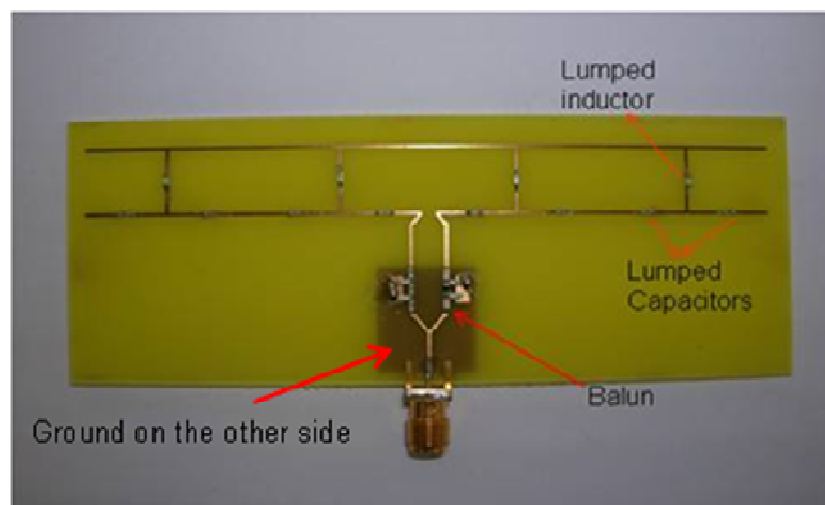


Figure 3-28. The prototype of the lumped left-handed antenna.

Simulated and measured reflection characteristics of the lumped left-handed antenna with a T-junction balun are compared in Figure 3-29. Two resonances were found at 473 MHz for $n = -1$ and 363 MHz for $n = -3$ from simulation. From measured result, the resonances were observed at 526 MHz and there was 53 MHz frequencies shift of 10% for $n = -1$. For the $n = -3$ mode the measured resonance was achieved at 408 MHz and there was 45 MHz frequencies shift of 11%. It is believed that the manufacturing tolerances (about 0.01 mm) and fabrication difficulties lead to these differences. It is also observed that there are two other dips in the reflection coefficient amplitudes, and they are due to the limited frequency bandwidth of the balun.

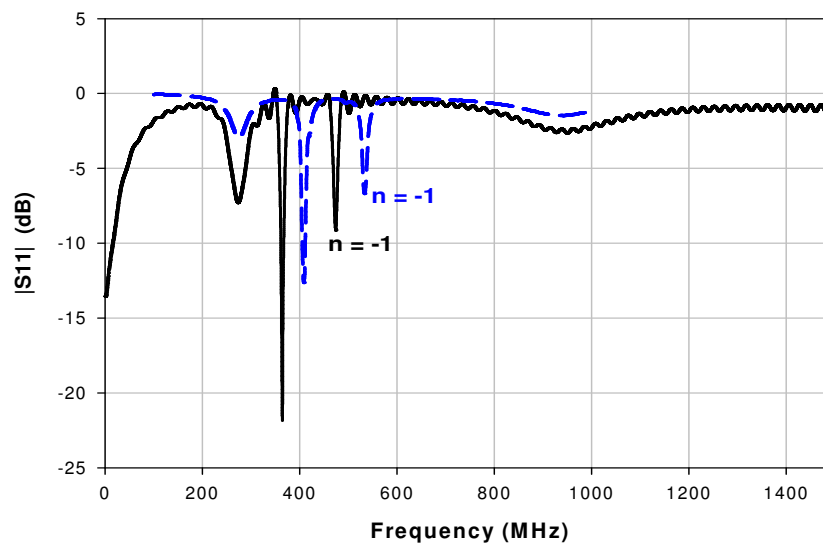


Figure 3-29. Reflection characteristics of lumped left-handed dipole antenna through balun. (Simulation: solid line, Measurement: dot line)

The simulated radiation pattern in the yz plane at 473 MHz is displayed at Figure 3-30, and compared with the measured one at 526 MHz as shown in Figure 3-31. The measured pattern gives bigger cross polarization due to the radiation and scattering from the balun

and cables feeding the dipole. The simulated efficiency is 16% at 473 MHz and simulated gain is -5 dBi. The measured gain at 526 MHz was -4 dBi, inclusive of the loss of 0.4 dB of the balun.

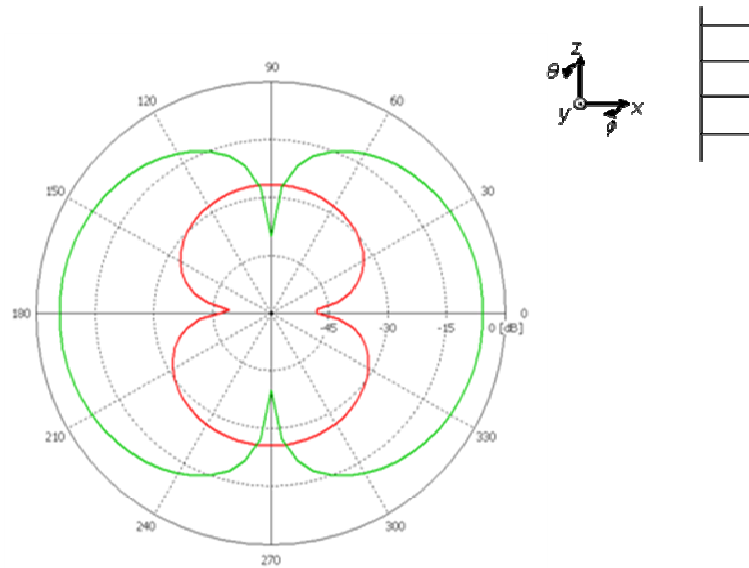


Figure 3-30. Simulated radiation pattern of lumped left-handed dipole antenna in yz plane at 473 MHz, $n = -1$. (green line: E_θ , red line: E_ϕ)

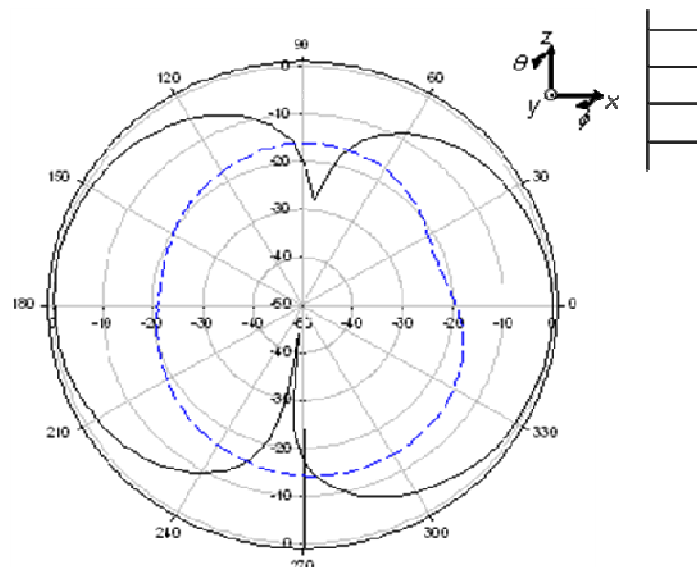


Figure 3-31. Measured radiation pattern of lumped left-handed dipole antenna in yz plane at 526 MHz, $n = -1$. (Solid line: E_θ , Dot line: E_ϕ)

3.3.2 Meandered Left Handed Dipoles

The antenna with a left-handed transmission line has a unique property that the wavelength of the induced current becomes shorter with decreasing frequency. One important feature of this left handed behaviour is that at higher mode numbers, the antenna becomes electrically smaller and hence has a well controlled radiation pattern. In a right handed antenna, higher order modes produce patterns with nulls in them due to their large electrical size. The left handed behaviour has applied to build an orthogonally polarized dipole antenna [23]. A dipole loaded with left-handed transmission line using a meandered configuration, with a higher mode current distribution, can give polarisation orthogonal to the dipole length.

The high mode number, at which a meandered dipole can give orthogonal polarisation, depends on the number of unit cells. The effect of cell number on polarization is analysed for clarifying the minimum cell number since more unit cells cause more loss and complicated structure.

3.3.2.1 Effect of Cell Number on Polarization

a. Analysis

Horizontal polarization is tailored through meandering the arms of the dipole. As shown in Figure 3-32(b), the current distribution of the straight dipole is parallel with its orientation, so it gives co-polarization. However, in Figure 3-32(a), the meander is arranged so that the peaks of the current standing wave occur on the horizontal sections of the meander, thus the radiated polarization is horizontal.

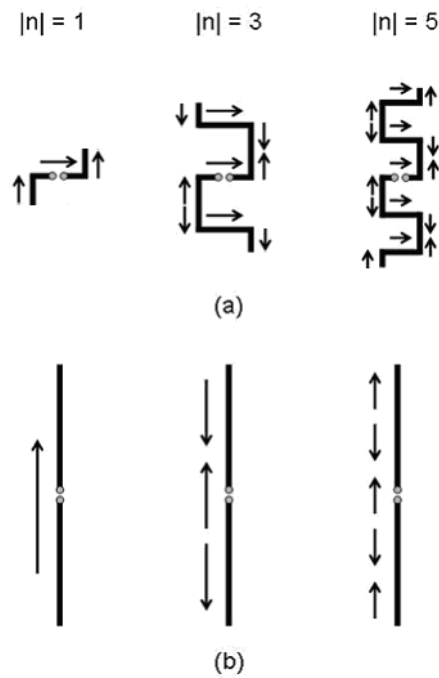


Figure 3-32 Principle of horizontal polarization. (a) Meandered left-handed current distribution. (b) Straight left-handed current distribution.

Also in Figure 3-32 (a), the direction of maximum radiation power moves as N ($|n|$) increases because of the inclined total radiation source. Here N is the number of unit cells and n is the number of the mode. In case of $N = 2$ ($n = -1$), it is clearly an inclined dipole with two orthogonal radiation source; In case of $N = 6$ ($n = -3$), the radiation source in horizontal direction becomes larger, so the inclination is relatively smaller. As N ($|n|$) increases, the horizontal radiation becomes much larger than the vertical radiation. So the direction of maximum radiation power will incline towards orthogonal direction with the orientation of the dipole.

b. Simulations

It has been shown above that the meandered left-handed dipoles give tilted radiation patterns. However, the minimum mode number $|n|$, in which the dipole gives cross

polarization, is still not clear. The effect of unit cell number on polarization of the meandered left-handed dipole will be studied numerically by simulations in CST. With cell number N from 2 to 18, the simulations models of meandered left-handed dipoles for mode number n from -1 to -9 have been shown in Figure 3-33. The parameters for each unit cell have been listed in Table 3-3.

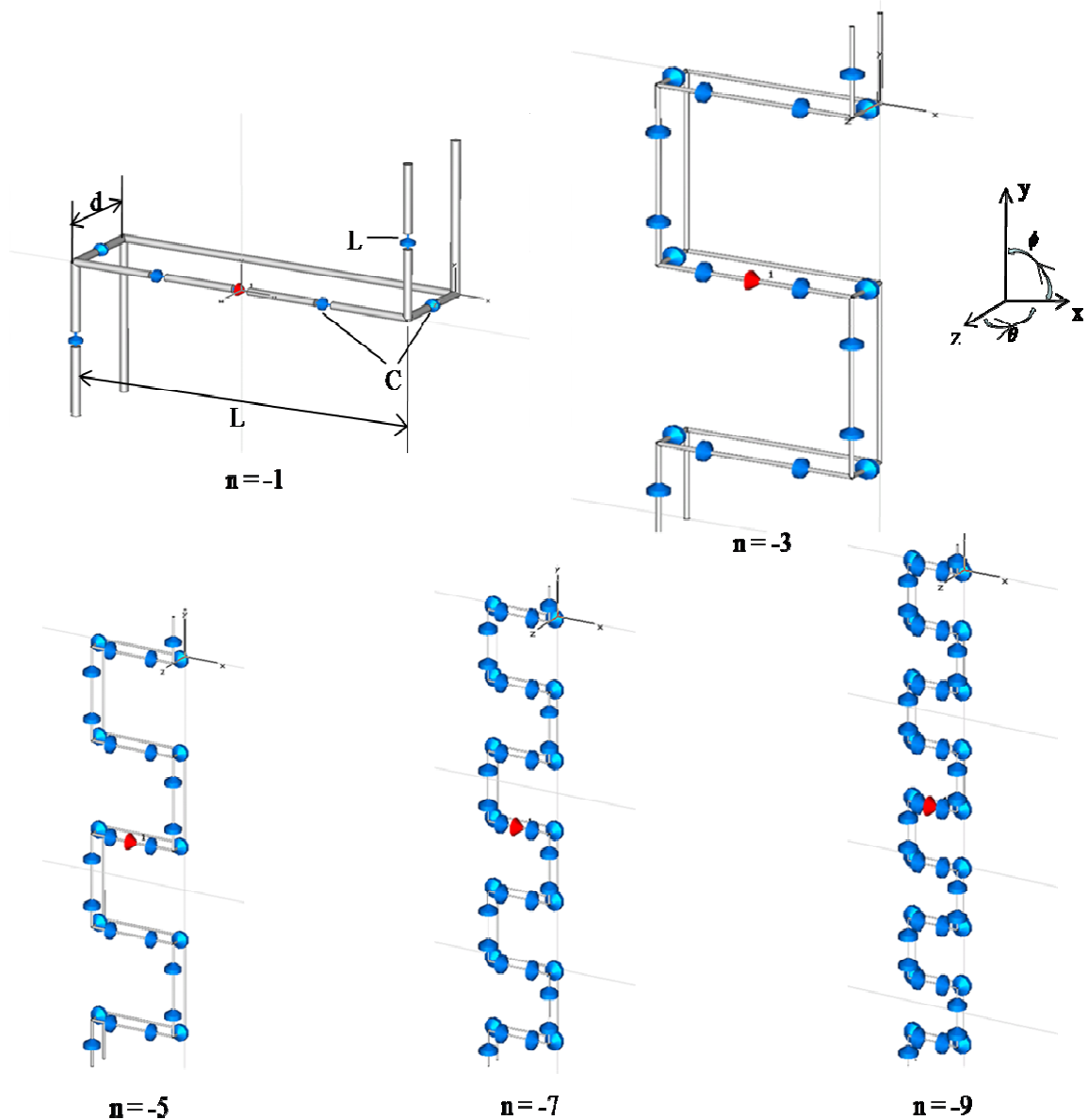


Figure 3-33. Simulation models of meandered left handed dipoles (n from -1 to -9).

Table 3-3 Parameters for unit cell of meandered dipoles.

Wire radius	0.25mm
Elements length	1mm
Distance between wires (d)	5mm
Length of cell (L)	20mm
Capacitance (C)	0.7pF
Inductance (L)	95nH

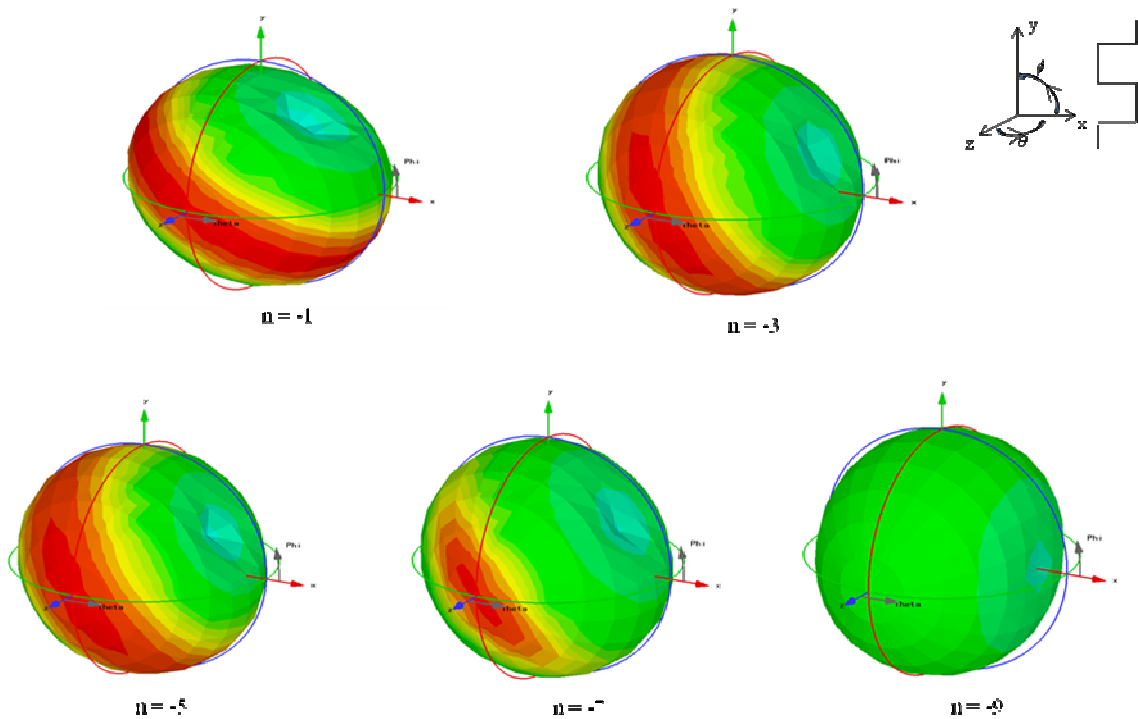
Figure 3-34 Farfield patterns of meandered left handed dipoles (n from -1 to -9).

Figure 3-34 shows the farfield radiation patterns for each simulation model. The meandered dipoles are placed along y axis (vertical direction) as shown in coordinate

system. They all give tilted patterns, which incline towards orthogonal direction with the orientation of dipoles as $|n|$ increases.

Table 3-4 Simulation performance of meandered left-handed dipoles.

Cell number (N)	2	6	10	14	18
Mode number (n)	-1	-3	-5	-7	-9
Resonance freq. (MHz)	425	443	410	433	397
Radiation efficiency (%)	32.3	10.6	7.8	13.1	0.9
Directivity in theta (dBi)	1.3	1.1	1	-0.6	-1.7
Directivity in phi (dBi)	2.3	1.7	1.7	0.1	-2

The simulation results are summarized in Table 3-4. As $|n|$ increases, the radiation efficiency decreases in relative resonance frequency. Although the directivities for theta component and ϕ component all decrease as efficiency reduces, the total cross-polarization increases. There is a trade-off between cross polarization and efficiency for meandered left handed dipoles. When $|n|$ increases to 9, the maximum directivity power for theta component (horizontal polarization part) becomes larger than that for phi component (vertical polarization part). So the main part of the farfield pattern is cross-polarized. The meandered dipole antenna is polarized orthogonal to its length in $n = -9$.

3.3.2.2 3D Meandered Left Handed Dipole

Other meandered structures of left handed dipoles have also been designed to study their special properties. A vertical oriented left handed dipole extending toward horizontal direction in 3D space will be presented, and it also can give an orthogonal polarization.

a. Configuration

The fundamental structure of the ladder network is the same as the straight left handed dipole antenna in Figure 3-5. The new configuration is composed of unit cells with a shunt inductor L and two series capacitors C , having a ladder network periodic structure of any number of cells with a meander arrangement. The dipole starts with vertical orientation, and then the meander parts extend towards z direction in 45 degrees. The configuration is shown in Figure 3-35, in which $N = 8$.

Similarly to the previous printed meandered dipole, the meander is arranged so that the peaks of the current standing wave occur on the horizontal sections of the meander, thus the radiated polarization is horizontal.

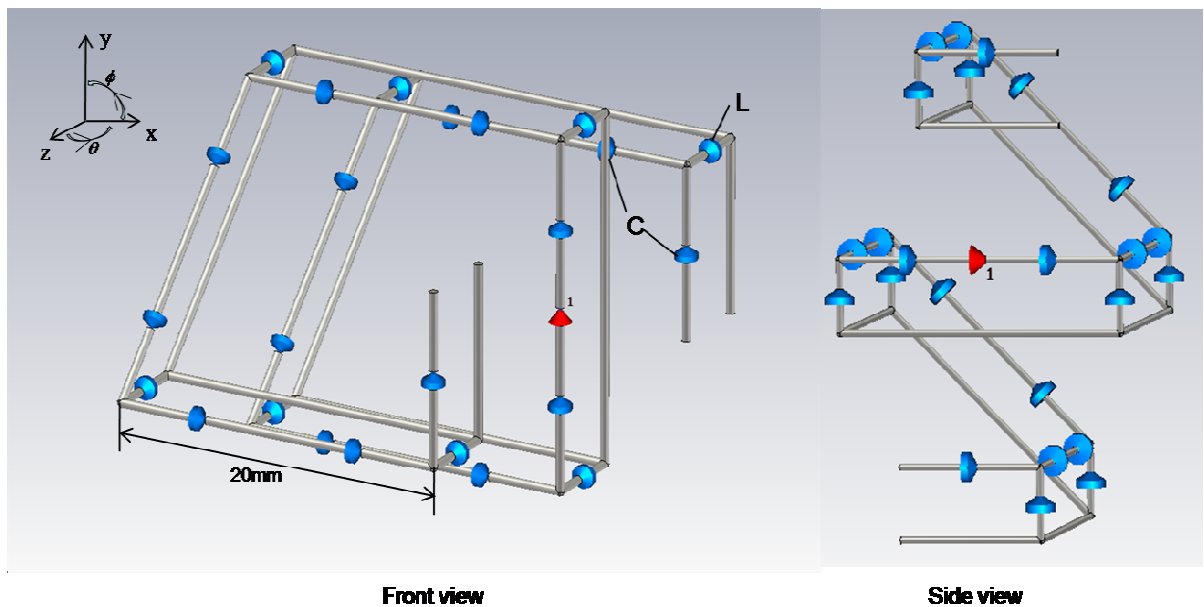


Figure 3-35. Configuration of 3D meandered left handed dipole.

b. Simulation Results

Simulated reflection characteristic of the 3D meandered dipole is shown in Figure 3-36. Lots of resonances are found due to the high number of unit cells, and the antenna is matched at frequency 560 MHz.

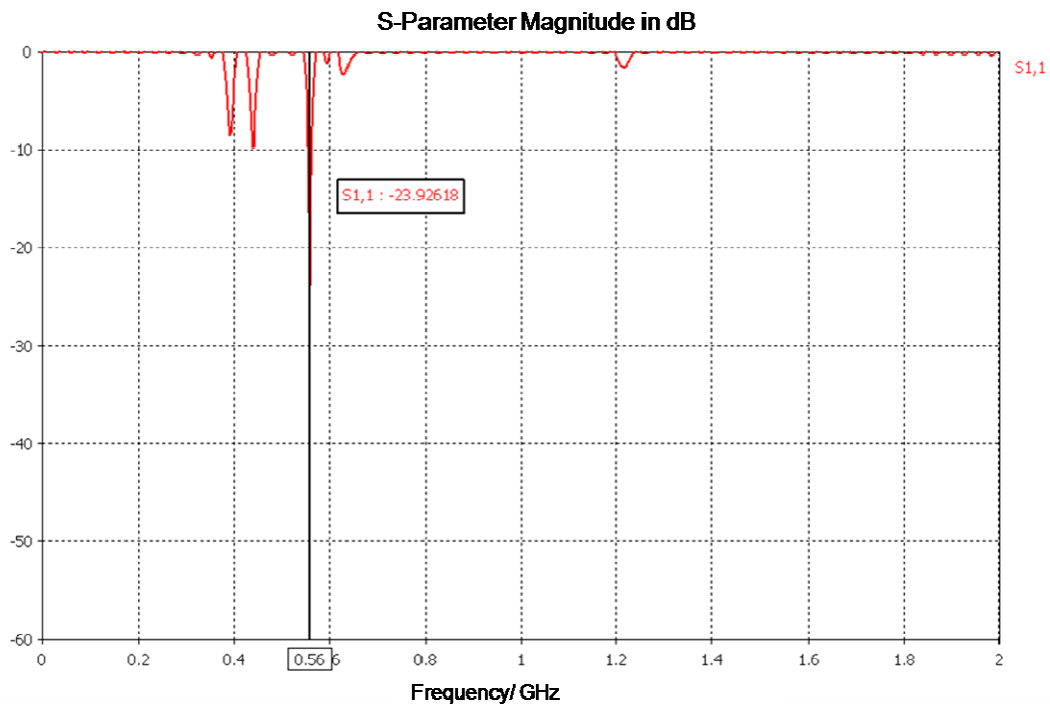


Figure 3-36. Reflection characteristic of the 3D meandered dipole.

The central meandered dipoles are placed along y axis (vertical direction) as shown in coordinate system. The farfield radiation patterns for theta and phi components are shown in Figure 3-37. The maximum gain is 0.02 dBi for theta component (horizontal polarization part) and is 0.01 dBi for phi component (vertical polarization part). So it can be concluded that the main part of the farfield pattern of the 3D meandered dipole is cross-polarized. Compared with 2D meandered dipoles (Figure 3-19), the 3D meandered dipole

can give orthogonal polarization with less number of unit cells and smaller size. 3D structure extends the design degrees of freedom for left handed meandered dipole antennas.

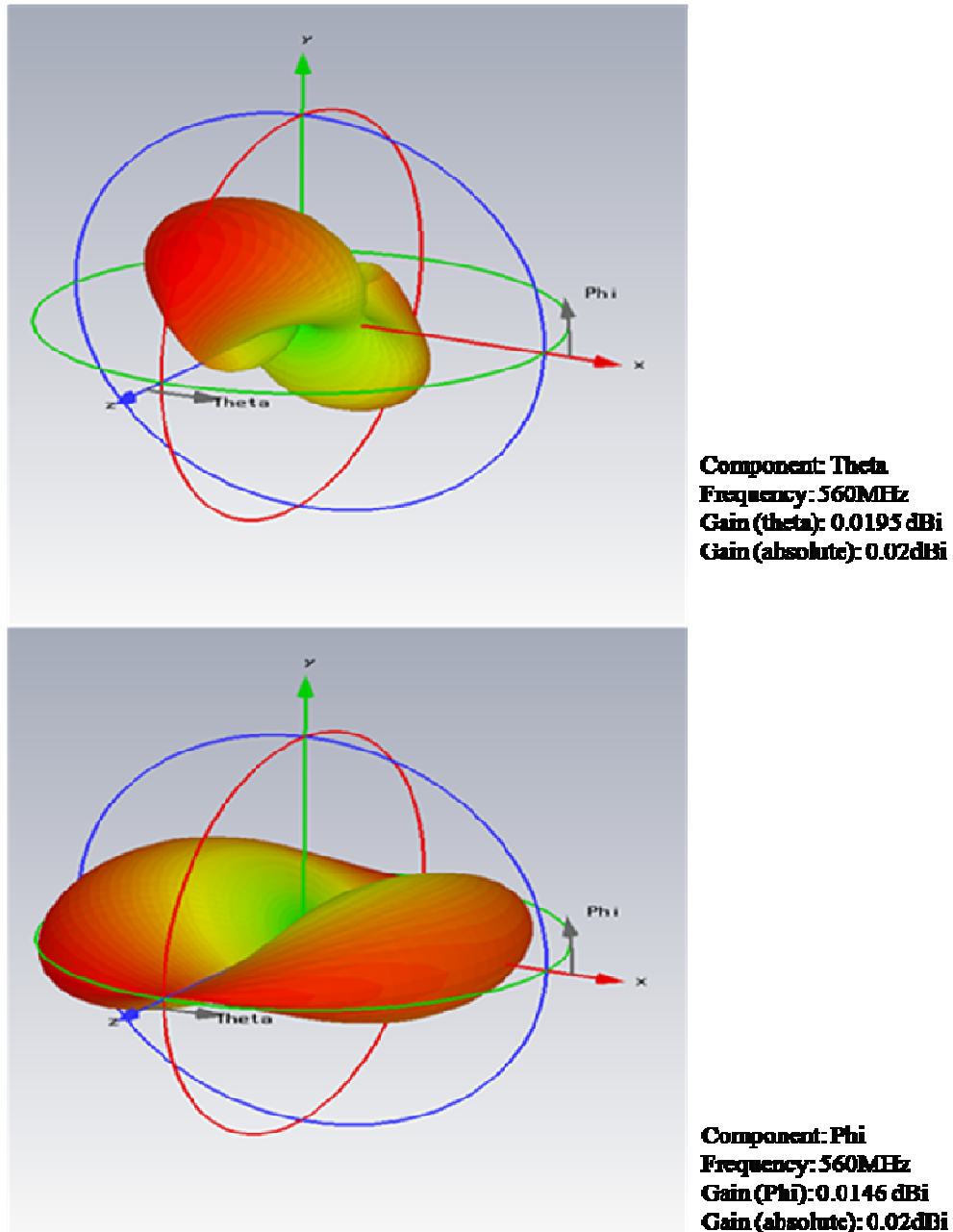


Figure 3-37 Farfield performance of the 3D meandered dipole.

3.4 Summary

The dipole antenna consisting of left handed transmission lines has been proposed. Analysis has shown that the relationship between the wavelength λ_a of induced current and the frequency is opposite to that of a conventional dipole of right-handed material, in that decreased frequency results in smaller wavelength.

The antenna has been implemented by both lumped and distributed elements. With lumped elements, the dipole antenna of length $0.16 \lambda_0$ gave an efficiency of 16%. For the distributed implementation, the efficiency was 27% and measured gain of the antenna with balun was -3.9 dBi in an $n = -1$ mode. It was experimentally confirmed that the proposed antenna structure contributed to the reduction of the antenna size. Loss remains a problem in left-handed dipoles. The establishment of low loss designs for loaded inductors and capacitors is an important further study.

A left handed dipole using a 2D meandered configuration, with a higher mode current distribution, can give polarisation orthogonal to the dipole length. A printed meandered left-handed dipole antenna working in an $n = -9$ mode is presented. It was experimentally confirmed that this antenna structure produces orthogonal polarization compared to an equivalent right-handed one. But the loss of meander inductors and interdigital capacitors, degrades the efficiency of the antennas, and the cross polarization is also high. It is clear that the efficiency is rather low and not sufficient for practical use.

Variations of the meandering allow choice of radiated polarization to be made. A 3D meandered structure of the left handed dipole has also been studied. The 3D meandered

dipole can give orthogonal polarization with less number of unit cells and smaller size, which extends the design degrees of freedom for meandered dipole antennas.

It can be found that the poor efficiency remains the main problem for left handed dipole antennas. A study of the efficiency of electrically small dipole antennas loaded with left-handed transmission lines is to be introduced in next chapter.

References

- [1] C. Caloz and T. Itoh, "Application of the transmission line theory of left-handed (LH) materials to the realization of a microstrip 'LH line'," *IEEE Antennas and Propagation Society International Symposium*, vol. 2, pp. 412-415, 2002.
- [2] G. V. Eleftheriades, O. Siddiqui, and A. K. Iyer, "Transmission line models for negative refractive index media and associated implementations without excess resonators," *IEEE Microwave Wireless Compon. Lett.*, vol. 13, pp. 51-53, Feb. 2003.
- [3] C. Caloz, H. Okabe, T. Iwai, and T. Itoh, "Transmission line approach of left-handed (LH) materials," presented at Proc. USNC/URSI National Radio Science Meeting, San Antonio, TX, June 2002.
- [4] C. Caloz and T. Itoh, "Novel microwave devices and structures based on the transmission line approach of meta-materials," presented at IEEE MTT-S Int. Symp., Philadelphia, PA, June 2003.
- [5] A. Lai, C. Caloz, and T. Itoh, "Composite Right/Left-Handed Transmission Line Metamaterials," *IEEE Microwave Magazine*, Sep. 2004.
- [6] A. Sanada, C. Caloz, and T. Itoh, "Planar distributed structures with negative refractive properties," *IEEE Trans. Microwave Theory Tech.*, vol. 52, pp. 1252–1263, Apr. 2004.
- [7] I. Lin, C. Caloz, and T. Itoh, "A branch-line coupler with two arbitrary operating frequencies using left-handed transmission lines," presented at IEEE-MTT Int. Symp. Dig., Philadelphia, PA, 2003.
- [8] A. Sanada, C. Caloz, and T. Itoh, "Zeroth order resonance in composite right/left-handed transmission line resonators," presented at Proc. Asia-Pacific Microwave Conf., Seoul, Korea, 2003.

- [9] L. Liu, C. Caloz, and T. Itoh, "Dominant mode (DM) leaky-wave antenna with backfire-to-endfire scanning capability," *Electron. Lett.*, vol. 38, pp. 1414–1416, 2000.
- [10] H. Iizuka and P. S. Hall, "A left-handed dipole concept," presented at Proc. Int. Workshop on Antenna Tech., New York, USA, Mar. 2006.
- [11] H. Iizuka, P. S. Hall, and A. L. Borja, "Dipole Antenna With Left-Handed Loading," *IEEE Antennas and Wireless Propag. Lett.*, vol. 5, pp. 483-485, Dec. 2006.
- [12] H. Iizuka and P. S. Hall, "Left handed dipole antennas and their implementations," *Trans. Antennas Propag.*, vol. 55, pp. 1246 -1253, May 2007.
- [13] H. R. Hertz, *Electric Waves*. London: Macmillan, 1893; Dover, 1962, This book is a collection of Hertz's papers during the years 1887 to 1891.
- [14] F. R. Terman, *Electronic Radio and Engineering*: McGraw-Hill Education, 1955.
- [15] S. J. Orfanidis, *Electromagnetic Waves and Antennas*, 2008.
- [16] W. Panofsky and M. Phillips, *Classical Electricity and Magnetism*: Addison-Wesley.
- [17] R. P. Feynman, *The Feynman lectures on physics / Feynman, Leighton, Sands*: Addison-Wesley, 1989.
- [18] J. Morin, J. Shea, and P. Lappen, *ARRL's Wire Antenna Classics - A collection of the best articles from ARRL publications*, vol. 1, First ed: The American Radio Relay League, Inc., 2005.
- [19] J. Z. Buchwald, "Reflections on Hertz and the Hertzian Dipole," *MIT and the Dibner Institute for the History of Science and Technology*, 2007.
- [20] J. Sevick, *Building and Using Baluns and Ununs: Practical Designs for the Experimenter*: Cq Communications, 1994.

-
- [21] *FEKO user manual, Suite 5.0, EM Software & System - S.A(pty) Ltd.* South Africa: Stellenbosch, 2005.
- [22] H. Iizuka and T. Watanabe, "Balanced Line to Unbalanced Line Transformer," *Japan Japanese patent 2005-198167*, Jan. 9, 2004.
- [23] H. Iizuka and P. S. Hall, "Orthogonally polarized dipole antenna using left handed transmission lines," presented at Proc. 36th Euro. Microwave Conf., Manchester, U.K., Sep. 10–15, 2006.
- [24] "CST Microwave Studio Tutorials," *Computer Simulation Technology*, www.cst.de, vol. Version 4, July 2002.
- [25] C. Caloz and T. Itoh, *Electromagnetic metamaterials: Transmission line theory and microwave applications*. NJ: Wiley-Interscience, 2006.
- [26] F. T. ULABY, *Fundamentals of Applied Electromagnetics*, Fifth ed: The University of Michigan, 1994.

CHAPTER IV EFFICIENCY OF ELECTRICALLY SMALL PERIODICALLY LOADED DIPOLE ANTENNAS

In 1967 Veselago proposed the theoretical investigation of left-handed material simultaneously exhibiting negative permittivity and permeability [13]. During the past forty years, left-handed metamaterials made by inserting periodic inclusions [10, 11, 13-15] with dimensions smaller than the guided wavelength, have attracted considerable attention in view of minimize antenna size [14, 16-23], which may lead to the development of new applications. Transmission lines loaded with reactive components that have left handed wave behavior have been applied to conventional dipoles design [24-27]. This left handed dipole has a unique feature that the wavelength of the induced current becomes shorter with decreasing frequency. Also increasing mode number occurs at decreasing frequency and the mode number n in the left handed region is defined by negative numbers. Dipoles loaded with left-handed transmission lines allow operation with higher order mode current distributions and small size [20], whereas a conventional dipole operating in a higher order mode is usually larger than a wavelength. Use in a meandered configuration, with a higher mode current distribution, left handed loading can give polarization orthogonal to the dipole length [26].

Two main features of dipoles with left-handed loading have been demonstrated above, namely size reduction and orthogonal polarized radiation in a higher order mode. In both of these, efficiency is a key parameter as the heavy loading increases the resistive loss, and it is important particularly in the case of size reduction to compare with conventionally loaded dipoles. In this section, an efficiency study is described of straight or meandered dipoles loaded with left-handed transmission line, and the comparison with right handed

loaded dipoles. In addition two types of optimized left handed dipoles with optimized efficiency are presented.

4.1 Dipole Antennas with Lumped Loading

The configuration of the dipole antenna with left-handed loading is shown in Figure 4-1. A dipole with periodic inductive loading, used as a comparison, is shown in Figure 4-2. The resonance frequency and the input impedance are controlled by the loading, independent of the length of the antenna [25]. The mode number n is based on the conventional resonant mode numbering. In the antenna with left-handed loading, increasing mode number occurs at decreasing frequency [20, 24]. The number, n , of resonances depends on the number of unit cells N . For example, in an antenna with $N = 4$, the resonance numbering is $n = -3, -2, -1$ in the range of frequency in the left handed region or $n = 1, 2, 3$ for the inductively loaded dipole, Figure 4-2, in the right handed frequency region. L-loading, straight CL-loading and meandered CL-loading dipoles will be compared in the next part for their impedance and efficiency properties with the same size reduction ratio.

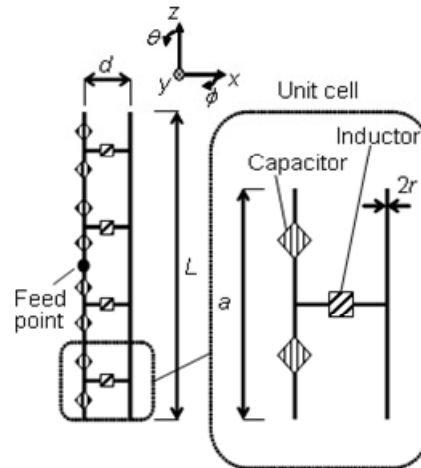
For size reduction, operation in a low mode number such as $n = -1$ would seem to be best efficiency, but the best number of unit cell is not clear. Simulated efficiency will be compared for two size reduction ratios and for various numbers of cells between left handed and right handed dipoles. Meandered left handed dipole will be compared with straight left handed dipole and right handed dipole in a high mode.

4.1.1 Configuration

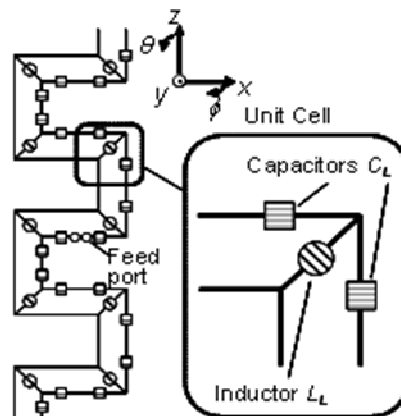
4.1.1.1 Dipole with Left Handed Loading

The antenna has a ladder network periodic structure which is shown in Figure 4-1. The unit

cell has a shunt inductor and two series capacitors which operate as a left-handed transmission line, L is the length of antenna, a is unit cell length, d is distance between the two wires, r is wire radius which is 0.3mm, and N is number of unit cells. N is equal to 4 in Figure 4-1 (a) and is 10 in Figure 4-1 (b).



(a)



(b)

Figure 4-1. Configuration of the loaded left handed dipole antenna.

(a) straight (b) meandered [24, 26]

4.1.1.2 Dipole with Periodic Inductive Loading

The configuration of the inductively loaded dipole is shown in Figure 4-2, in which $N = 4$.

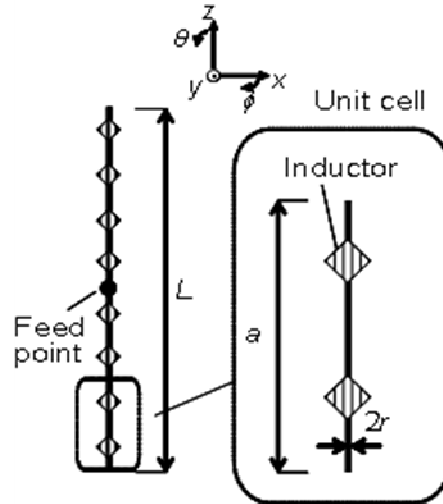


Figure 4-2. Configuration of the loaded right handed dipole antenna.

4.1.2 Simulation Performance

The performance of the antenna in free space is investigated numerically using the commercial simulator "CST" [28]. The antenna radiation efficiency is defined as the ratio of gain to directivity or equally the ratio between the radiated to input power of the antenna. Conductivity for copper wires is 5.8×10^7 S/m and lumped elements are assumed with loss resistors as indicated in the manufacturer's datasheets, [29], (Johanson Technology).

4.1.2.1 Performance for Size Reduction Dipoles in $|n| = 1$ Mode

At two size reduction ratios $0.18 \lambda_0$ and $0.07 \lambda_0$, where λ_0 is free space wavelength, the inductively loaded dipole has been compared to the left handed loaded dipoles operating in the $n = -1$ mode. Simulated efficiency has been compared for two size reduction ratios and

for various numbers of cells among straight L-loading, straight CL-loading and meandered CL-loading dipoles.

a. Performance for 4 Unit Cell Periodically Loaded Dipoles with $|n|=1$

The values of the loading inductors and capacitors are chosen to all achieve an $|n|=1$ resonance at a frequency around 530 MHz. For the straight antennas the length is set close to 100 mm, which is $0.18 \lambda_0$ and $kr = 0.55$ where r is the radius of the radian sphere. For the meandered case the length of 88 mm and width of 44 mm also give $kr = 0.55$. Simulated performance with $N = 4$ are listed in Table 4-1. For all the simulation models, the wire radius r is 0.3 mm, and the distance between the two wires, d , for straight or meandered left handed models is 10 mm.

Table 4-1: Simulated performance of 4 cell loaded dipole antennas with $|n|=1$, $kr = 0.55$ ($0.18 \lambda_0$).

Dipole configuration	Antenna length L (mm)	Cap. (pF)	Induc. (nH)	Freq. (MHz) at $ n =1$	Input Imp. (Ω)	Rad. Effic. (%)	Gain (dBi)
StraightL	100		40	531	18.6	68.5	0.1
Straight CL	100	0.5	120	527	72.6	48.4	-1.4
Meandered CL	Length 88 Width 44	0.5	55	524	78	66.2	-0.3

In the case of the straight antennas, the efficiency reduced from 68.5% to 48.4% for CL loading. This is assumed to be due to resistive loss in the extra components. The efficiency is increased to 66.2% when the CL loaded dipole is meandered. It is believed the improved

radiation factor in the meandered dipole is because currents are in phase on horizontal sections [26]. The gains can be compared to 1.5 dBi obtained from Harrington's equation (4.2) for the maximum gain.

It is extremely hard, in a small dipole with conventional inductive loading to get matching at 50Ω . This difficulty leads to various techniques in which the antenna is fed some way down its length [4], where a more suitable impedance can be found. These techniques are not needed in left handed loaded antennas. Left handed loading shows greater degrees of freedom than conventional type to achieve a desired impedance at the terminals.

The simulations are repeated for smaller dipole antenna size, $kr = 0.22$. The antenna frequency is around 535 MHz and length 40 mm, $0.07 \lambda_0$. The simulation parameters and results are shown in Table 4-2.

Table 4-2: Simulated performance of 4 cell loaded dipole antennas with $|n|=1$, $kr = 0.22$ ($0.07 \lambda_0$).

Dipole configuration	Antenna length L (mm)	Cap. (pF)	Induc. (nH)	Freq. (MHz) at $ n =1$	Input Imp. (Ω)	Rad. Effic. (%)	Gain (dBi)
Straight L	40		56	536	14.8	17.4	-6
Straight CL	40	0.35	180	537	26.8	6.7	-10.2
Meandered CL	length 35.2 width 17.6	0.3	85	534	40	4.4	-12.1

It can be seen that for antenna size of $0.07 \lambda_0$ and $kr = 0.22$, the impedance of the inductively loaded dipole is 14.8Ω comparing with straight CL-loading and meandered CL-loading of 26.8Ω and 40Ω respectively. Again the left handed dipoles have a better impedance at the expense of efficiency. The efficiency and gain are all very low as expected from the Harrington-Chu limits. However for this smaller antenna size, the meandered is no better than the straight dipole and both left handed antennas have significantly lower efficiency than conventional loading. The gains can be compared to -3 dBi for the maximum obtainable gain from equation (4.1).

In order to examine the efficiency of these left handed antennas and compare them to conventional ones, the gain of the antennas of two sizes are plotted together with the Harrington limit in Figure 4-3. It can be seen that left handed loading does reduce the efficiency compared to the inductive loading.

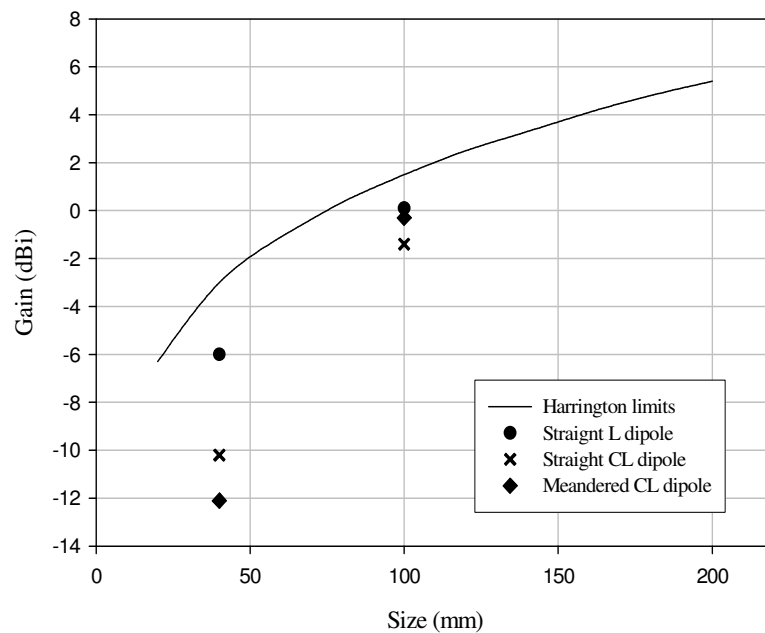


Figure 4-3. Gain vs. size of dipole antennas.

b. Efficiency of Periodically Loaded Dipoles for Various Numbers of Cells in the $|n|=1$ Mode

For size reduction, efficiency is a key parameter as the heavy loading increase the resistive loss. For efficiency, operation in a low mode number and $n = -1$ would seem best, but the best number of unit cells is not clear. Figure 4-4 show simulated efficiency for two size reduction ratios and for various numbers of cells.

For the antenna size of $0.18 \lambda_0$, in the inductive-loading case, it is expected that the efficiency reduces with the number of loading elements. This is why a single inductive loading is usually recommended in an electrically small monopole. However the reverse is true for the left handed loading, the efficiency increased with the number of unit cells. The inductively loaded dipole gives highest efficiency 72% for $N = 2$, but the left handed dipole becomes comparable with right handed dipole when increasing to 6 unit cells and even gives better efficiency with $N=8$. Efficiency is also increased when the dipole is meandered and is comparable to the conventional inductive loading when $N = 4$. Gain shows the same decreasing trend for inductively loaded dipoles but increases for CL-loading with increasing cell numbers.

Some understanding of these trends can be given by considering simple equivalent circuits containing only the resistive components in the L and C equivalent circuits. The manufacturer's data [29] shows that the value of these resistances varies non linearly with L or C values. The resistance increases with increasing L with a gradient >1 for values used for series L loading and falls for increasing C with a gradient >1 . If we assume that for a series L loaded antenna, the value of each inductor is L_{total} / N , where L_{total} is some notional

value of L required for a given size reduction factor and N is the number of loading components then the non linear relationship means that the total resistance on the antenna is always $> NR_1$, where R_1 is the resistance of L needed for one component or L_{total} . Therefore a single inductor will always give highest efficiency.

If CL loading is used, then because higher inductor values are needed as the number of loading cells is increased, due to their shunt or parallel connection, the associated resistances also increase. For the values of L needed in this case the gradient of R against L is now <1 , which results in a total loss resistance that reduces with N . The same trend occurs if the loss resistors associated with capacitors are considered.

These hypotheses, based on the non linear R-L and R-C relationships in the component equivalent circuits, whilst intuitively satisfying, may not be necessary to explain the efficiency trend of the CL loading with number of cells. A cascaded ABCD matrix analysis of T networks of loss resistors showed a trend of reducing total loss resistance with increasing N even when a linear R-L and R-C relationships are assumed. It is increasingly hard to give intuitively satisfying explanations of why this happens as improved models of the structure are considered, such as the ABCD matrix model, or indeed the CST model, due to their inherent complexity but all of these models seem to support the trends noted in the full simulations and measurements.

For the smaller antenna size of $0.07 \lambda_0$, inductively loaded dipoles give poor efficiencies around the value of 17% and there is about 2 percent fluctuation for different unit cell numbers, Figure 4-4. We do not feel that it is appropriate to draw conclusions from these

results as it is believed that the accuracy of the simulation in finding efficiency is of the order of a few percent. The meandered CL-loading is no better than the straight CL-loading dipole and both have significantly lower efficiency than conventional loading. However, the results show the same trend that the efficiency will increase with the number of unit cells for the left-handed loading.

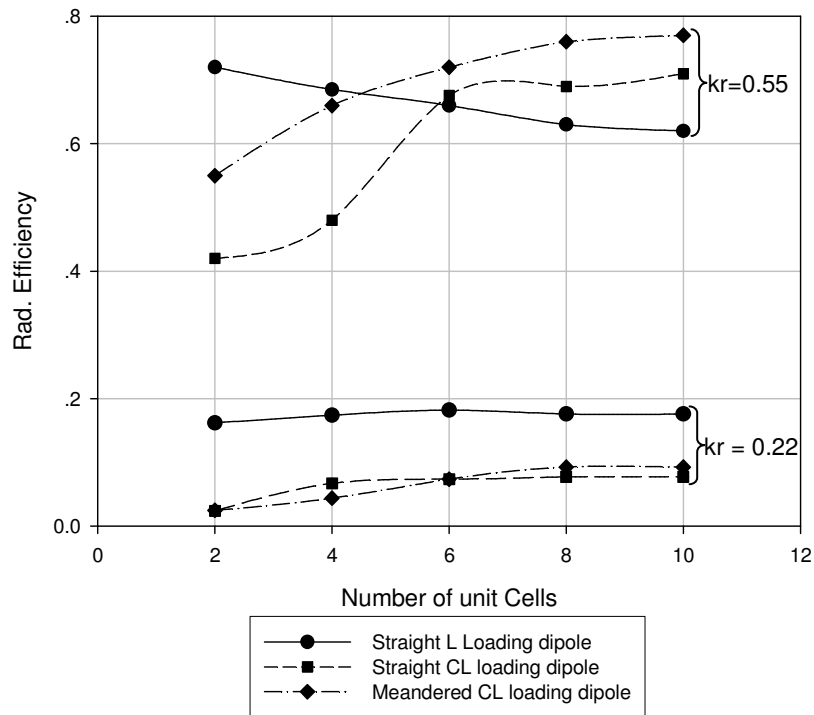


Fig. 4-4. Efficiency of periodically loaded dipole antennas with $|n|=1$, for $kr = 0.55$ ($0.18 \lambda_0$) and $kr = 0.22$ ($0.07 \lambda_0$).

4.1.2.2 Performance of Dipole Antennas with a High Order Mode $|n| = 7$

To the best of our knowledge, orthogonal polarization is a unique property of the meandered CL-loading dipole in a high order mode. For $|n| = 7$, simulations have been made to compare efficiency between straight inductive loading, CL-loading and meandered

CL-loading with 8 unit cells, shown in Table 4-3.

It can be seen that the required loading value in inductive loading is much bigger than it is in CL-loading which results in an efficiency of 0.02%. The currents on the two wires of the straight CL-loaded dipole are out of phase, and the radiation resistance is therefore very small. However the effect of these out of phase currents for straight dipole can be reduced by meandering the arms of dipole. This may explain why the meandered CL-loading dipole has 10 times better efficiency than that of inductive loading and 4 times better than straight CL-loading.

Table 4-3. Simulated performance of 8 cell loaded dipole antennas with $|n|=7$, $kr = 0.48$ ($0.15 \lambda_0$).

Structure	Ant. length L (mm)	Ant. width (mm)	Cap. (pF)	Induc. (nH)	Freq. (MHz) at $ n =7$	Imp. (Ω)	Rad. Effic. (%)	Gain (dBi)
Straight L	100	0.6		800	459	673	0.02	-35.9
Straight CL	100	0.6	0.5	65	458	32	0.07	-30.2
Meandered CL	96	24	0.6	50	462	32	0.29	-24.5

4.1.2.3 Bandwidth Performance of Left Handed Dipoles.

Bandwidth performance of left handed dipoles has also been studied. Based on the previous left handed dipole simulations, the bandwidth for $|S_{11}| < -10$ dB of straight and meandered dipoles with different unit cell numbers is calculated at resonance $n = -1$ and shown in Table 4-4 and Table 4-5.

Table 4-4. Bandwidth of straight CL loading dipoles at resonance $n = -1$.

Unit cells (N)	Dipole length (mm)	Freq.(MHz) at $n = -1$	Rad. Efficiency	Bandwidth $ S_{11} < -10$ dB
2	100	535	42%	0.48%
4	100	527	48%	0.67%
6	102	532	68%	0.48%
8	100	530	69%	0.54%
10	100	527	71%	0.51%

Table 4-5. Bandwidth of meandered CL loading dipoles at resonance $n = -1$.

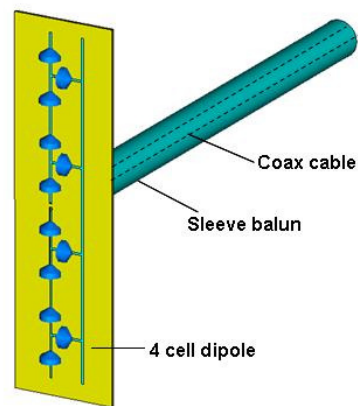
Unit cells (N)	Dipole length (mm)	Dipole width (mm)	Freq.(MHz) at $n = -1$	Rad. Efficiency	Bandwidth $ S_{11} < -10$ dB
2	70	70	526	55%	0.68%
4	88	44	524	66%	0.4%
6	96	32	517	72%	0.62%
8	96	24	526	76%	0.72%
10	97	19.4	523	78%	0.78%

It can be seen that with the same length, either straight or meandered left handed dipole antennas with various unit cell numbers all give narrow bandwidth of below 1%. The relationship between bandwidth and the antenna size is the same as conventional antennas. It can be concluded that small dipole antennas are inherently narrow band and left handed loading does not therefore change things very much.

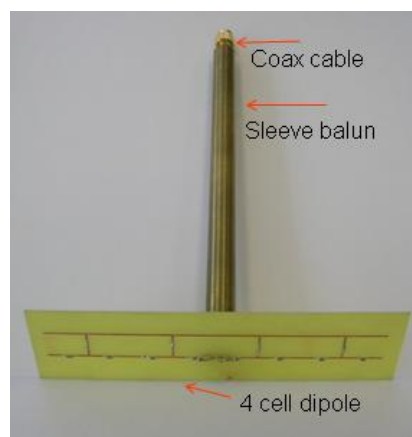
4.1.3 Implementation of 4 Cell Left Handed Dipole

A 4 cell left handed dipole has been implemented with a balun and then measured to verify CST simulation results. The 4 cell dipole simulation model and prototype are shown in Figure 4-5, and implementation is on an FR4 substrate with a thickness of 0.8mm and a relative permittivity of 4.4. The parameters of the antennas and components are based on Table 4-1 (Straight CL).

A coaxial sleeve balun has been used to feed the dipole and its configuration is shown in Figure 4-6. Sleeve balun is a tube that is coupled to the outer of the coax cable at approximately $0.93 \lambda/4$ from the antenna feed point. D is the outer radius of the sleeve and d is the outer radius of the coax. The ratio D/d should be around 2.5 to 4. The open end of the tube facing the antenna element should be as close as possible. In effect this tube is a shorted $\lambda/4$, at its open end the impedance looking back down the coax is high, thus preventing RF current developing on the outer of the coax. The sleeve balun we fabricated in figure 4-5 is 142 mm long shorted at the end furthest from the dipole and its outer radius D is 4 mm.



(a)



(b)

Figure 4-5. left handed dipole with 4 unit cells, (a) Simulation model (b) Prototype.

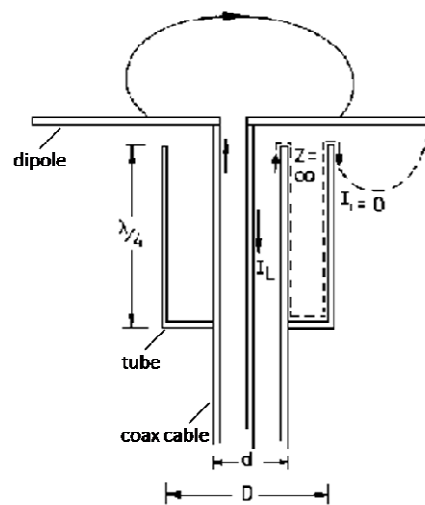


Figure 4-6. Configuration of a coaxial sleeve balun.

Simulated and measured reflection coefficient is compared in Figure 4-7. Two resonances at 442 MHz and 337 MHz where $n = -1$ and -3 were obtained from simulation. From measured result, the resonance was observed at 418 MHz and there was 24 MHz frequencies shift of 5.4% for the $n = -1$. For the $n = -3$ mode the resonance almost agrees with the simulation. We believed that the unavoidable manufacturing tolerances (about 0.01 mm) and fabrication difficulties led to these differences. In particular it was found difficult to exactly duplicate the connection geometry at the feed point and differences of up to 3 mm occurred in the distance of the antenna and balun terminals due to the need for additional wire connections. The results also show that the presence of mismatch loss increased the bandwidth.

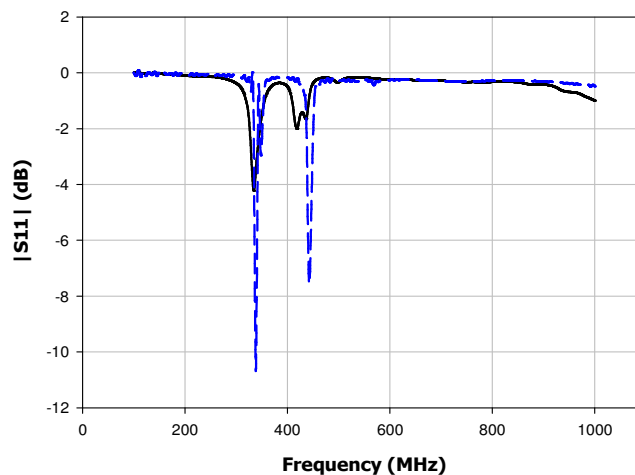


Figure 4-7. S11 Magnitude in dB of 4 unit cell left handed dipole.

(Simulation: dash line; Measurement: solid line)

Gain, measured using the substitution method with a standard dipole with known gain values is shown in Table 4-6 compared to the simulation. An error budget for this measurement was calculated. Primary error contributions came from radiation and

scattering from the balun and cables feeding both the standard gain dipole and left handed dipole. Overall measurement errors are of the order of 1.5 dB, which we believe to be the main contribution to the difference between simulated and measured gain. Many of the contributions to our error budget are of a bias type as opposed to a random type and will all tend to give a lower measured gain compared to simulations.

Table 4-6. Simulated and measured gain for 4 cell left handed dipole.

Simulated frequency (n=-1)	Simulated gain ($kr = 0.46$)	Measured frequency (n=-1)	Measured gain ($kr = 0.44$)
442 MHz	-4.1 dBi	418 MHz	-6 dBi

4.2 Optimized Loaded Dipole Antennas

4.2.1 Dipole with Optimized Component Configuration

Previous implementations of the left handed dipole have been implemented with interdigitated capacitors and meander line inductors [25] and gave good dipole patterns and impedance matching with an efficiency of 27% for length $0.17 \lambda_0$ ($kr = 0.57$). However, the efficiency remains low due to losses in the loading structure. The establishment of low loss designs for loaded inductors and capacitors is studied in this section.

In an implementation with distributed elements, the resistive loss in the metallization of the components, resistivity of the substrate and capacitive coupling effects to the substrates contribute to the total loss. By comparing the meandered and spiral inductors, we can see that the current flow is in the same direction for all the parallel strips of the spiral inductor, whereas for the meandered inductor, two adjacent strips will have opposing current flows, leading to phase cancellation that reduces the mutual inductance. Thus for a desired inductance, the spiral inductor has a lower resistive loss than the meandered inductor. Also, an advantage of using parallel plate capacitors instead of interdigitated capacitors is lower conductor loss due to their wider metal area and capacitance density [30]. To reduce losses, a unit cell implementations with two series parallel plate capacitors and a shunt spiral inductor is applied. The configuration will be shown in Figure 4-8.

The parallel plate capacitor and spiral inductor are designed using following equations (4.3) and (4.4). Equation (4.3) [30] is used for calculating the capacitance of the parallel plate capacitor where A is the area of the plate and D is the distance between two parallel

plates. ϵ_0 is the permittivity of free space and ϵ_r is the relative permittivity. Equation (4.4) is a modified Wheeler (MW) expression [31], where μ_0 is the free space permeability, N is the number of turns, W is the turn of strip conductor width, S is the gap or spacing between turns, d_{out} is the outer diameter, d_{in} is the inner diameter, d_{avg} is the average diameter and ρ is the fill ratio, equal to $(d_{out} - d_{in}) / (d_{out} + d_{in})$. k_1 and k_2 in equation (3) are constants given by 2.34 and 2.75 for square spiral layout.

$$C = \frac{\epsilon_0 \epsilon_r A}{D} \quad (4.3)$$

$$L = k_1 \mu_0 \frac{N^2 d_{avg}}{1 + k_2 \rho} \quad (4.4)$$

Table 4-7 (a) Parameters of the simulation model.

Length L of the antenna	Length a of unit cell	Distance d of wires	Width w of wire	Number N of unit cells
100mm	25mm	16mm	0.88mm	4

(a)

Table 4-7 (b) Parameters of the optimized components.

	Parallel plate capacitor	Spiral square inductor
Parameters	$\epsilon_r = 2.6$ $A = 3.43\text{mm}$ $D = 0.6\text{mm}$	$N = 5$ $W = 500\mu\text{m}$ $S = 500\mu\text{m}$ $d_{in} = 1.5\text{mm}$ $d_{out} = 10\text{mm}$
Equivalent lumped value	0.45pF	140nH

(b)

4.2.1.1 Configuration

The printed left-handed dipole antenna with parallel plate capacitors and spiral inductors is shown in Figure 4-8, and is implemented on Teflon substrate with a thickness of 0.6mm and relative permittivity of 2.6. The parameters of the antenna and optimized components are listed in Table 4-7. Conductivity of 5.8×10^7 S/m for copper and loss tangent of 0.0015 for the dielectric substrate were used for the simulation.

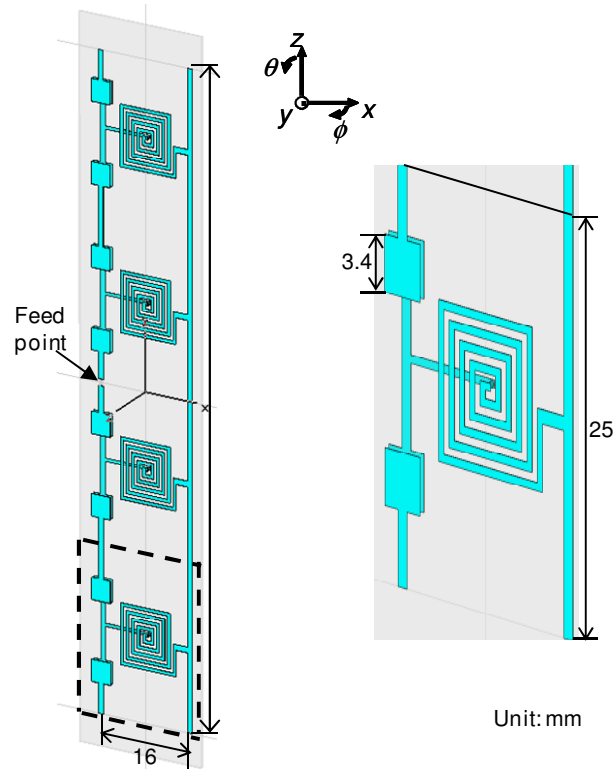


Figure 4-8. Configuration of the optimized distributed dipole antenna.

4.2.1.2 Simulated and Measured Performances

Two resonances at 483 MHz and 368 MHz for $n = -1$ and -3 respectively were observed from simulation. An input impedance with a real part of 56Ω was achieved at $n = -1$. An $S_{11} < -10$ dB bandwidth of 0.49% is achieved at $n = -1$. From the farfield simulation results, the radiation efficiency was improved to 73.8% at 483 MHz due to the application of low loss optimized components. The simulated gain is 0.8 dBi.

A T-junction balun is used for the measurement [32]. The configuration of the balun is shown in Figure 4-9. The balun has an impedance of 50Ω for the unbalanced port and 56Ω for the balanced port (design process described in Appendix E). A simulated S parameter file from CST was imported into ADS [33] and connected to the T-junction balun for

schematic simulation. After being combined with the balun, two more dips were observed at the two sides of simulated S11 plot from ADS.

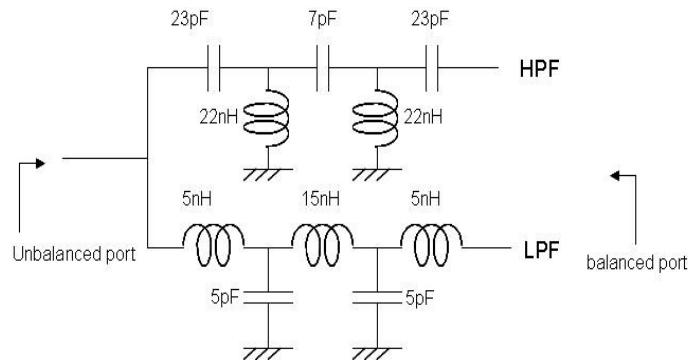


Figure 4-9. Configuration of T-junction balun.

Figure 4-10 shows the fabricated dipole with the T-junction balun. The balun allows easy PCB fabrication but will affect the antenna performance because of the coupling between them. The balun also introduces a small extra loss to the radiating system, which is measured with back to back baluns to be 0.4 dB.

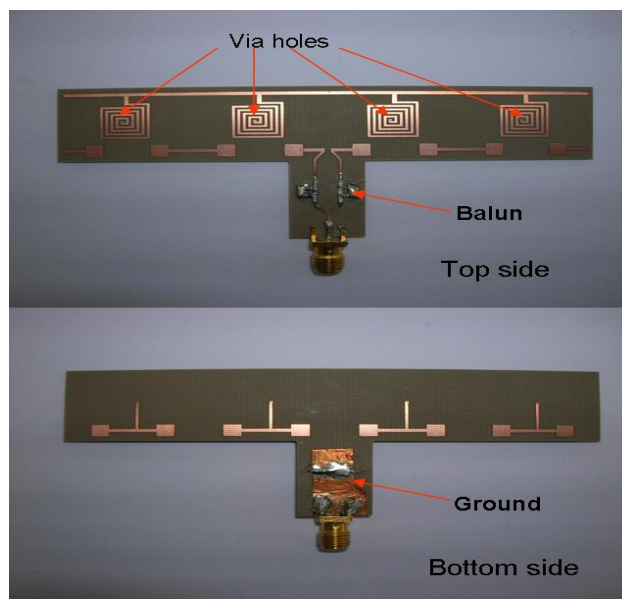


Figure 4-10. Photograph of the optimized left-handed antenna.

Simulated and measured reflection coefficient magnitudes of the optimized dipole with a T-junction balun are compared in Figure 4-11. Frequencies of 487 MHz and 374 MHz were observed for the $n = -1$ and -3 modes from measurement. Agreement between simulation and measurement was good, although there were frequency shifts of 0.8% for the $n = -1$ mode and 2.1% for $n = -3$. Two more dips were also found in the measured reflection coefficient, due to the presence of the balun.

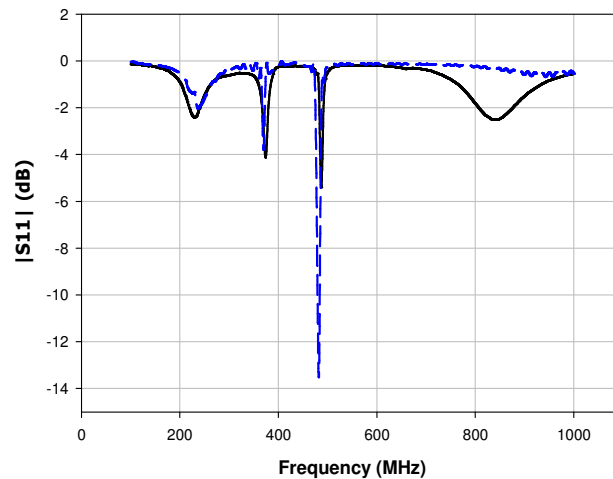


Figure 4-11. S 11 Magnitude of optimized left handed antenna with balun.

(Simulation: dash line; Measurement: solid line)

Figure 4-12 shows simulated and measured radiation patterns in the xz plane at 487 MHz, typical of an electrically small dipole. Cross polarization was lower than -12 dB from measurement, which is bigger than simulation due to extra radiation from the balun and cables feeding the dipole. The substitution method was used for gain measurement and the measured gain was -1.9 dBi, taking into account the balun's loss of 0.4 dB. The 2.3 dB differences between the simulated and measured gain is due to limitations in the measurements.

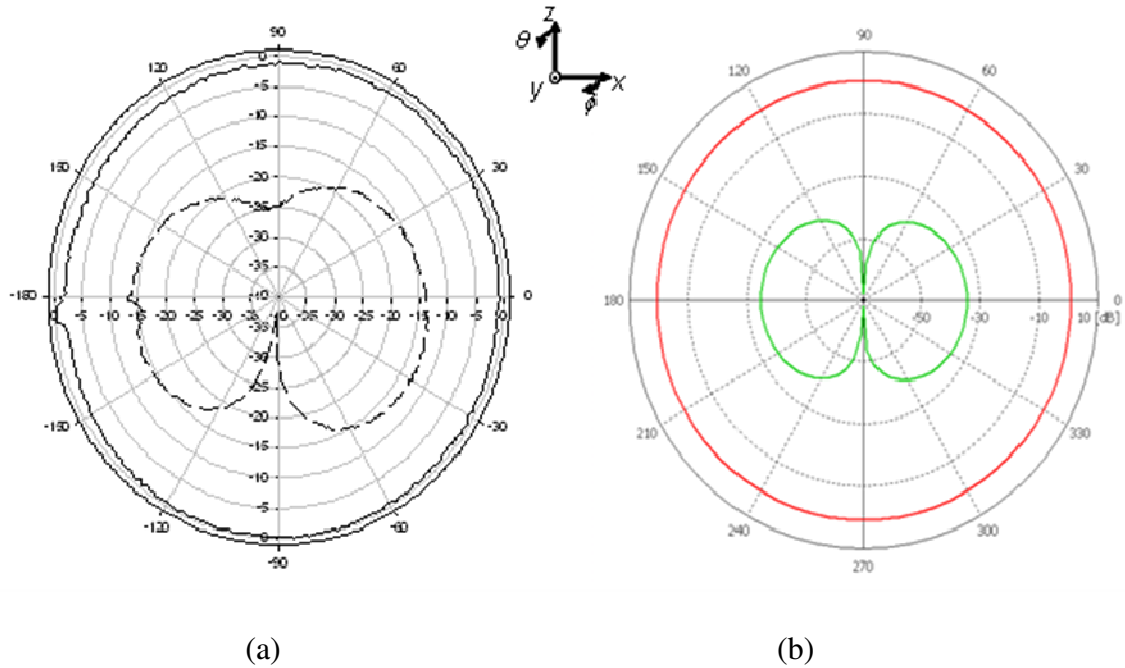


Figure 4-12. (a) Measured radiation pattern for the optimized antenna in xz plane, real line: E_{θ} , dashed line: E_{ϕ} . (b) Simulated radiation pattern for the optimized antenna in xz plane, red line: E_{θ} , green line: E_{ϕ} .

4.2.1.3 Comparisons

a. Simulation Comparisons

Simulations were made for the lumped loading left handed dipole (CL-loading) and right handed dipole (inductive loading) to compare with the optimized distributed loading left handed dipole. For the lumped loading structures, simulated models are based on Figure 4-1 (a) and Figure 4-2. The same values for the lumped inductors and capacitors were applied for lumped CL-loading during simulations, namely 0.45 pF and 140 nH. The value of lumped inductors used for lumped L-loading is 40 nH. Comparisons of the simulation results are shown in Table 4-8. It can be seen that an increase in gain of 2.5 and 0.7 dBi

was obtained from the optimized loading simulation, over the CL-loading and L-loading antennas. The efficiency of the optimized antenna is equivalent to an L-loaded dipole with 2 cells, as shown in Figure 4-4.

Table 4-8. Simulation results for different loading structure of 4 unit cell dipole.

Implementation (loading structure)	L- loading	CL- loading	Optimized lumped loading
Antenna enclosed radius (r)	50mm	50mm	50.8mm
Number of unit cells	4	4	4
Resonance frequency at $ n =1$	531MHz	533MHz	483MHz
Value of kr	0.56	0.55	0.51
Input impedance	18.6 Ω	78 Ω	56 Ω
Rad. Efficiency	68.5%	41%	73.8%
Gain	0.1dBi	-1.7dBi	0.8dBi

b. Measurement Comparisons

The above simulated dipole with lumped CL-loading was also built and measured, and shown in Figure 4-13. Two resonances were found at 536 MHz for $n = -1$ and 434 MHz for $n = -3$. The measured gain at 536 MHz was -4 dBi, inclusive of the loss of 0.4 dB of the

balun. The measured results for the lumped loaded dipole are compared with the optimized distributed loaded dipole in Table 4-9. There is about 2 dB difference between the simulated and measured gain results mainly because of the radiation and scattering from the balun and cables feeding the dipoles. Whilst not agreeing well with the simulations due to the limitations in the measurements, the results do show the trend and validate the improvement of antenna gain in the implementation with parallel plate capacitors & spiral inductors.

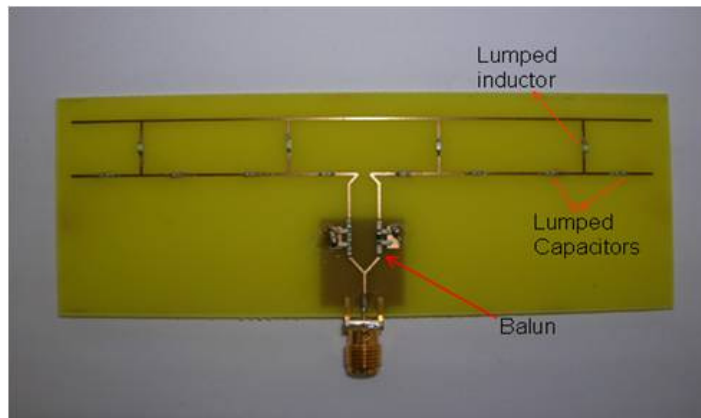


Figure 4-13. Photograph of the lumped left-handed antenna.

Table 4-9. Measured results for two implementations of left handed antenna.

($L = 140 \text{ nH}$, $C = 0.45 \text{ pF}$)

Implementation (Unit cell components)	Lumped L & C	Parallel plate capacitor & spiral inductor
Resonance frequency (at -1 mode)	526MHz	487MHz
Gain	-4dBi	-1.9dBi

4.2.2 Dipole with Non-linear Loading

The loss in the loading elements is proportional to the current intensity and the resistance. If the resistance of the elements, located where the current intensity is high, is reduced, the total loss will be reduced. Such non-linear loading along the dipole has been studied and is reported here. The dipole is fed in the centre where the current intensity is large so a low value of the loading is applied in middle and higher towards outside. The built in optimizer in CST was used to find the best capacitor and inductor values everywhere independently for matching impedance and best efficiency.

Simulations for a straight 6 unit cell dipole with linear or non linear CL-loading along dipole length were performed based on the model shown in Figure 4-14. Linear CL-loading with the element value of 0.7 pF and 120 nH was firstly simulated and obtained efficiency is 67.5%. Non-linear CL-loading simulations are then performed based on linear parameters. Lower values of the loading capacitors and inductors are applied in the middle location and other C & L values are adjusted to produce the same resonance frequency and impedance. In the simulations, C (1) or L (1) is changed and then other C & L values are adjusted to produce the same resonance frequency and impedance.

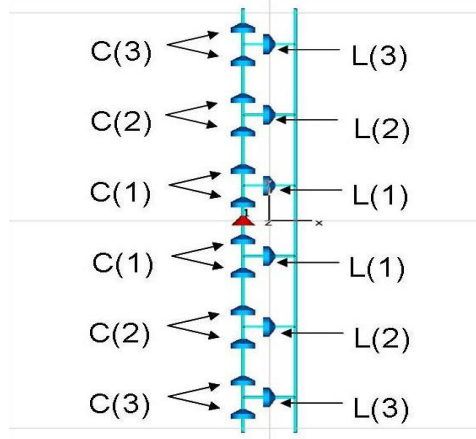


Figure 4-14. Configuration of left handed dipole with non linear loading.

Results are summarized in Table 4-10. It has been found that non-linear loading with central capacitance of 0.6 pF and inductance of 115 nH give improvement in dipole efficiency from 67.5 to 69.5%.

Table 4-10. Simulation results for non linear CL loading 6 unit cell dipole.

C(1) (pF)	C(2) (pF)	C(3) (pF)	L(1) (nH)	L(2) (nH)	L(3) (nH)	Freq, $n=-1$ (MHz)	Imp. (Ω)	Effici. (%)	Gain (dBi)
0.7	0.7	0.7	120	120	120	532	72.2	67.5	-0.04
0.6	0.7	0.9	120	120	120	533.8	73.7	68	-0.002
0.5	0.7	3	120	120	120	532.9	73.6	67.6	-0.03
0.8	0.7	0.5	120	120	120	532	73.5	67.3	-0.05
0.7	0.7	0.7	140	120	125	524.8	80	66.5	-0.1
0.7	0.7	0.7	115	120	115	537.4	76.2	69.4	0.2
0.6	0.7	0.9	112	120	115	540.1	76	69.5	0.2

4.3 Summary

The efficiency of dipole antennas loaded with left-handed transmission lines has been investigated and compared to conventional inductive loading.

Both conventional and left handed loading can give size reduction. For an antenna size of $0.18 \lambda_0$ with 4 unit cells, periodically loaded, conventional inductive loading gives best efficiency. Meandered CL-loading gives better efficiency than straight CL-loading and is comparable with inductive loading. Both meandered and straight left handed loading show greater degrees of freedom than the conventional right handed loading which allows a desired impedance to be obtained. However at a size of $0.07 \lambda_0$ the meandered dipole is no better than the straight dipole and both left handed antennas have significantly lower efficiency than conventional right handed loading.

The efficiency of the conventional inductively loaded dipole reduces with increasing number of cells, whilst those with left-handed loading increase. For high mode numbers left handed loading is more efficient than inductive loading.

When parallel plate capacitors and spiral inductors are applied for low loss distributed loading the radiation efficiency improves substantially to 73.8% as compared to previous implementations and the improvement is experimentally validated. Some small improvement is found by non-linear loading along the dipole length.

It can be concluded that in a low order mode, the efficiency of L-loading dipole is better

with low number of unit cell. If the number of cell increases, CL-loading presents comparable and even better performance. In a high mode the meandered left handed dipole gives the best efficiency due to the phase distribution, presenting orthogonal polarization as well. The dipole with optimized lumped loading presents the best performance in impedance and efficiency, even better than the conventional inductive loading.

References

- [1] L. J. Chu, "Physical Limitations of Omni-Directional Antennas," *Journal of Applied Physics*, vol. 19, pp. 1163-1175, Dec. 1948.
- [2] R. C. Hansen, "Fundamental Limitations in Antennas," *Proc. of the IEEE*, vol. 69, pp. 170-182, Feb. 1981.
- [3] R. F. Harrington, "Effect of Antenna Size on Gain, Bandwidth, and Efficiency," *Journal of Research of the National Bureau of Standards-D. Radio Propagation*, vol. 64D, Jan.-Feb. 1960.
- [4] J. R. James, A. J. Schuler, and R. F. Binham, "Reduction of Antenna Dimensions by Dielectric Loading," *Electron. Lett.*, vol. 10, pp. 263-265, 27th June 1974.
- [5] J. S. McLean, "A Re-Examination of the Fundamental Limits on the Radiation Q of Electrically Small Antennas," *IEEE Trans. Antennas Propag.*, vol. 44, pp. 672-676, May 1996.
- [6] G. S. Smith, "Efficiency of electrically small antennas combined with matching networks," *IEEE Trans. Antennas Propag.*, vol. AP-40, pp. 369-373, May 1977.
- [7] H. A. Wheeler, "Fundamental Limitations of Small Antennas," *Proceedings of the IRE*, pp. 1479-1484, Dec. 1947.
- [8] H. A. Wheeler, "The Radian Sphere Around a Small Antenna," *Proceedings of the IRE*, pp. 1325-1331, Aug. 1959.
- [9] R. W. Ziolkowski and A. Erentok, "Metamaterial-Based Efficient Electrically Small Antennas," *IEEE Trans. Antennas Propag.*, vol. 54, pp. 2113-2130, July 2006.
- [10] J. R. James and R. M. Burrows, "Resonance Properties of Dielectric-loaded Short Unipoles," *Electron. Lett.*, vol. 9, pp. 300-302, 12th July 1973.

- [11] J. R. James and A. Henderson, "Electrically short monopole antennas with dielectric or ferrite coatings," *PROC. IEE*, vol. 125, pp. 793-803, Sept. 1978.
- [12] K. L. Wong and Y.-F. Lin, "Small broadband rectangular microstrip antenna with chip-resistor loading," *Electron. Lett.*, vol. 33, pp. 1593-1594, Sept. 1997.
- [13] V. G. Veselago, "The electrodynamics of substances with simultaneously negative values of ϵ and μ ," *Sov. Phys. Usp.*, vol. 10, pp. 509-514, Jan.-Feb. 1968.
- [14] G. V. Eleftheriades, A. K. Iyer, and P. C. Kremer, "Planar negative refractive index media using periodically L-C loaded transmission lines," *IEEE Trans. Microwave Theory Tech.*, vol. 50, pp. 2702-2712, Dec 2002.
- [15] H. Iizuka and P. S. Hall, "A left-handed dipole concept," presented at Proc. Int. Workshop on Antenna Tech., New York, USA, Mar. 2006.
- [16] A. L. Borja, P. S. Hall, Q. Liu, and H. Iizuka, "Omnidirectional loop antenna with left-handed loading," *IEEE Antennas and Wireless Propag. Lett.*, vol. 6, pp. 495-498, Feb. 2007.
- [17] C. Caloz and T. Itoh, "Transmission line approach of left-handed (LH) materials and microstrip implementation of an artificial LH transmission line," *IEEE Trans. Antennas Propag.*, vol. 52, pp. 1159-1166, May 2004.
- [18] C. Caloz, A. Sanada, and T. Itoh, "A novel composite right-/left-handed coupled-line directional coupler with arbitrary coupling level and broad bandwidth," *IEEE Trans. Microwave Theory Tech.*, vol. 52, pp. 980-992, Mar. 2004.
- [19] G. Goussetis, A. P. Feresidis, and J. C. Vardaxoglou, "Periodically loaded dipole array supporting left-handed propagation," *Proc. IEE Microwaves, Antennas and Propag.*, vol. 152, pp. 251-254, Aug. 2005.

- [20] H. Iizuka, P. S. Hall, and A. L. Borja, "Dipole Antenna With Left-Handed Loading," *IEEE Antennas and Wireless Propag. Lett.*, vol. 5, pp. 483-485, Dec. 2006.
- [21] C. J. Lee, K. M. K. H. Leong, and T. Itoh, "Design of resonant small antenna using composite right/left-handed transmission line," presented at Proc. IEEE Antennas Propag. Society Int. Symp., Washington DC, USA, Jul.2005.
- [22] M. Schuessler, J. Freese, and R. Jakoby, "Design of compact planar antennas using LH-transmission lines," *Proc. IEEE Int. Symp. Microwave Theory and Tech.*, vol. 1, pp. 209-212, Jun. 2004.
- [23] O. F. Siddiqui, M. Mojahedi, and G. V. Eleftheriades, "Periodically loaded transmission line with effective negative refractive index and negative group velocity," *IEEE Trans. Antennas Propag.*, vol. 51, pp. 2619-2625, Oct. 2003.
- [24] P. S. Hall and Q. Liu, "Dipoles and loop antennas with left handed loading," presented at 2008 Loughborough Antennas & Propagation Conference, Loughborough, UK, 17-18 March 2008.
- [25] H. Iizuka and P. S. Hall, "Left handed dipole antennas and their implementations," *Trans. Antennas Propag.*, vol. 55, pp. 1246 -1253, May 2007.
- [26] H. Iizuka and P. S. Hall, "Orthogonally polarized dipole antenna using left handed transmission lines," presented at Proc. 36th Euro. Microwave Conf., Manchester, U.K., Sep. 10–15, 2006.
- [27] Q. Liu, P. S. Hall, and A. Lucas-Borja, "Dipole with left handed loading with optimised efficiency," presented at 2nd European Conference on Antenna and Propagation, Edinburgh, UK, Nov 2007.

- [28] "CST Microwave Studio Tutorials," Computer Simulation Technology, www.cst.de, vol. Version 4, July 2002.
- [29] "RF Ceramic Chip Inductors and Multi-Layer High-Q Capacitors datasheet," Johanson Technology, www.johansontechnology.com.
- [30] H. Samavati, A. Hajimiri, A. R. Shahani, G. N. Nasserbakht, and T. H. Lee, "Fractal Capacitors," *IEEE Journal of Solid-state Circuits*, vol. 33, Dec. 1998.
- [31] Mohan, S. S., and e. al., "Simple Accurate Expressions for Planar Spiral Inductances," *IEEE J. Solid-State Circuits*, vol. 34, pp. 1419-1424, October 1999.
- [32] H. Iizuka and T. Watanabe, "Balanced Line to Unbalanced Line Transformer," Japan Japanese patent 2005-198167, Jan. 9, 2004.
- [33] "ADS Advance Design System 2005A," Schematic, Agilent Technologies.

CHAPTER V LOOP ANTENNAS USING LEFT HANDED TRANSMISSION LINES

Transmission lines loaded with reactive components that have left handed wave behaviour have been applied to many forms of antennas to investigate the new properties that those antennas have [1-3]. The idea of the left-handed transmission lines has been also extended to small antennas constructed on a ground plane [4-6]. Recently Dr. Iizuka etc have shown how left-handed transmission lines can be incorporated into dipole antennas [1, 2, 7-9], which are discussed in the last two chapters. Two main features of dipoles with left handed loading have been demonstrated, namely size reduction and orthogonal polarized radiation in a higher order mode. A study for the efficiency of electrically small dipole antennas loaded with left-handed transmission lines is also be introduced including a low loss design on distributed inductors and capacitors.

Loop antennas are another typical vehicle antennas for the use of car radio, TV etc. The printed circuit board structure allows mounting on glass or roof panel of vehicles. However, multipath is usually a problem for the application of car TV in town. In this chapter, left handed transmission lines will be applied to conventional loop antenna designs to investigate their new features in the performance. Left-handed loop antennas could give size reduction when used in cars around 500MHz. A novel loop antenna with switched pattern against multipath could be a solution for the vehicle diversity need.

5.1 Basic Loop Antenna Properties

Basic loop antenna development and properties are firstly reviewed. A coil of large diameter, used as an antenna, especially in direction-finding equipment and in radio receivers is called a loop antenna. The loop antenna is another simple, inexpensive, and very versatile antenna type. A typical loop antenna consists of a conducting coil of any convenient cross section, generally circular or rectangular, that emits and receives radio energy [10]. All planar loops are directional antennas with a sharp null, and have a radiation pattern similar to the dipole antenna with E and H fields interchanged.

5.1.1 Small / large Loop Antennas

A loop is considered a small loop if it is less than $1/4$ of a wavelength in circumference. Most directional receiving loops are about $1/10$ of a wavelength. It has been shown that a small loop (circular or square) is equivalent to an infinitesimal magnetic dipole whose axis is perpendicular to the plane of the loop [10]. The fields radiated by an electrically small loop can be seen uniform with a constant current along the loop. The far-field pattern for a small loop, in each of its principal planes, can be obtained by assuming that each of its sides is a small linear dipole of constant current and length. Loop antennas with electrically small circumferences or perimeters have small radiation resistances that are usually smaller than their loss resistances. Thus they are very poor radiators, and they are seldom employed for transmission in radio communication. The ways to increase the radiation resistance of the loop are by increasing (electrically) its perimeter or the number of turns, or to insert a ferrite core of very high permeability [10].

A large loop antenna is similar to a dipole, except that the ends of the dipole are connected to form a circle, triangle or square. Typically a loop is a multiple of a half or full wavelength in circumference. A circular loop gets higher gain (about 10%) than the other forms of large loop antenna, since gain of this antenna is directly proportional to the area enclosed by the loop [10]. However, circles can be hard to support in a flexible coil, making square and triangle loop antennas much more popular. Large loop antennas have no need for a ground plane and are more immune to localized noise.

The loop usually has its strongest signal in the plane of the loop and the nulls in the axis perpendicular to the plane of the loop. Thus loops are somewhat directional along the axis of highest gain [11]. A loop can be used for direction finding by rotating the plane of the antenna until the signal disappears. However, there is an ambiguity in the direction as planar loops have a 180 degree symmetry. Other methods must be used to determine if the signal is in front or behind the loop. Frequently, a dipole and a loop are used together, to obtain a combined cardioid or heart-shaped radiation pattern with a sharp null on only one side.[11]

5.1.2 Particular Loop Antennas

There are two special cases of loop antennas which are neither short nor long, and have particular characteristics. Half wavelength loop, a half wave dipole curved into a circle, can be mounted in the horizontal plane as a horizontally polarized omnidirectional antenna [11]. Full wavelength loop, an element of the Quad antenna, radiates on its axis (unusual for a loop) and polarizes according to the alignment of the feed position [11].

In 1940, a unique antenna was introduced [12], which was later called Alford loop antenna after one of the authors. This loop antenna had a design that made it a good radiator, and at the same time made it horizontally polarized with an omnidirectional pattern. This was made possible by the way it was fed as shown in Figure 5-1. By feeding the two centre conductors with a current that is equal in amplitude but opposite in phase, the radiation of the currents on these conductors will have opposite directions, and will hence cancel each other. Therefore, on the four sides the currents will be travelling in the same direction and the four arms on the side forms a square loop. As a result, the wanted uniform current distribution is obtained, but still with a fairly large circumference, approximately a wavelength.

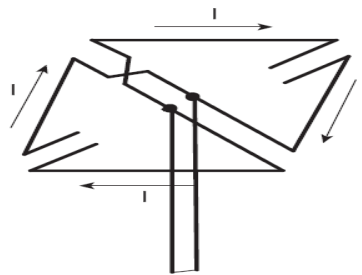


Figure 5-1. Sketch of an Alford loop antenna [12].

In 1985, a version of this antenna was implemented using printed circuit technology [13]. The antenna is made out of a dielectric substrate which has a Z type structure printed on both sides. The two Z are orientated in a manner such that the diagonal of the Z overlap and the arms form a square loop (shown in Figure 5-1). The antenna is fed by a coaxial probe connected to one side of the structure. The inner conductor of the probe is then connected to the other side via a hole in the centre. This makes the current distribution on

both sides equal in magnitude, but gives it a 180-degree phase difference. This causes the radiation of the currents on the diagonal to cancel each other, but on the arms a uniform current distribution is obtained. Since the current distribution is uniform, the antenna will radiate a horizontally polarized wave with an omnidirectional pattern.

5.2 Omnidirectional Left Handed Loop Antenna

Omnidirectional loops based on the Alford loop principle have been shown [12, 14, 15], but have some problems with input impedance matching and the uniformity of the currents along the loop. On the one hand, a small loop antenna will have an omnidirectional pattern, but a very small radiation resistance and high reactance. On the other hand, a larger loop antenna will have a reasonable radiation resistance but the current distribution along the loop will become non-uniform and may not yield an omnidirectional pattern. The same omnidirectional performance can be obtained using reactive loading derived from left handed transmission line concepts. A loop antenna with left-handed loading will be proposed to investigate its new features in the performance [16].

5.2.1 Configuration

Fig 5-2 shows how the left handed loading concept can be applied to a loop [17]. Here the two wire transmission line is formed into a loop and fed at the break in the outer loop as shown. The loop antenna, loaded by a left-handed ladder network composed of 4 unit cells. The unit cell has a shunt inductor L_L and two series capacitors C_L . These components determine the operating mode at a given frequency, where phase constant β can be negative, zero, or positive. The phase constant of such a line applied to the loop is similar as the one applied to a left handed dipole defined in equation (3.13). Thus, the antenna is left-handed at lower frequencies and right-handed at higher frequencies with a transition frequency, which can be shown to work in the $n = 0$ mode under appropriate design conditions.

The capacitors C_L are put on one side of the ladder network, which also has the feed point. The currents I_1 and I_2 on the two wire transmission line are in opposite directions, as might be expected, and cancellation in the far field would normally reduce the radiation significantly. Loading the line with capacitors on one side only results in the two currents having significantly different amplitudes, and this difference leads to strong radiation. The proposed loading also allows good impedance matching to be achieved.

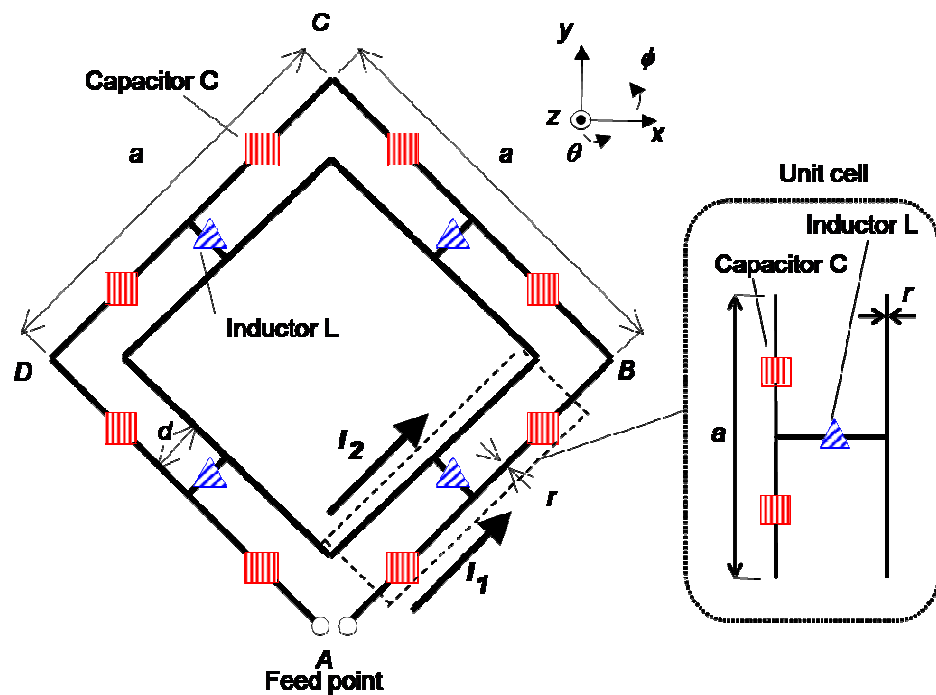


Figure 5-2. Conceptual model of a left-handed loop antenna [16].

5.2.2 Performances

5.2.2.1 Simulation Model and Prototype Antenna

The performance of the antenna is investigated numerically using the commercial simulator CST. The printed left-handed loop antenna loaded with series lumped capacitors and shunt lumped inductors is shown in Figure 5-3, which is implemented on FR4

substrate with a thickness of 0.8mm and dielectric permittivity of 4.4. The parameters of the simulation model, shown in Table 5-1, were specified so that an antenna would have one wavelength circumference, λ_0 , at about 500 MHz and 50Ω impedance. The equivalent circuits of the components included a loss value specified by the manufacturer. Conductivity of $5.8e7$ S/m for copper and loss tangent of 0.017 for dielectric substrate were used for the simulation.

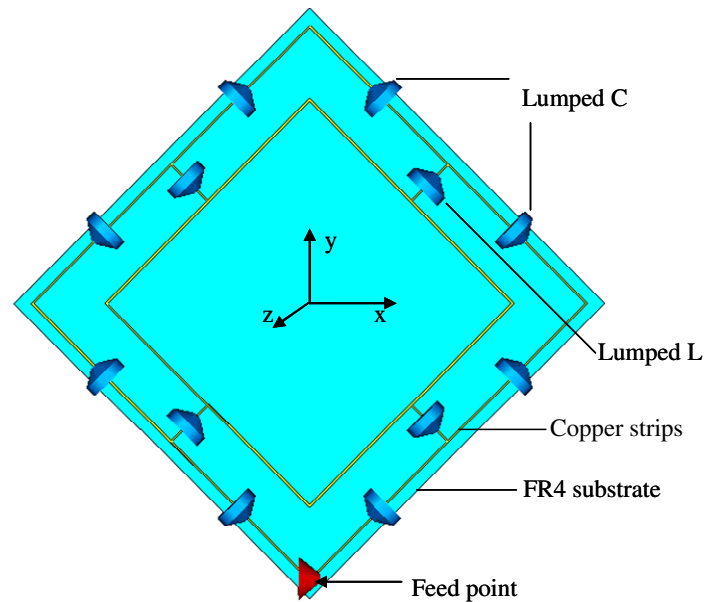


Figure 5-3. Simulated model of left-handed loop antenna in CST.

Table 5-1 Parameters of the Simulation Model.

Circumference L	600 mm
Length a of unit cell	150 mm
Distance d of wires	20 mm
Width r of strip line	0.7 mm
Number N of unit cells	4
Capacitance of C_L	1 pF
Inductance of L_L	220 nH
Length of LC elements	1.5 mm

A prototype loop antenna was implemented with a balun [19] used in the measurement as shown in Figure 5-4. The balun has impedance of 50 ohm for the balanced port and 50 ohm for the unbalanced port (design process described in Appendix E). The frequency bandwidth of the balun for $|S_{11}| < -10$ dB starts at 330 MHz and ends at 700 MHz. The configuration including parameters of the balun is shown in Figure 5-5. The balun introduces a small extra loss of about 0.4 dB, which reduces the overall radiation efficiency.

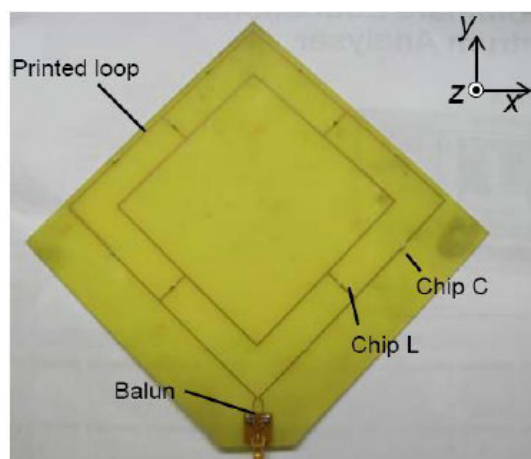


Figure 5-4. A Prototype of Left-Handed Loop Antenna. [16]

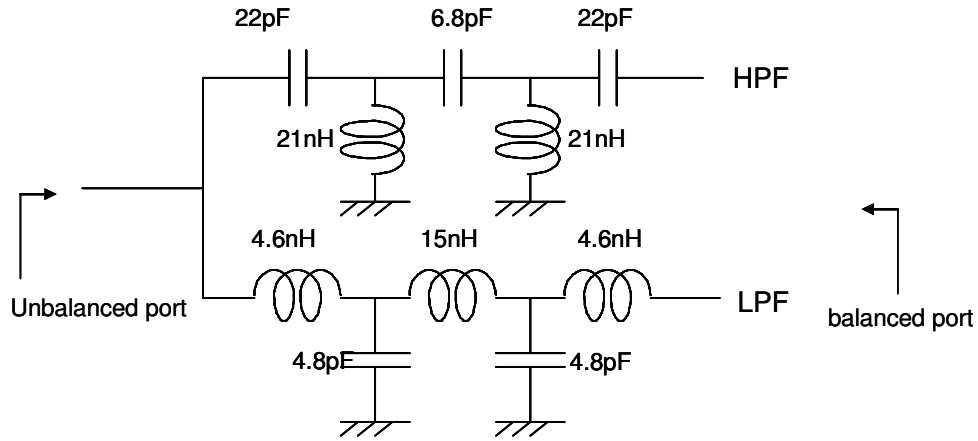


Figure 5-5. Configuration of T-junction Balun for the left handed loop antenna.

5.2.2.2 Simulated and Measured Results

a. Reflection Characteristics

Reflection characteristics are shown in Figure 5-6. Several resonances are observed. These can be understood by considering conventional resonance numbering as in (5.2). This gives the relationship between the resonance number n , the length L of the loop antenna, and the wavelength λ_a of the current induced on the antenna.

$$L = |n| \frac{\lambda_a}{2} \quad (5.2)$$

The number n is a negative integer, zero, or a positive integer. It decreases with decreasing frequency.

In Figure 5-6, a resonance in the $n = 0$ mode was observed at 500 MHz for measurement and at 546 MHz for simulation. The bandwidth, for less than -10 dB return loss, is 2.26% for measurement and 1.74% for simulation. This difference is attributed to use of printed circuit construction, compared to wires in free space as in the simulations, and in particular the loss in the FR4 substrate giving a lower Q factor and hence wider bandwidth. The loop

antenna is matched in its input port at even modes and the lowest resonance observed was $n = -N = -4$.

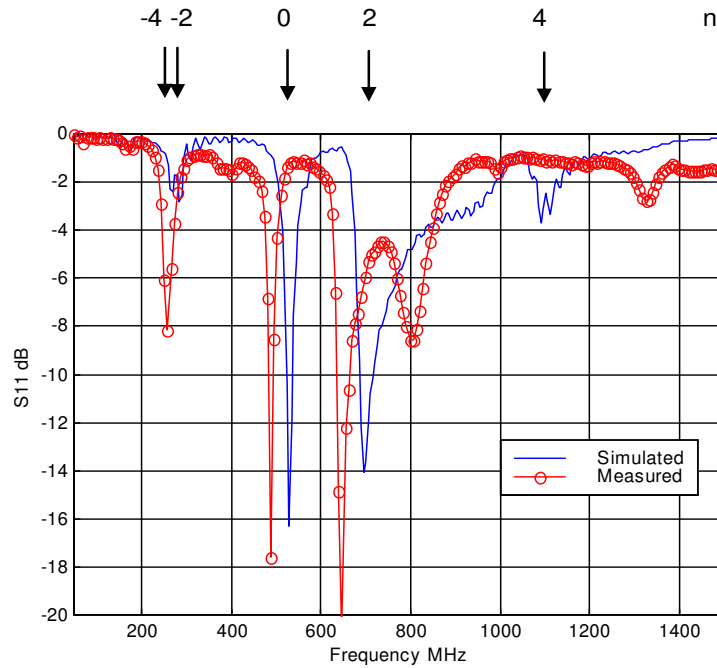


Figure 5-6. Return loss characteristic (S11 Amplitude). [16]

The input return loss characteristics are further explained in relationship between frequency and phase constant β , shown in Figure 5-7. Capacitance and inductance of loaded elements are adjusted so that the antenna operates in the $n = 0$ obtained at 546 MHz where the wavelength is infinite and the phase constant is zero.

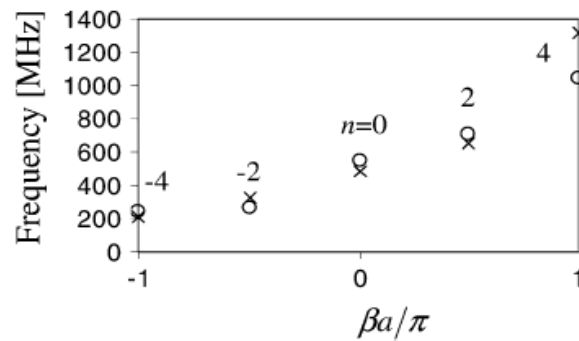


Figure 5-7. Relationship between the frequency and phase constant β . [16]

b. Near Field Distributions

Current distributions on wires in the plane of the loop at 546 MHz are shown in Figure 5-8. A voltage of 1V was applied at the feed point. Currents I_1 and I_2 have different amplitude levels in Figure 5-8 (a) and are out of phase in Figure 5-8 (b). The summation of currents I_1 and I_2 becomes flat amplitude and phase distributions, and consequently omnidirectional radiation pattern is obtained in the plane of the loop.

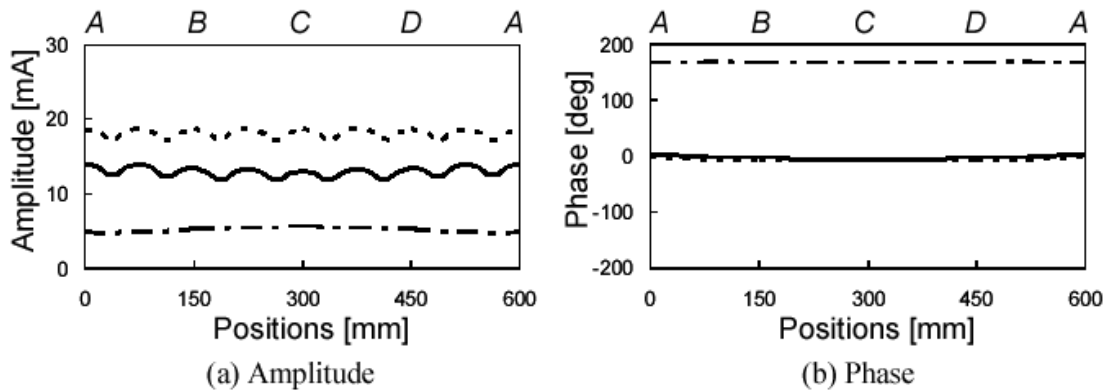


Figure 5-8. Current distributions at 546 MHz ($n = 0$). (----: I_1 , -.-.: I_2 , —: I_1+I_2).[17]

Figure 5-9 shows the simulated absolute near H-field distribution for various modes in the z -plane. Similar field distribution are shown at modes $|n| = 2$ and $|n| = 4$ for both left- and right-handed performance, with two and four current peaks, respectively. The field distribution in the $n = 0$ mode shows uniform current amplitude distribution, as expected.

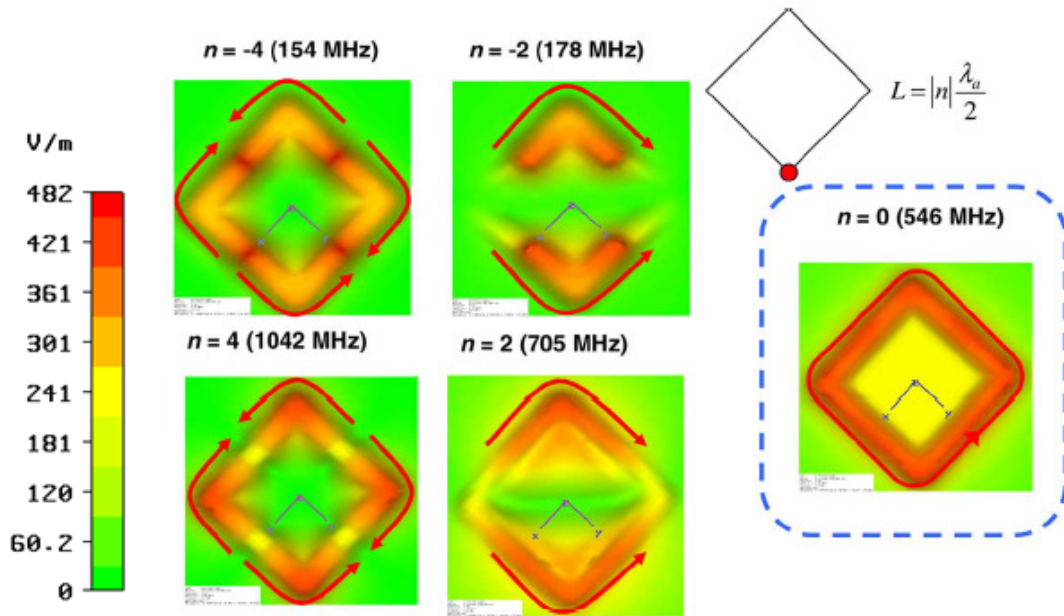


Figure 5-9. Simulated absolute near H-field distribution. Distributions at $n = -4$ (154 MHz), $n = -2$ (178 MHz), $n = 0$ (546 MHz), $n = 2$ (705 MHz), $n = 4$ (1042 MHz) modes. (Inset shows feeding point).[16]

c. Far Field Radiation Patterns

The antenna radiation efficiency is defined as the ratio between the radiated to accepted (input) power of the antenna. Likewise, the gain is the ratio of the radiation intensity in a given direction from the antenna to the accepted intensity averaged over all directions. Simulations show that efficiency in the $n = 0$ mode is 94% and that although the $n = 0$ mode cannot be achieved with conventional L loading, in the $n = -2$ and 2 mode achieved with left handed and conventional loading respectively, the efficiencies are 10% and 50%. The left-handed antenna has a lower operating frequency but also lower efficiency and gain.

Figure 5-10 (a) and (b) show measured radiation patterns in the xy and zx planes in the $n = 0$ mode (at 546 MHz). The coordinate system is shown in Figure 5-3. The omnidirectional pattern is obtained in the plane of the loop (xy plane) with small cross polarization below -50 dB. The antenna has two nulls in the z axis perpendicular to the plane of the loop. The simulated gain is 1.4 dBi at 546 MHz.

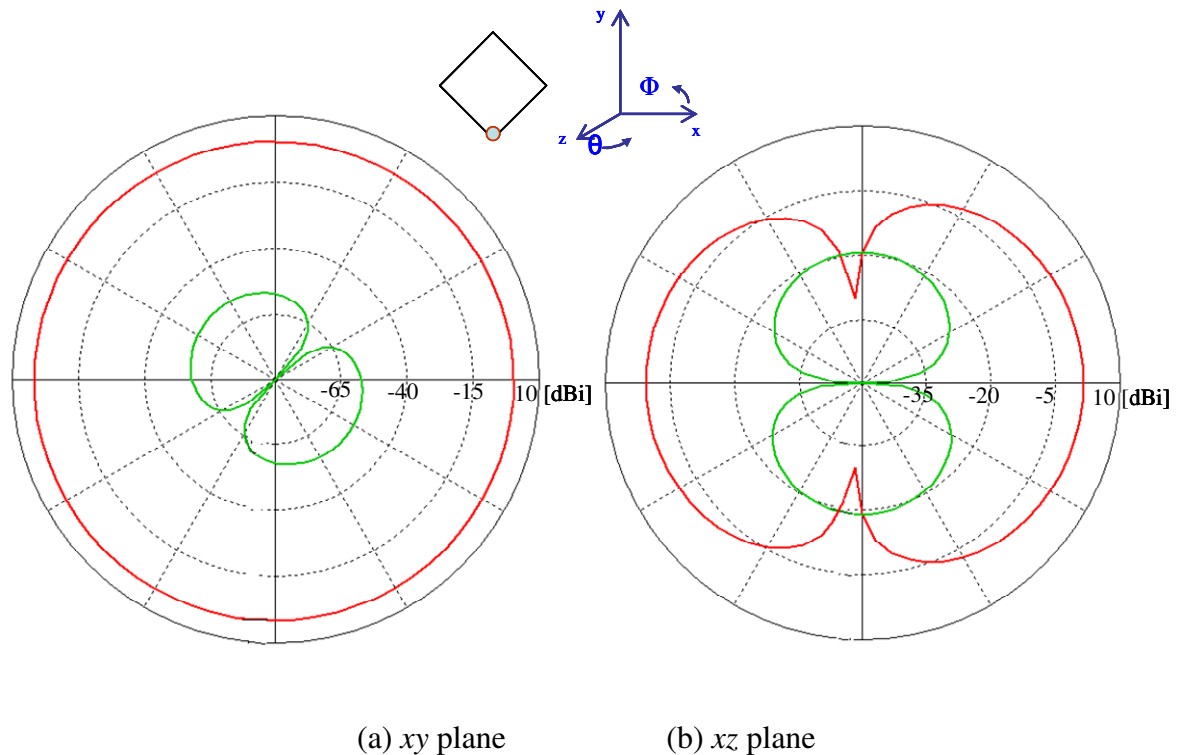


Figure 5-10. Simulated radiation patterns of the left handed loop antenna.

(Freq. = 546 MHz at the $n = 0$, Red line: E_ϕ , Green line: E_θ)

The measured radiation patterns in the xy and zx planes in the $n = 0$ mode, which was obtained at 500 MHz, are plotted in Figure 5-11. The coordinate system is shown in Figure 5-4. Measured patterns at 500 MHz show deviations of up to 3 dB from omnidirectional with cross polarisation below -20 dB in the plane of the loop (xy plane). Two nulls were also found in the zx plane. Agreement between simulation and measurement was relatively

good. The measured gain is 0.3 dB at 500 MHz. The measured gain is about 1 dB worse than the simulated result due to the extra loss from the balun and possible error during the measurements.

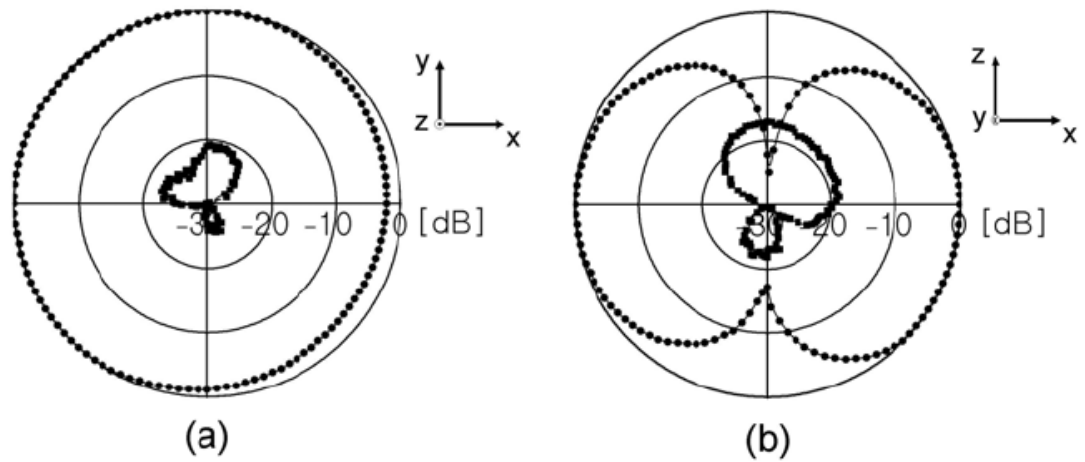


Figure 5-11. Measured radiation patterns of the left handed loop antenna.

(a) xy plane (b) zx , freq. = 500 MHz, $n = 0$. Circle symbol: E_ϕ , Square symbol: E_θ .

Table 5-2 Gain of the left handed loop antenna.

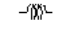
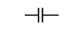

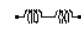
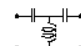
	Resonance frequency	Gain
Simulation	546MHz	1.4dBi
Measurement	500MHz	0.3dBi

d. Comparisons

The left handed loop antenna is also compared with other right handed periodically loading loop antennas. Table 5-3 shows results from simulations of loops with various right-handed and left-handed loading, operating in different modes. Efficiency was simulated using CST software. All loops have four unit cells with $L_L = 220$ nH and $C_L = 1$ pF. The C and L

equivalent circuits used were based on those recommended by the surface mount component manufacturer, Johanson [20] and contained loss resistances of the order of 1Ω . The loops all have a length of 600 mm and the unloaded dipole resonant frequency at $|n| = 2$ and $|n| = 4$ is 470 MHz and 900 MHz, respectively. Left-handed loading shows a matched input impedance and an efficiency of 93.77% in the $n = 0$ mode. In higher order modes, efficiency decrease significantly and input impedance becomes larger. Right-hand LC loading gives the greatest size reduction at $n = 2$ but the efficiency is very poor at 0.52%. Periodic inductive loading gives best efficiency at 50.36%, but worst input impedance than the other loadings.

Table 5-3. Simulated Performance of Loop Antennas with various Configurations Of unit Cell. (4 identical cells per loop, $L_L = 220$ nH, $C_L = 1$ pF) [16]

Unit cell			Frequency (MHz)	Impedance (Ω)	Efficiency (%)	Mode (n)
 $L_L/2$	$C_L/2$		-	-	-	0
			165	43	0.52	2
			252	102	12.24	4
 $L_L/2$		-	-	-	-	0
			226	79	50.36	2
			352	140	3.9	4
 $L_L/2$	$C_L/2$		550	50	93.77	0
			178	214	10.37	-2
			154	264	0.21	-4

5.2.3 Summary

A loop antenna using a ladder network with left-handed loading has been proposed. Various modes can be easily obtained in the loop. The antenna having one wavelength, λ_0 , circumference, gives an omnidirectional pattern in the plane of the loop, working in an $n = 0$ mode. In contrast, a conventional right-handed loop with the same dimensions has a figure of eight pattern in the plane of the loop. The antenna is compared to loops with other loading arrangements. The left-handed loading achieves good performance maintaining a 50Ω impedance matching without a high loss of efficiency. It is clear that the proposed left-handed antenna structure significantly extends the design degrees of freedom for loop antennas.

References

- [1] P. S. Hall and Q. Liu, "Dipoles and loop antennas with left handed loading," presented at 2008 Loughborough Antennas & Propagation Conference, Loughborough, UK, 17-18 March 2008.
- [2] Q. Liu, P. S. Hall, and A. Lucas-Borja, "Dipole with left handed loading with optimised efficiency," presented at 2nd European Conference on Antenna and Propagation, Edinburgh, UK, Nov. 2007.
- [3] R. W. Ziolkowski and A. Erentok, "Metamaterial-Based Efficient Electrically Small Antennas," *IEEE Trans. Antennas Propag.*, vol. 54, pp. 2113-2130, July 2006.
- [4] C. J. Lee, K. M. K. H. Leong, and T. Itoh, "Design of resonant small antenna using composite right/left-handed transmission line," presented at Proc. IEEE Antennas Propag. Society Int. Symp., Washington DC, USA, Jul.2005.
- [5] S. Otto, A. Rennings, C. Caloz, P. Waldow, and T. Itoh, "Composite right/left-handed λ -resonator ring antenna for dual-frequency operation," presented at Proc. IEEE Int. Symp. Antennas Propag., Washington, DC, Jul. 2005.
- [6] M. Schuessler, J. Freese, and R. Jakoby, "Design of compact planar antennas using LH-transmission lines," *IEEE Int. Symp. Microwave Theory and Tech.*, vol. 1, pp. 209-212, Jun. 2004.
- [7] H. Iizuka and P. S. Hall, "A left-handed dipole concept," presented at Proc. Int. Workshop on Antenna Tech., New York, USA, Mar. 2006.
- [8] H. Iizuka and P. S. Hall, "Left handed dipole antennas and their implementations," *IEEE Trans Ant and Prop.*, vol. 55, pp. 1246 - 1253, May 2007.

- [9] H. Iizuka, P. S. Hall, and A. Lucas Borja, "Dipole antenna with left handed loading," *IEEE Antenna, Propagation Wireless Letters*, vol. 5, pp. 483-485, Dec 2006.
- [10] C. A. Balanis, *Antenna Theory, Analysis, and Design*. New York: Wiley, 1982.
- [11] A. W. Rudge, K. Milne, A. D. Olver, and P. Knight, *Handbook of Antenna Design*, vol. 2: Peter Peregrinus Ltd., 1983.
- [12] A. Alford and A. Kandoian, "Ultra-high frequency loop antennae," *Electrical Communication*, vol. 18, pp. 255-265, 1940.
- [13] A. Fenn, "Arrays of horizontally polarized loop-fed slotted cylinder antennas," *IEEE Transactions on Antennas and Propagation*, vol. 33, pp. 375-382, 1985.
- [14] H. R. Chuang, "Omni-directional horizontally polarized Alford Loop Strip Antenna," *US patent 5,767,809*, June 1998.
- [15] C. C. Lin and H. R. Chuang, "A 2.4 GHz omni-directional horizontally polarized planar printed antenna for WLAN applications," presented at Proc. IEEE Int. Symp. Antennas Propag., Columbus, OH, Jul. 2003.
- [16] A. L. Borja, P. S. Hall, Q. Liu, and H. Iizuka, "Omnidirectional loop antenna with left-handed loading," *IEEE Antennas and Wireless Propag. Lett.*, vol. 6, pp. 495-498, Feb. 2007.
- [17] H. Iizuka and P. S. Hall, "Omnidirectional Left-Handed Loop Antenna," presented at IEEE AP-S International Symposium, Albuquerque, USA, July 2006.
- [18] A. Lai, C. Caloz, and T. Itoh, "Composite right/left-handed transmission line metamaterials," *IEEE Microw. Mag.*, vol. 5, pp. 34-50, Sep. 2004.
- [19] H. Iizuka and T. Watanabe, "Balanced Line to Unbalanced Line Transformer," *Japan Japanese patent 2005-198167*, Jan. 9, 2004.

- [20] "RF Ceramic Chip Inductors and Multi-Layer High-Q Capacitors datasheet,"
Johanson Technology, www.johansontechnology.com.

CHAPTER VI DUAL MODE RECONFIGURABLE LEFT HANDED LOOP ANTENNA

A loop antenna loaded with left-handed transmission lines has been presented. The zero order mode gives rise to omnidirectional patterns in the plane of the loop, with good input impedance matching and efficiency. The resonant frequency is controlled by the loading values, independent on the length of the antenna. It has been found through extensive simulations that increasing the required loading capacitor values decreases the resonance frequency at the relevant mode number [1]. Namely, different mode number can be obtained at the same resonance frequency with variation of capacitance of loading capacitors. Therefore, a tunable left handed loop antenna will be developed.

Left handed loop antennas can be used in vehicles for receiving radio, TV signals etc. The printed circuit board structure allows them mounting on glass or roof panel of vehicles. The dual mode loop antenna is specially designed for vehicle diversity application because the switchable patterns are capable against the multipath problem.

6.1 Configuration

The configuration of loop antenna using a left-handed transmission line is introduced above in Figure 5-2, [2]. There the two-wire transmission line is formed into a loop and fed at the break in the outer loop as shown. The loading is performed by inserting series capacitors and shunt inductances in a number of unit cells. Various modes can be obtained in the loop. An omnidirectional pattern in the plane of the loop with a null in the z axis is obtained while working in an $n = 0$ mode and a pattern with a null at $\phi = 45^\circ$ in the plane of the loop can be obtained in an $|n| = 2$ mode. (as shown in Figure 5-9)

Using tunable varactors instead of the capacitors in the loop antenna configuration, a varactor-loaded left handed loop antenna will be proposed with reconfigurable radiation patterns [3]. The antenna has two varactors in each unit cell and can provide dual required radiation patterns in the plane of the antenna at a constant frequency in the UHF band. One important point for the antenna is a bias technique for the varactors on antenna lines that does not degrade the radiation pattern.

The first prototype built in Birmingham of the dual mode reconfigurable loop antenna is shown in Figure 6-1. Eight varactors were loaded in the outer loop, and extra wires were added to provide DC voltage. However, the measured radiation pattern for this loop is unstable and distorted due to the extra radiation from the hanging down wires. So the design to integrate the bias circuit into the loop antenna is needed.

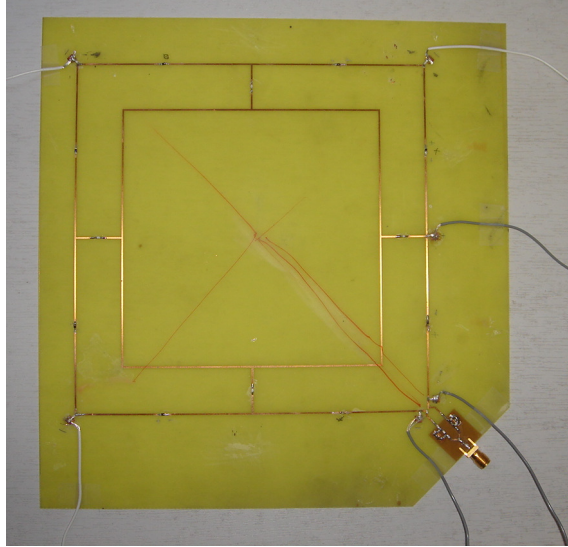


Figure 6-1. Prototype antenna of reconfigurable left handed loop.

The new configuration of the varactor-loaded loop antenna is shown in Figure 6-2 (a) and partial DC bias circuit is magnified in Figure 6-2 (b) to clarify the DC bias paths. Five slits were inserted on the strips of the outer loop so that the DC voltage may be supplied to the loaded varactors via the antenna lines. Some DC-isolation capacitors and RF-choke resistors were attached, with capacitance of 0.1 μ F and resistance of 10K Ω . In terms of RF design, the DC-isolation capacitors were loaded on the lines having slits so that each line works as one entity. In terms of DC, the slits divide the strip lines into two parts, where one could act as DC anode while the other act as DC cathode. Besides the RF-choke resistors short the same polarity parts together.

The parameters of the reconfigurable loop antennas are based on the original ones of the left handed loop antenna (Table 5-1). The antenna was implemented on FR4 substrate with a thickness of 0.8mm and a relative permittivity of 4.6. The size of the loop is 150 x 150 mm, with spacing between the wires of 20 mm, width of strip = 1.4 mm, number of unit

cells = 4 and loading inductor value of 220 nH. The width of the slits is chosen to be 0.2mm due to the technology limitation. The width of strips is set larger than the one in Table 5-1 for the need of components etching. Simulations will be compared between the loop with or without the slits.

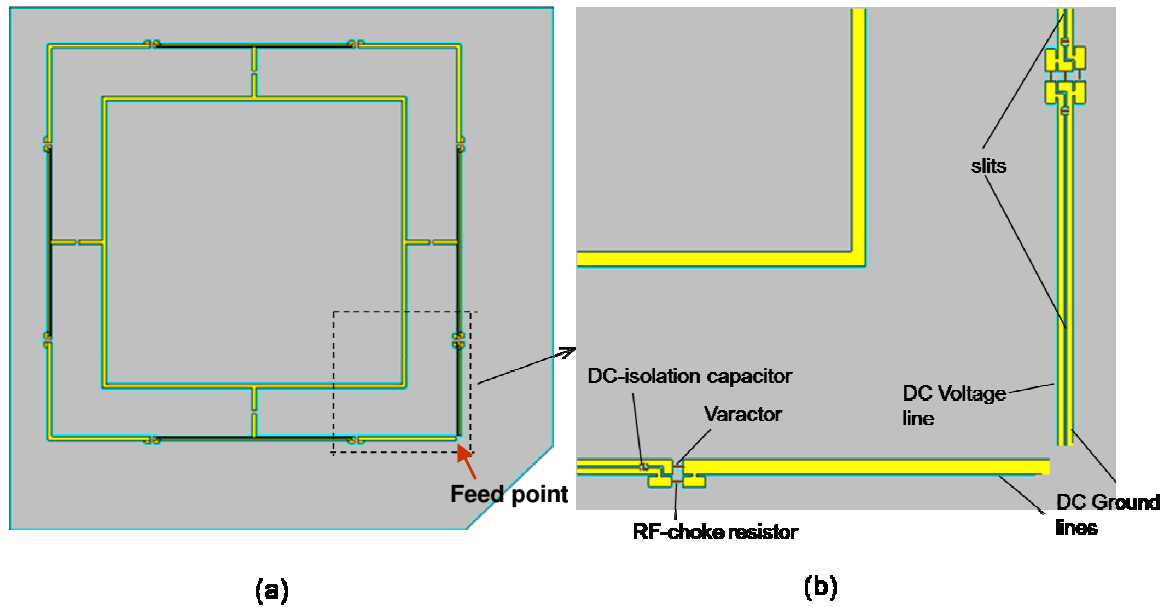


Figure 6-2. (a) Configuration of a varactor-loaded left handed loop antenna. (b) Partial DC bias circuit on antenna lines.

6.2 Performance

6.2.1 Simulation results

The antenna of Figure 6-2 in free space was numerically investigated by the commercial simulator CST [4]. First, simulations of return loss are compared between the loop with and without slits to verify the bias circuit. The capacitors are 1pF here. As shown in Figure 6-3, two curves of $|S_{11}|$ are close to each other. The bias circuit gives no extra effect on the original loop antenna in RF region.

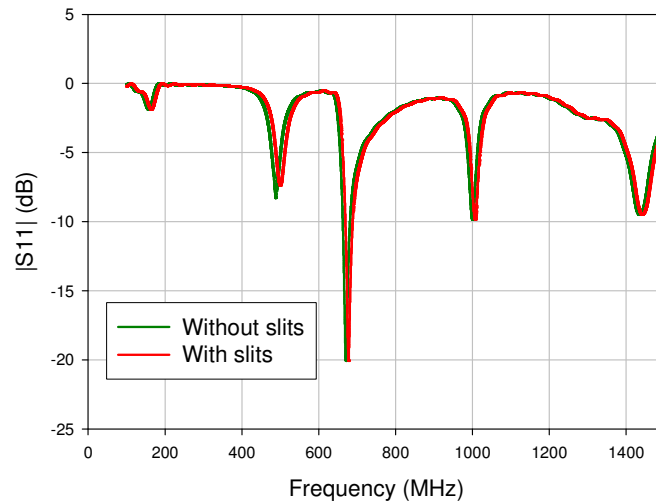


Figure 6-3. Comparison of the loop antenna return losses.

During the simulations, ideal capacitors with variation of the capacitance are applied. The antenna shows resonance frequency at 500 MHz in an $n = 0$ mode with loading capacitance equal to 1 pF. The resonant frequency is controlled by the loading values and the second order mode, $n = 2$ can be achieved at 500 MHz when the loading value of the capacitors is increased to 15 pF. The simulated results by CST for two values of capacitors are summarized in Table 6-1.

Table 6-1. Simulated results for the dual mode loop antenna.

C value	L value	At $n = 0$ mode				At $n = 2$ mode			
		Resonance	Imp.	Effic.	Gain	Resonance	Imp.	Effic.	Gain
1 pF	220 nH	500 MHz	104 Ω	62%	1dBi	670 MHz	53 Ω	70%	1.4dBi
15 pF	220 nH	Not clear				500 MHz	56 Ω	93%	1.9dBi

Figure 6-4 shows the simulated return loss characteristic in amplitude with the two capacitance values. Two modes $n = 0$ and $n = 2$ can be achieved for the loop antenna at 500 MHz with variation of the capacitance from 1 pF to 15 pF.

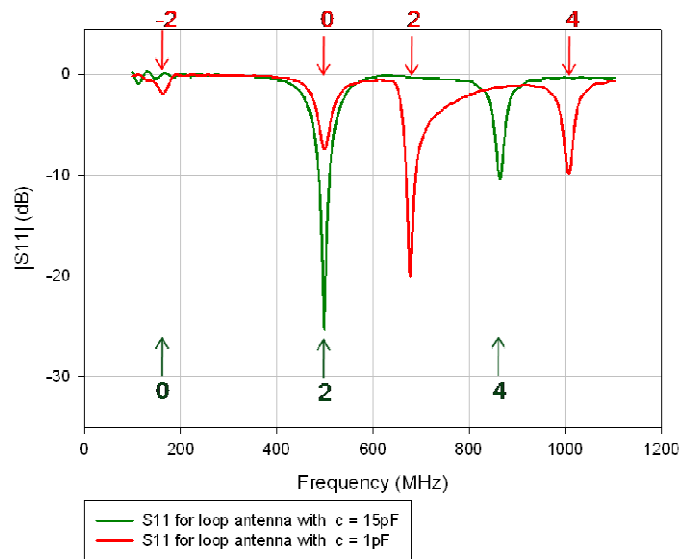


Figure 6-4. Simulated return loss in amplitude.

Near field distributions and far field radiation patterns of the loop antenna at two modes are shown in Figure 6-5 (a) and (b). The $n = 0$ mode gives a nearly uniform current distribution and an omnidirectional pattern with a null to z axis. The current distribution in the $n = 2$ mode has two peak waveforms, and will produce a pattern with a null at $\phi = 45^\circ$ in plane of the loop. Simulations show that efficiency in the $n = 0$ mode is 62% and in the $n = 2$ mode is 93%.

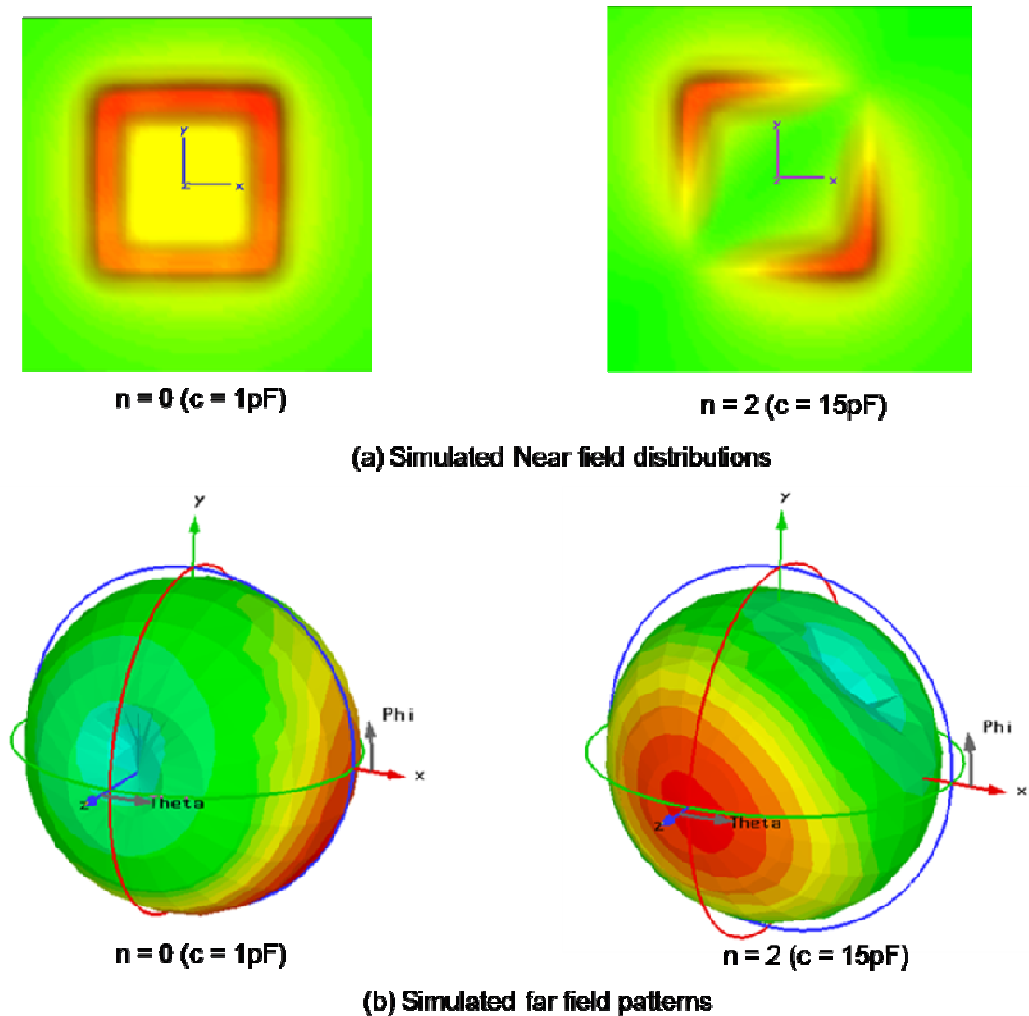


Figure 6-5. Simulated near and far field performances at 500 MHz.

6.2.2 Measurement results

A prototype antenna was built and measured to verify the numerical investigation presented above. The picture of the antenna is shown in Figure 6-6 (a) with a balun used to feed the antenna. The balun [5] consists of a high pass filter (HPF), low pass filter (LPF), and T junction. The configuration of the balun is indicated in Figure 6-6 (b) with the DC bias design. In terms of DC, the slits split each antenna strip into two parts, one of which is used as DC voltage supplying line for the varactors and the other part is DC ground line. During the measurements, a Bias Tee is connected at the unbalanced port of the balun with the network analyzer. From the balun's LPF side, DC voltage is inputted via the balanced port of the balun then passes through one part of the antenna strip while DC ground is through the other part. The DC ground line is also shorted with RF ground via the RF-choke resistor. The lumped element values set for the balun are the same as shown in Figure 5-5 to give 50 ohm impedance for the balanced port and 50 ohm for the unbalanced port and broad bandwidth.

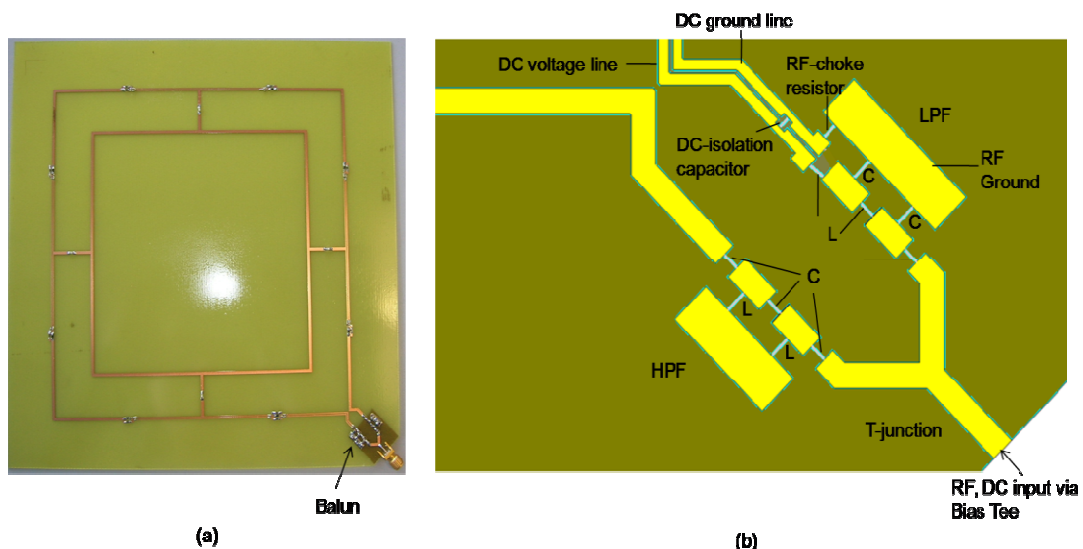


Figure 6-6. (a) Prototype antenna of varactor-loaded left handed loop.

(b) Configuration of the feeding balun.

Measured return loss performance is shown in Figure 6-7. The resonant frequency is controlled by the value of varactor. The zero mode was achieved at 452 MHz with varactors' capacitance equal to 1pF as shown in red line. Another mode, $n = 2$ was obtained at the same frequency when varactors were tuning to capacitance of 12 pF as shown in green line. There is 48 MHz frequency shift compared with simulated return loss in Figure 6-4 mainly due to the presence of the balun. It can also be seen that the measured plot drop down because of the extra loss from the balun, connectors, cables and Bias Tee during measurements.

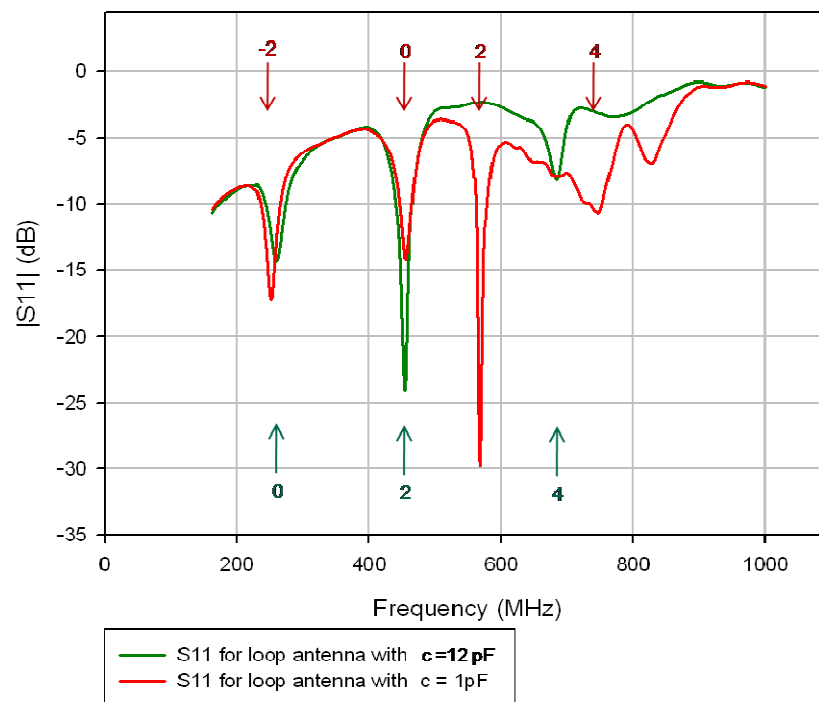


Figure 6-7. Measured return loss in amplitude.

Figure 6-8 shows simulated and measured radiation patterns in the plane of the loop in both $n = 0$ and $n = 2$ modes. It is a circle in the $n = 0$ mode and has two lobes with two nulls at $\phi = 45^\circ$ and 135° in the $n = 2$ mode. Agreement between simulation and

measurement was relatively good. In general the measurement results show that the validity of the numerical investigation is confirmed by the prototype antenna.

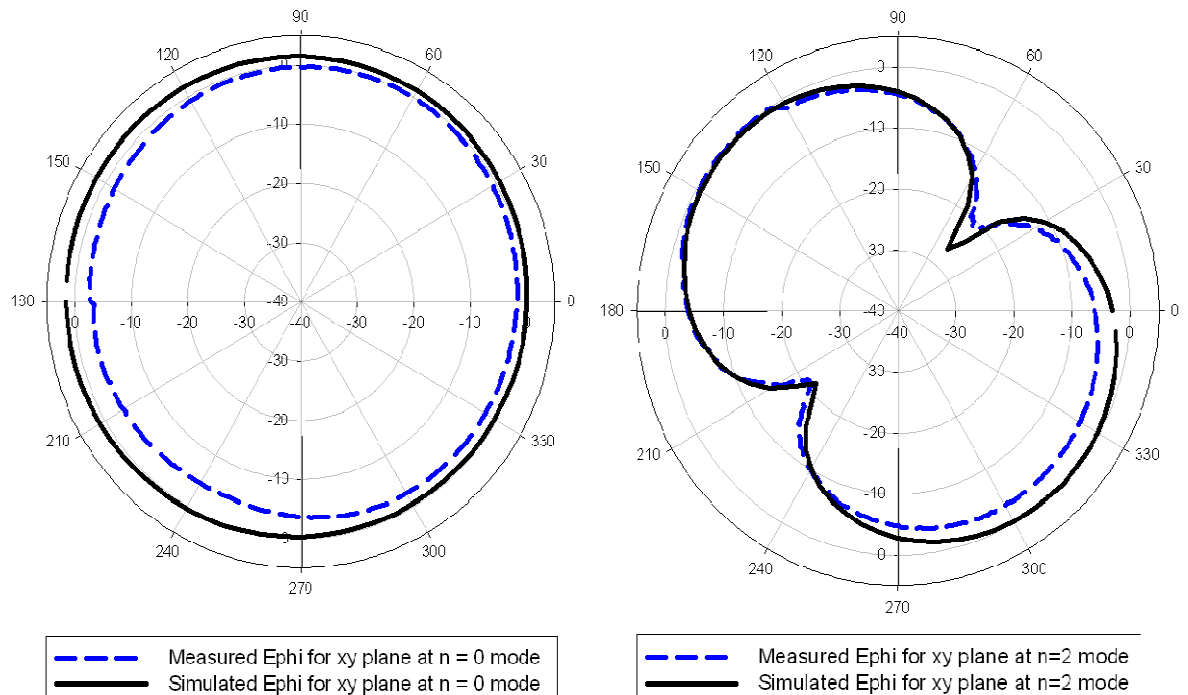


Figure 6-8. Radiation pattern in xy plane in $n=0$ and $n=2$ modes.

(Simulation: solid line; Measurement: dot line)

The measured gains are -0.1 dBi and 0.4 dBi for the $n=0$ and 2 mode at 452 MHz. Comparisons between the measurements and simulations are listed in Table 6-2. The gains are worse than the simulated results due to the extra loss from the balun and possible error during the measurements.

Table 6-2. Gain results of the reconfigurable left handed loop antenna.

	Resonance frequency	Gain	
		at $n = 0$ mode	at $n = 2$ mode
Simulation	500MHz	1dBi	1.9dBi
Measurement	452MHz	-0.1dBi	0.4dBi

6.3 Summary

A novel varactor-loaded left handed reconfigurable loop antenna is presented. By tuning the loading varactors, the loop gives an omnidirectional pattern with a null to z axis while working in the $n = 0$ mode and can switch to a pattern with a null at $\phi = 45^\circ$ in the plane of the loop in the $n = 2$ mode. A bias circuit has been designed for the varactors on antenna lines without degrading the radiation pattern. The prototype antenna shows good agreement between the simulated performances and the measured results. This switched pattern loop antenna could be used for vehicle diversity application.

References

- [1] H. Iizuka and P. S. Hall, "Left handed dipole antennas and their implementations," *IEEE Trans Ant and Prop.*, vol. 55, pp. 1246 - 1253, May 2007.
- [2] A. L. Borja, P. S. Hall, Q. Liu, and H. Iizuka, "Omnidirectional loop antenna with left-handed loading," *IEEE Antennas and Wireless Propag. Lett.*, vol. 6, pp. 495-498, Feb. 2007.
- [3] Q. Liu and P. Hall, "Varactor-loaded left handed loop antenna with reconfigurable radiation patterns," presented at IEEE International Symposium on Antennas & Propagation, Charleston, SC USA, 2009.
- [4] "CST Microwave Studio Tutorials," *Computer Simulation Technology*, www.cst.de, vol. Version 4, July 2002.
- [5] H. Iizuka and T. Watanabe, "Balanced Line to Unbalanced Line Transformer," *Japan Japanese patent 2005-198167*, Jan. 9, 2004.

CHAPTER VII CONCLUSIONS AND FUTURE WORK

7.1 Conclusions

The topic of this PhD research in 'Antennas using Left Handed Transmission Lines' makes use of the backward wave phenomenon to create some novel antennas that give practically useful size reduction and other new characteristics. Collaborators in this work at Toyota Research Center wish to put these novel designs on their cars. Metamaterials could give practically useful size reduction and be used to make an electrically small antennas. The printed circuit board structure allows antennas mounting on glass or in roof panel of cars.

This thesis presents a numerical and experimental study on the performance of linear antennas based on left-handed transmission lines. New features arising in their performance and various designs for optimised capability and useful applications for the two types of antennas, dipoles and loops, are summarised as follows.

7.1.1 Conclusions for Left Handed Dipoles

A dipole antenna using a left handed transmission line ladder network structure has been proposed. Simulation results have shown the unique feature of reduced wavelength of induced current with decreasing frequency, which is opposite to that of a conventional dipole of right-handed material. The resonance frequency and input impedance are controlled by loading element values, independent on the length of the antenna. The left-handed loading achieves a useful size reduction while maintaining a straightforward impedance matching with some loss of efficiency. Another important feature of this left handed behaviour is that at higher mode numbers, the antenna becomes electrically smaller

and hence has a well controlled radiation pattern. In a right handed antenna, higher order modes produce multi-lobed patterns due to their large electrical size. It is also shown that the relationship between bandwidth and the antenna size is the same as a conventional antenna.

The dipole antenna has been implemented by both lumped and distributed elements. With lumped elements, the dipole antenna of length $0.16 \lambda_0$ gave an efficiency of 16%. With the distributed elements, consisting of interdigitated capacitors and meandered line inductors, the efficiency was improved to 27% and measured gain of the antenna with balun was -3.9 dBi in an $n = -1$ mode. It was experimentally confirmed that the proposed antenna structure contributed to the reduction of the antenna size. However, loss remains a problem in left-handed dipoles.

A meandered left-handed dipole antenna working in an $n = -9$ mode is presented. It has been shown that this antenna structure produces orthogonal polarization to its length compared to an equivalent right-handed one. A prototype has been designed and constructed. Results confirm the good input matching and radiation pattern, although gain is low due to losses in the loading structure.

The efficiency of dipole antennas loaded with left handed transmission lines has been investigated and compared to conventional inductive loading. In a low order mode, the efficiency of L-loading dipole is better with low number of unit cell. If the number of cell increases, CL-loading presents comparable and even better performance. In a high mode the meandered left handed dipole gives the best efficiency due to the phase distribution,

presenting orthogonal polarization as well.

Optimized designs for improving left handed dipole efficiency have been developed. When parallel plate capacitors and spiral inductors are applied for low loss distributed loading the radiation efficiency improves substantially to 73.8% as compared to previous implementations and the improvement is experimentally validated. Some small improvement is found by non-linear loading along the dipole length.

It can be concluded that, in left handed dipoles, the loading results in size reduction, straightforward matching and the possibility of operating in higher order modes with well controlled radiation patterns. The use of higher order modes allows orthogonal polarisation to be obtained, which is thought to be a feature unique to these antennas. However, efficiency is low due to losses in the loading structure and the bandwidth is narrow. The dipole with optimized distributed loading presents the best performance in impedance and efficiency, even better than the conventional inductive loading.

7.1.2 Conclusions for Left Handed Loop Antennas

A loop antenna using a ladder network with left-handed loading has been proposed. Various modes can be easily obtained in the loop. The antenna having one wavelength circumference, gives an omnidirectional pattern in the plane of the loop, working in an $n = 0$ mode. In contrast, a conventional right-handed loop with the same dimensions has a figure of eight pattern in the plane of the loop. The antenna is compared to loops with other loading arrangements. The left-handed loading achieves good performance maintaining a 50Ω impedance matching without a high loss of efficiency.

A novel varactor-loaded left handed reconfigurable loop antenna is presented. By tuning the loading varactors, the loop gives an omnidirectional pattern with a null to z axis while working in the $n = 0$ mode and can switch to a pattern with a null at $\phi = 45^\circ$ in the plane of the loop in the $n = 2$ mode. A bias circuit has been designed for the varactors on antenna lines without degrading the radiation pattern. The prototype antenna shows good agreement between the simulated performances with the measured results.

It can be concluded that various modes can be obtained in a left handed loop antenna. The zero order mode gives rise to omnidirectional patterns in the plane of the loop, with good efficiency. A novel dual mode reconfigurable loop antenna can be achieved with varactors loaded. The loop gives an omnidirectional pattern with a null to z axis while working in an $n = 0$ mode and a pattern with a null at $\phi = 45^\circ$ in the plane of the loop in an $n = 2$ mode. The dual mode loop antenna could be used in vehicle diversity application because the switchable patterns are capable against the multipath problem.

7.2 Future Work

As we know, left handed transmission lines applying to antenna design give rise to many new features, such as size reduction and impedance matching. However, the potential tradeoff is poor efficiency due to extra loading, and it's not sufficient for practical use. Efficiency improvement is an important further study for left-handed antenna design. The study on distributed inductor and capacitor design for low loss has been developed. Some alternative ways can be investigated in the future.

- The gain approaches the Harrington limit only if the antenna efficiently utilizes the available volume within the enclosed sphere. It has been shown that the efficiency is increased when the CL-loaded dipole is meandered. Thus variations in the transmission line loading architecture may be effective, such as bending the dipole or loop.
- Amplifiers could be used to overcome loss, as in the microstrip based right/left-handed leaky wave antenna [1].

Efficiency and bandwidth are two key aspects in the practical realization of small antennas. This thesis presents a systematic study on the efficiency of linear antennas based on left-handed transmission lines. However bandwidth of small left-handed antennas is still narrow. External matching network for broadband has been investigated for the electrically small left handed loading antennas. However, the result is not obvious. An alternative way of using varactors in the loading is possible to obtain a tunable antenna operating in a wide frequency range in both left-handed and right-handed fundamental modes. Attention should be paid for two points. Firstly, different varactor values need to be chosen to

produce no gaps between the resonances. Secondly, a good matching for all the modes has to be obtained.

It has been found that the use of meandered left-handed dipole structure allows orthogonal polarisation to be obtained at a higher order modes. To build a circularly polarized antenna using CRLH transmission line can be carried out in the future. A possible configuration of circular polarized antenna is shown in Figure 7-1, in which a switcher or 90 degree phase shifter is used for switching the polarization among co, cross, or circular ones.

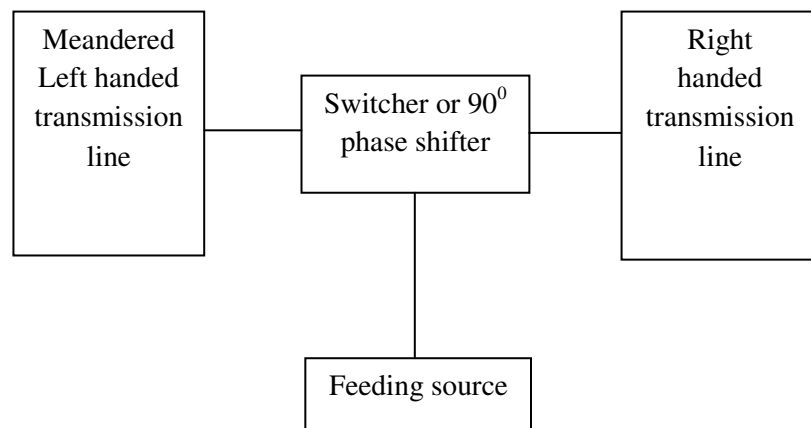


Figure 7-1. Configuration of circular polarization antenna.

References

- [1] F. P. Casares-Miranda, C. Camacho-Penalosa, and C. Caloz, "High-gain active composite right/left-handed leaky-wave antenna," *IEEE Trans. Antennas Propag.*, vol. 54, pp. 2292-2300, Aug. 2006.

APPENDIX A TELEGRAPHER'S EQUATIONS

The Telegrapher's Equations [1] are a pair of linear differential equations which describe the voltage and current on an electrical transmission line with distance and time. They were developed by Oliver Heaviside [2] who created the transmission line model, and are based on Maxwell's Equations. Following sections A.1-A.4 are mostly selected from [1,2].

A.1. Lossless Transmission Line

Based on the transmission line model, each short segment of the transmission line consists of a series resistor R , a series inductor L , a shunt capacitor C , and a shunt conductance G .

The line voltage $V(x)$ and the current $I(x)$ can be expressed in the frequency domain [1] as:

$$\frac{\partial V(x)}{\partial x} = -(R + j\omega L)I(x) \quad (\text{A.1})$$

$$\frac{\partial I(x)}{\partial x} = -(G + j\omega C)V(x) \quad (\text{A.2}).$$

When the elements R and G are negligibly small the transmission line is considered as a lossless structure. In this hypothetical case, the model depends only on the L and C elements which greatly simplifies the analysis. For a lossless transmission line, the second order steady-state (assuming a sinusoidal wave $E = E_0 \cdot e^{-j\omega(\frac{x}{c}-t)}$) Telegrapher's equations [1] are:

$$\frac{\partial^2 V(x)}{\partial x^2} + \omega^2 LC \cdot V(x) = 0 \quad (\text{A.3})$$

$$\frac{\partial^2 I(x)}{\partial x^2} + \omega^2 LC \cdot I(x) = 0 \quad (\text{A.4}).$$

These are wave equations which have plane waves with equal propagation speed in the forward and reverse directions as solutions. The physical significance of this is that electromagnetic waves propagate down transmission lines and in general, there is a

reflected component that interferes with the original signal. These equations are fundamental to transmission line theory [1, 3, 4].

A.2 Lossy Transmission Line

When the loss elements R and G are not negligible, the original differential equations describing the elementary segment of line become [1]

$$\frac{\partial}{\partial x}V(x,t) = -L\frac{\partial}{\partial t}I(x,t) - RI(x,t) \quad (\text{A.5})$$

$$\frac{\partial}{\partial x}I(x,t) = -C\frac{\partial}{\partial t}V(x,t) - GV(x,t) \quad (\text{A.6}).$$

By differentiating the first equation with respect to x and the second with respect to t , and some algebraic manipulation, we obtain a pair of hyperbolic partial differential equations each involving only one unknown [1]:

$$\frac{\partial^2 V(x)}{\partial x^2} = \Gamma^2 V(x) \quad (\text{A.7})$$

$$\frac{\partial^2 I(x)}{\partial x^2} = \Gamma^2 I(x) \quad (\text{A.8})$$

where

$$\Gamma = \sqrt{(R + j\omega L)(G + j\omega C)} \quad (\text{A.9}).$$

Note that these equations resemble the homogeneous wave equation with extra terms in V and I and their first derivatives. These extra terms cause the signal to decay and spread out with time and distance. If the transmission line is slightly lossy (small R and $G = 0$), signal strength will decay over distance as $e^{-\alpha x}$, where $\alpha = R/2Z_0$ and the characteristic impedance is:

$$Z_0 = \sqrt{\frac{R + j\omega L}{G + j\omega C}} \quad (\text{A.10}).$$

The solutions for $V(x)$ and $I(x)$ are [1]:

$$V(x) = V_+ e^{-\Gamma x} + V_- e^{\Gamma x} \quad (\text{A.11})$$

$$I(x) = \frac{1}{Z_0} (V_+ e^{-\Gamma x} - V_- e^{\Gamma x}) \quad (\text{A.12}).$$

The constants V_{\pm} and I_{\pm} must be determined from boundary conditions. For a voltage pulse $V_{in}(t)$, starting at $x = 0$ and moving in the positive x -direction, then the transmitted pulse $V_{out}(x, t)$ at position x can be obtained by computing the Fourier Transform, $\tilde{V}(\omega)$, of $V_{in}(t)$, attenuating each frequency component by $e^{-\text{Re}(\Gamma)x}$, advancing its phase by $-I_m(\Gamma)x$, and taking the inverse Fourier Transform [5].

A.3 Input Impedance of a Transmission Line

The characteristic impedance Z_0 of a transmission line is the ratio of the amplitude of a single voltage wave to its current wave. Since most transmission lines also have a reflected wave, the characteristic impedance is generally not the impedance that is measured on the line.

For a lossless transmission line, it can be shown that the impedance measured at a given position l from the load impedance Z_L is

$$Z_{in}(l) = Z_0 \frac{Z_L \cos(kl) + Z_0 j \sin(kl)}{Z_0 \cos(kl) + Z_L j \sin(kl)} \quad (\text{A.13})$$

where $k = \frac{2\pi}{\lambda}$ is the wave number [1].

For the special case where $kl \approx n\pi$ where n is an integer (meaning that the length of the line is a very close to a multiple of half a wavelength), the expression reduces to the load impedance so that $Z_{in} = Z_L$ for all n . This includes the case when $n = 0$, meaning that the length of the transmission line is negligibly small compared to the wavelength. The

physical significance of this is that the transmission line can be ignored (i.e. treated as a wire) in either case [1].

Another special case is when the load impedance is equal to the characteristic impedance of the line (i.e. the line is matched), in which case the impedance reduces to the characteristic impedance of the line so that $Z_{in} = Z_0$, for all l and all λ .

In calculating k , the wavelength is generally different inside the transmission line to what it would be in free-space and the velocity constant of the material the transmission line is made of needs to be taken into account when doing such a calculation [4].

A.4 Direction of Signal Propagations

The wave equations above indicate that there are two solutions for the travelling wave: one forward and one reverse. Assuming a simplification of being lossless (requiring both $R=0$ and $G=0$) the solution can be represented as [6]:

$$V(x,t) = f_1(\omega t - kx) + f_2(\omega t + kx) \quad (\text{A.14})$$

where:

$$k = \omega \sqrt{LC} = \frac{\omega}{v} \quad (\text{A.15})$$

k is the wave number and has units of radians per meter,

ω is the angular frequency (in radians per second),

f_1 and f_2 can be any functions whatsoever, and

$v = \frac{1}{\sqrt{LC}}$ is the waveform's speed of propagation.

f_1 represents a wave traveling from left to right in a positive x direction whilst f_2 represents a wave traveling from right to left. It can be seen that the instantaneous voltage at any point x on the line is the sum of the voltages due to both waves.

Since the current I is related to the voltage V by the telegrapher's equations, we can write

$$I(x,t) = \frac{f_1(\omega t - kx)}{Z_0} - \frac{f_2(\omega t + kx)}{Z_0} \quad (\text{A.16})$$

where Z_0 is the characteristic impedance of the transmission line, which, for a lossless line is given by $Z_0 = \sqrt{\frac{L}{C}}$ [7].

APPENDIX B ANTENNA PARAMETERS

Antenna, which serves as the transducer between the controlled energy within the system and the radiated energy in free space, is the key element in today's wireless communication systems. There are several critical parameters affecting an antenna's performance, such as return loss, input impedance, radiation pattern, gain, antenna efficiency, and polarization etc. The importance of each parameter is very dependent on the antenna application. Some fundamental antenna parameters which are related to this work will be introduced next.

B.1 Return loss

Scattering Parameters [8], or s-parameters, are the reflection and transmission coefficients between the incident and reflection voltage waves mostly operating at radio frequency and microwave frequencies. S-parameters change with the measurement frequency and each parameter is typically characterized by magnitude and phase. The expression in decibels is $20\log(S_{ij})$ because s-parameters are voltage ratios of the waves. The return loss S_{11} represents the input reflection coefficient of the antenna and is mostly concerned in this work.

The return loss S_{11} of an antenna can be regarded as a measure of the ratio between the power reflected back from the antenna feeding point to that fed to the antenna at a particular frequency or band of frequencies. When a transmission line is terminated with the load impedance, Z_L , which is not equal to the characteristic impedance of the transmission line, Z_0 , not all the incident power is transmitted into the termination. Part of the incident power is reflected back so that phase addition and subtraction of the incident and reflected waves creates a voltage standing wave on the transmission line. The return loss is related voltage standing wave ratio (VSWR) defined as the following equations:

$$S_{11} = \frac{V_{\text{reflected at port1}}}{V_{\text{towards port1}}} = \Gamma = \frac{Z_{\text{input}} - Z_0}{Z_{\text{input}} + Z_0} \quad (\text{B.1})$$

Where Γ is the reflection coefficient, Z_{input} is antenna input impedance, and Z_0 is characteristic impedance (typically=50Ω). The return loss in dB is calculated from:

$$\text{Return loss (dB)} = -10\log\Gamma^2 = -20\log\Gamma. \quad (\text{B.2})$$

A typical return loss S_{11} magnitude in decibel for a dipole antenna obtained by using software CST Microwave Studio [9] is shown in Figure B-1. Theoretically, if the entire power is reflected back, S_{11} will be 0 dB. While if the power is completely absorbed and radiated by the antenna, the value will be $-\infty$ dB. A low return loss value, usually lower than -10 dB, corresponds to a good matching at the specific frequency. A $|S_{11}| < 10$ dB bandwidth is considered as the useful band in this work, which indicates a 10% power reflection, and the minimum dB value point is defined as the centre resonant frequency.

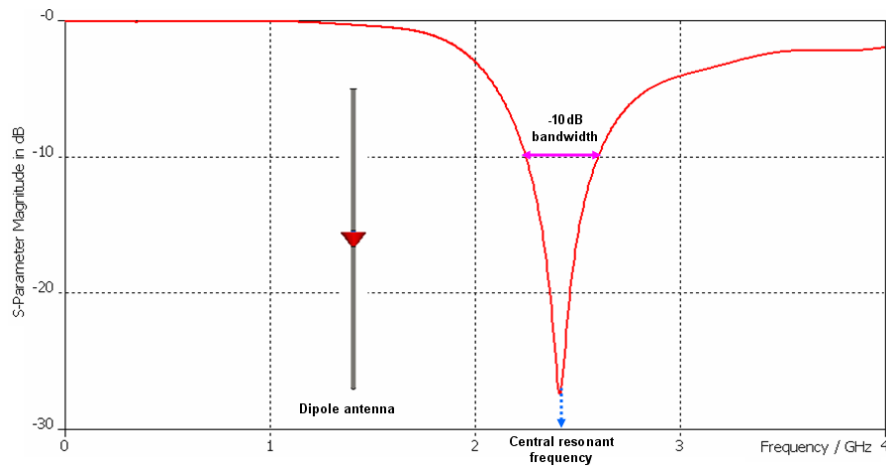


Figure B-1. Return Loss ($|S_{11}|$) of a dipole antenna at 2.4 GHz.

B.2 Input Impedance

Input impedance is defined as “the impedance presented by an antenna as its terminals or the ratio of the voltage to current at a pair of terminals or the ratio of the appropriate components of the electric to magnetic fields at a point” [10]. It can represent the antenna as part of a circuit or network.

During antenna design, the input impedance should exactly match the output impedance of the source for maximum power transfer. The input impedance of an antenna is generally a function of frequency. Therefore, the antenna generally matches to the interconnecting transmission line and other associated terminal only within a bandwidth. The impedance

match performance can be determined by the amount of power reflected back at the port of the antenna. It is related to the reflection coefficient Γ at the input of the antenna as

$$|\Gamma|^2 = \frac{P_{reflect}}{P_{incident}} = \frac{|Z_{input} - Z_c|^2}{|Z_{input} + Z_c|^2} \quad (\text{B.3})$$

where Z_{input} is the antenna's complex input impedance and Z_c is the characteristic impedance of the transmission line [11].

B.3 Radiation Pattern

Radiation pattern of an antenna is the graphical representative of antennas radiation properties in the spatial domain. According to the space coordinates, antenna radiation properties can be measured in three regions: (a) reactive near-field, (b) radiating near-field and (c) far-field region [10]. Only within the far-field region, the angular field distribution of an antenna is independent of the distance from the antenna. The far-field region is conventionally given when the distance away from the antenna is greater than $2D^2/\lambda$, where D is largest dimension of the antenna and λ is operating wavelength. In general, the radiation pattern is determined by the far-field radiation properties and is represented as a function of the directional coordinates.

The radiation pattern is three-dimensional, and can be displayed in a meaningful manner of 2D cutting planes. For antennas with linear polarization properties, the radiation properties are generally described in terms of their principle E-plane and H-plane. The E-plane is a cutting plane which is associated with the electric field vectors, and the H-plane is associated with the magnetic field vectors.

B.4 Directivity and Gain

Two other antenna parameters which can be derived from the radiation pattern properties are directivity, D and antenna gain, G . The directivity is a measure of how strongly the antenna pattern is focused in the particular direction of its maximum reception sensitivity compared to other directions. It is defined as “the ratio of the radiation intensity in the peak

intensity direction to the averaged radiation intensity in all other directions” [10]. The definition can be expressed as

$$D(\theta, \phi) = \frac{\text{power radiated per unit solid angle}}{\text{average power radiated per unit solid angle}} \quad (\text{B.4})$$

Antenna gain is a measure of the directive property of the antenna, and indicates how efficiently the antenna transforms available input power into radiating power as compared to a referenced antenna element in a particular direction [10]. It is usually measured in units of dBi (decibels as referenced to an isotropic antenna element) or dBd (decibels as referenced to a dipole antenna element, where 0 dBd = 2.1 dBi). It can be expressed as

$$G(\theta, \phi) = \frac{\text{power radiated per unit solid angle}}{\text{input (accepted) power}} \quad (\text{B.5})$$

B.5 Polarization

Polarization is the sum of the electric field (E-plane) orientations over time projected onto an imaginary plane perpendicular to the direction of motion of the radio wave [10]. Antenna polarization is determined by the physical structure of the antenna and by its orientation. In the most general case, polarization is elliptical (the projection is oblong), meaning that the antenna varies over time in the polarization of the radio waves. Two special cases are linear polarization when the ellipse collapses into a line and circular polarization in which the ellipse varies maximally.

The polarization is expressed with reference to the electric field. Co-polarization is the polarization in which the antenna is intended to radiate. Cross-polarization is the measure of discrimination to oppositely polarized electromagnetic waves (e.g. the discrimination that a vertically polarized antenna has to horizontally polarized radio waves or the polarization orthogonal to a specified reference polarization). When plotted along with the principal plane pattern of the antenna on a relative dB scale, cross-polarization is simply the difference between the co-polarized level and the cross-polarized level in any given direction.

APPENDIX C CST MICROWAVE STUDIO

Simulation plays an essential role regarding the evaluation and expectation of the antenna characteristics and behaviour. The main commercial simulation software employed in this work is CST Microwave Studio[®], which is the product of CST-Computer Simulation Technology [9]. The software package will be briefly introduced briefly from its user manual, as well as the fundamental theory behind them.

CST Microwave Studio[®] is a fully featured electromagnetic software package based on the Finite Integration Technique (FIT). This numerical method provides a universal spatial discretization scheme, applicable to various electromagnetic analysis and design, ranging from static field calculations to high frequency applications whether in time or frequency domain.

The background theory of CST Microwave Studio so called Finite Integration Technique was first introduced by Weiland in 1977 [12]. FIT discretizes the *integral* form of Maxwell's equations, rather than the differential one which is employed by Finite Difference Time Domain (FDTD) method. The FIT equations are presented in Equation (B.1).

$$\text{Faraday's Law: } \oint_{\partial A} \vec{E} \cdot d\vec{s} = - \int_A \frac{\partial \vec{B}}{\partial t} \cdot d\vec{A}$$

$$\text{Ampere's Law: } \oint_{\partial A} \vec{H} \cdot d\vec{s} = \int_A \left(\frac{\partial \vec{D}}{\partial t} + \vec{J} \right) \cdot d\vec{A}$$

$$\text{Gauss's Law for electricity: } \oint_{\partial V} \vec{D} \cdot d\vec{A} = \int_V \rho \cdot dV$$

$$\text{Gauss's Law for magnetism: } \oint_{\partial V} \vec{B} \cdot d\vec{A} = 0 \quad (\text{C.1})$$

E [V/m] =electric field vector; B [Wb/m²] =magnetic flux density vector;

H [A/m] =magnetic field vector; D [C/m²] =electric flux density vector;

J [A/m²] = displacement current density; ρ [C/m³] =volume charge density.

In order to solve these equations numerically, a finite calculation domain must be defined, enclosing the necessary space region. The next step is to decompose the computational domain into a finite number of tetra- or hexahedra unit cells, and electric and magnetic field vectors can be aligned on the facet of these cells, as shown in Figure C-1. Under the decomposition, all the cells have to fit exactly to each other. This decomposition yields the finite simplified cells complex G , which serves as computational grid [13]. The spatial discretization of Maxwell's equations is finally performed on these grid systems. The calculation process is repeated for all grid cells within the boundary until the desired accuracy is reached.

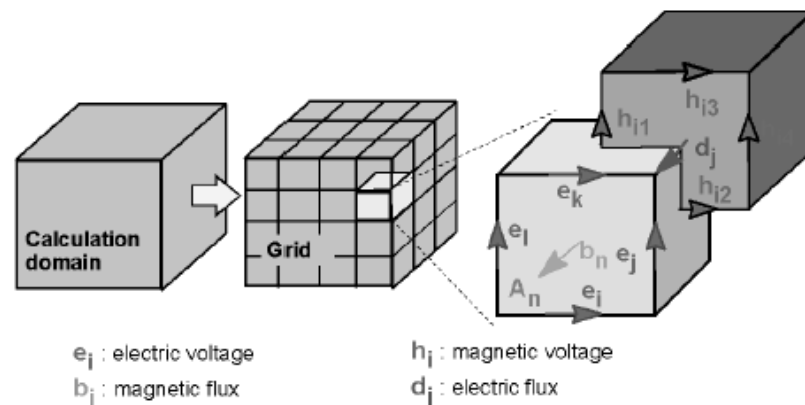


Figure C-1. Decomposition of the computational domain in FIT [14].

CST Microwave Studio contains three different simulation tools (transient solver, frequency domain solver, eigenmode solver) to best fit particular applications. The most flexible tool, transient solver, is a time domain simulator, which is also the mainly used solver in this project. It is remarkably efficient for the most kinds of high frequency applications. The entire broadband frequency behaviour of the simulated object can be obtained from only one calculation run. CST is also distinctive on its windows-based operating interface and graphic feedback for the definition of object that is being developed. Another outstanding feature of CST is that the mesh properties can be very flexible. The mesh of an objective can be defined in high density to achieve high accuracy result, or sub-grid mesh system can be used to save computational resources when processing electrically large objects.

Like other 3-D full wave simulation softwares, there are some disadvantages in CST Microwave Studio. For example, the software is based on a method which requires the discretization of the entire calculation volume; therefore the application is limited by the electrical size of the structure. In general, CST Microwave Studio is a reliable software tool for most microwave applications.

APPENDIX D ANTENNA MEASUREMENT

D.1 Background to Antenna measurement

Antenna measurement is an important part for evaluating and verifying an antenna's performance during the designing procedure. All the antennas can be specified by a common set of parameters. Typical parameters used in antenna evaluation include the input impedance, polarization, radiation pattern, radiation efficiency and gain. All of these parameters can be measured through various means. I would like to thank my colleague Mr. Wei Zhang for providing me the Figure D-1, D-2 and D-3.

D.2 Antenna Test Range

The choice of an antenna test range depends on many factors, such as the directivity of the antenna under test, frequency range and desired test parameters. Often the physical features of the antenna (size, weight and volume) can also have influence on the selection of an antenna range. During selecting an antenna range to evaluate antenna performance, care must be taken to ensure the performance metrics are measured with sufficient accuracy. Some commonly used antenna test ranges are shown in the Figure D-1.

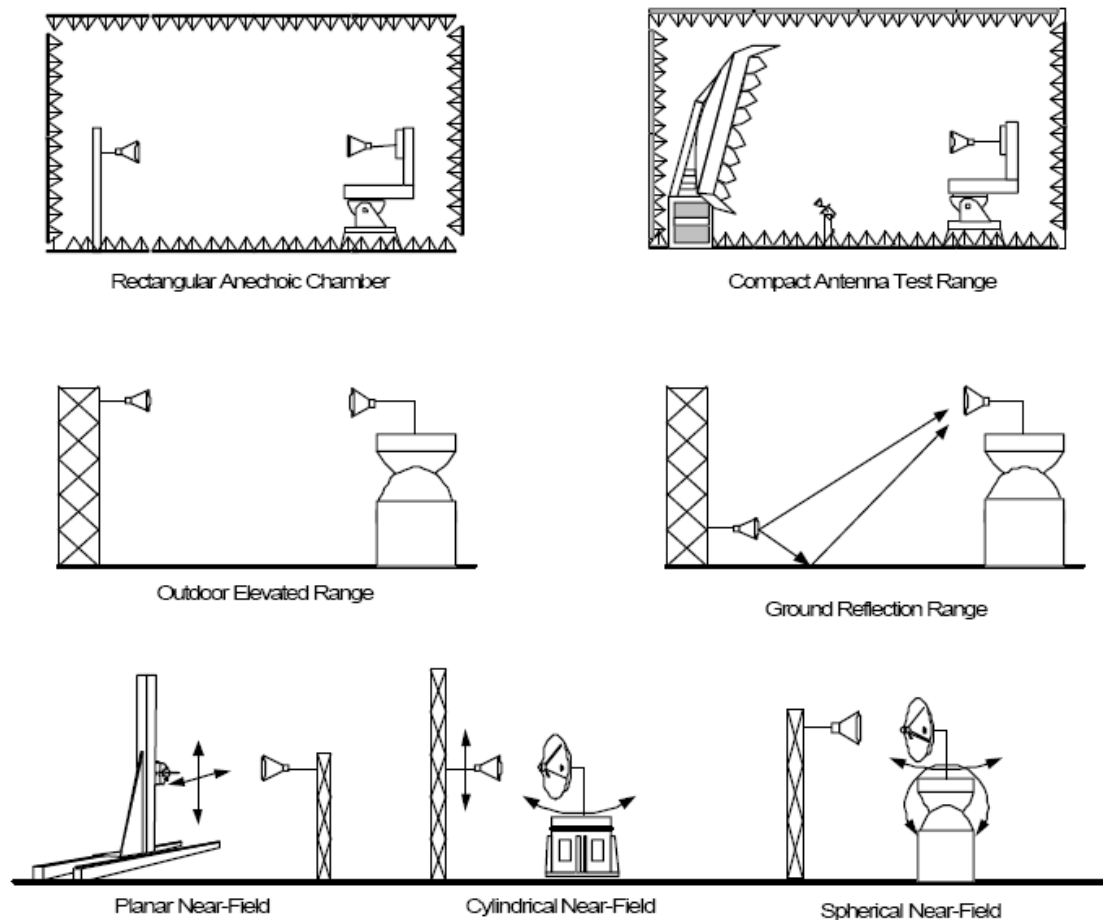


Figure D-1 Antenna test ranges.

D.3 Antenna Range Instrumentation

Regardless of the type of antenna range to be chosen, the instruments which operate the range are very similar. The instrumentation for antenna measurement consists of four subsystems:

1. Positioning and Control
2. Signal Source
3. Receiving
4. Recording and Processing.

The test antenna is installed on a positioner and is usually tested as the receiving mode. The motion of the positioner, such as rotation of the test antenna, is controlled by a positioner control device which is usually located in the control room. The positioner

control device provides position data for the positioner and the recording/processing subsystem.

A signal source provides the RF signal for the remote receiving antenna. The signal source can be permanently fixed on the ground or floor, or located on a table near the source antenna, depending on the frequency of operation and mechanical considerations. The source control device is usually located in the control room with the measurement and control instrumentation.

To process the received signal for recording, microwave receivers are employed on the antenna range to accept the receiving signals from the test antenna and to convert these signals to lower frequencies for processing. Since the signals are usually low level, microwave receivers offer many advantages including improved dynamic range, better accuracy, and rejection of unwanted signals that may be present in the area.

Data storage is conveniently handled by a variety of media including a floppy disk, local hard drive, removable drives or bulk data storage on a local network. After data acquisition is completed, an analysis software can plot the measured data, such as return loss, radiation pattern, gain, and so on, into a variety of data plotting formats such as rectangular, polar and three-dimensional plots.

Often, a computer subsystem is added to the instrumentation to automate the entire measurement procedure.

D.4 Typical Applications of Antenna Range Instrumentation

D.4.1 Near-Field Range

Near-field ranges are used where large antennas are to be tested indoors in a relatively small space. This type of range uses a small RF probe antenna that scans over a surface surrounding the antenna under test. Typically separation between the probe and the antenna structure is about 4 to 10 wavelengths. During the measurement, near-field amplitude and phase information is collected over a discrete matrix of points. This data is then transformed to the far-field using Fourier techniques. The resulting far-field data can then

be displayed in the same formats as conventional far-field antenna measurements. Near-field ranges usually are configured for automatic control. Both the large numbers of measurements and the need of transformation from the near-field data to the far-field, require the use of a computer system for data acquisition, reduction and display. The antenna may be tested in the transmit mode, receive mode, or both.

There are many scanning coordinate systems possible for collecting the near-field data.

Three techniques are in common usage:

1. Planar Near-Field Method
2. Cylindrical Near-Field Method
3. Spherical Near-Field Method

The Figure D-2 is one example of a planar near-field application where the test antenna is to be tested in both transmit and receive modes.

control, so a single positioner control unit is used to control all the range axes as well as the short range length.

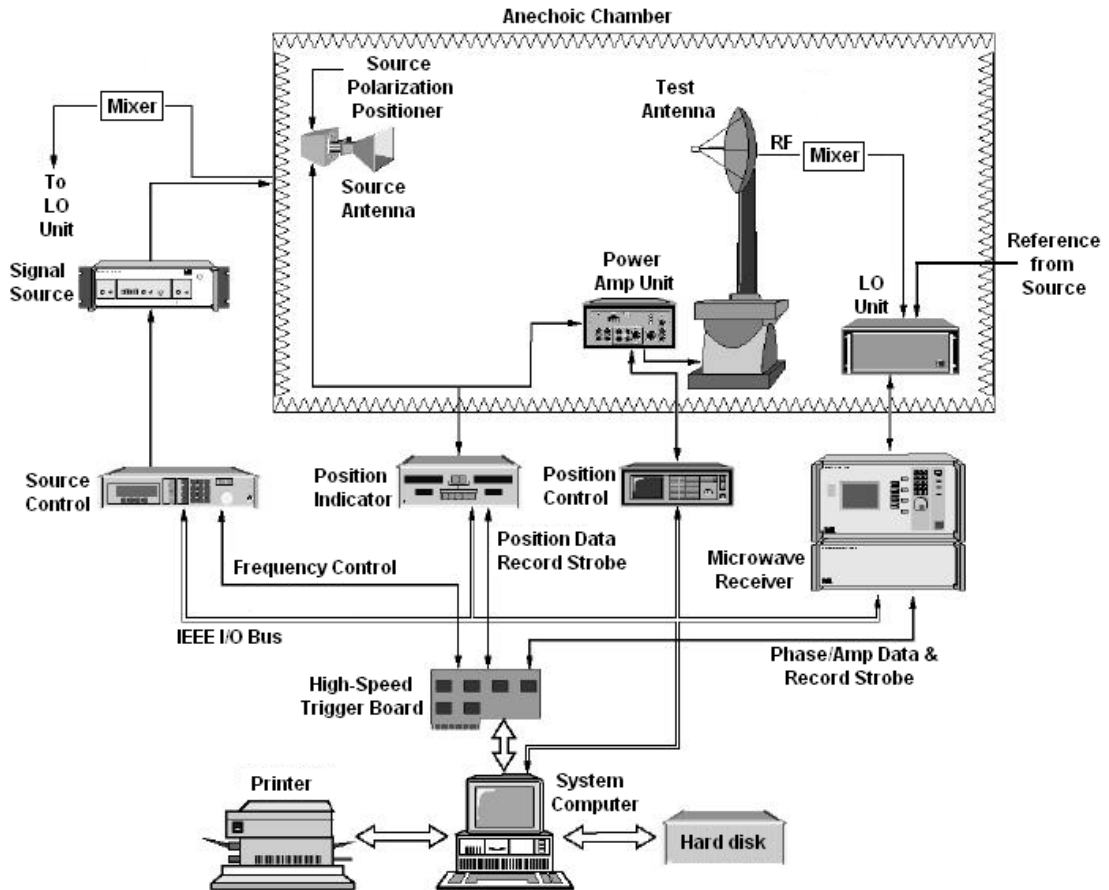


Figure D-3. Indoor Far-Field Range.

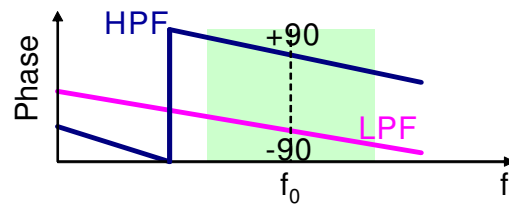
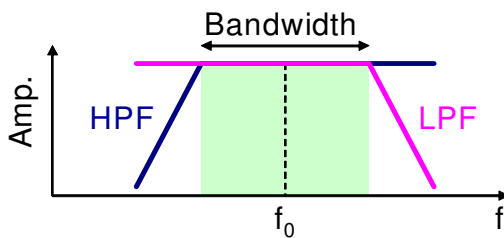
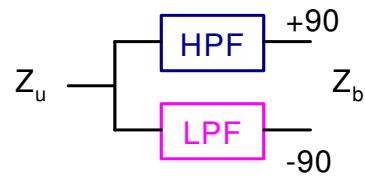
APPENDIX E WIDEBAND LC BALUN

I would like to thank Dr. H. Iizuka from Toyota Research Centre for providing me the contents in Appendix E.

Concept of wideband LC balun

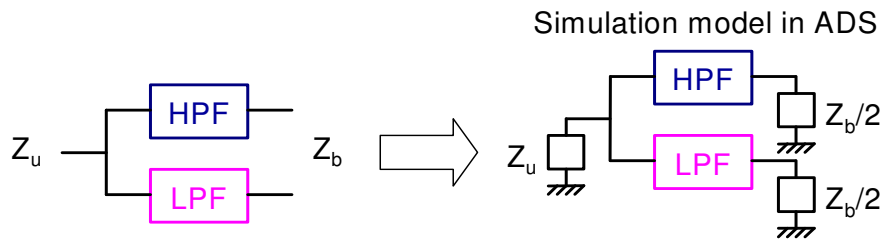
I have a patent (J.P. patent 2005-198167) in Japan.
But the document is written in Japanese. I have not published.
Thus, I briefly describe the design.

LC balun consists of HPF, LPF,
and T junction.



HPF and LPF are designed so that phase may be +90 deg and -90 deg
at the center frequency f_0 .
Bandwidth of the balun increases with increasing the order of filters.
I use the 5th order balun.

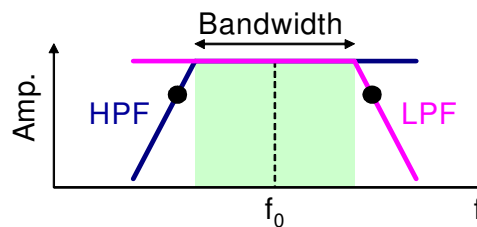
Design of balun



The balun is simulated by ADS as three-port model.

Characteristic impedance of filters: $((2Z_u)(Z_b/2))^{1/2} = Z_u Z_b^{1/2}$

3dB down frequency for LPF: $(1/0.47035)f_0$ } These lead phases of +90 & -90 for HPF & LPF at f_0 .
 3dB down frequency for HPF: $0.47035f_0$



Example of design of balun(1/2)

Example

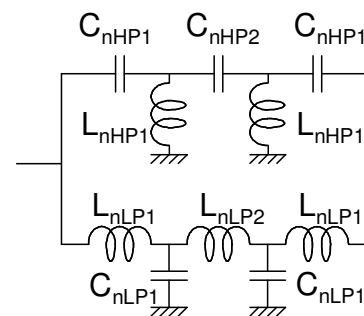
Frequency: $f_D = 550$ MHz

Impedance: $Z_u = 50\Omega$, $Z_b = 50\Omega$

Normalized balun is first considered.
(5th order Butter worth)

LC elements

HPF:	LPF:
$C_{nHP1} = 1.61803$ H	$L_{nLP1} = 0.61803$ H
$C_{nHP2} = 0.5$ H	$L_{nLP2} = 2.0$ H
$L_{nHP1} = 0.61803$ F	$C_{nLP1} = 1.61803$ F



Characteristic impedance

$$Z_{n0LP} = Z_{n0HP} = 1\Omega$$

3dB down frequency

$$f_{nLP} = 1/(2\pi) \text{ Hz,}$$

$$f_{nHP} = 1/(2\pi) \text{ Hz}$$

Example of design of balun(2/2)

Then, values are converted.

Frequency converter:

$$M_{HP} = f_D / (f_{nHP} / 0.47035) = 1625 * 10^6$$

$$M_{LP} = f_D / (f_{nLP} * 0.47035) = 7347 * 10^6$$

Impedance converter:

$$K = (Z_u Z_b)^{1/2} / Z_{n0HP} = (Z_u Z_b)^{1/2} / Z_{n0LP} = 50$$

HPF:

$$C_{nHP1} = C_{nHP1} / M_{HP} / K = 19.9 \text{ pF}$$

$$C_{nHP2} = C_{nHP2} / M_{HP} / K = 6.15 \text{ pF}$$

$$L_{nHP1} = L_{nHP1} / M_{HP} * K = 19.0 \text{ nH}$$

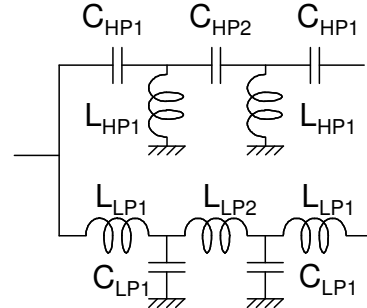
Equations were revised.

LPF:

$$L_{nLP1} = L_{nLP1} / M_{LP} * K = 4.21 \text{ nH}$$

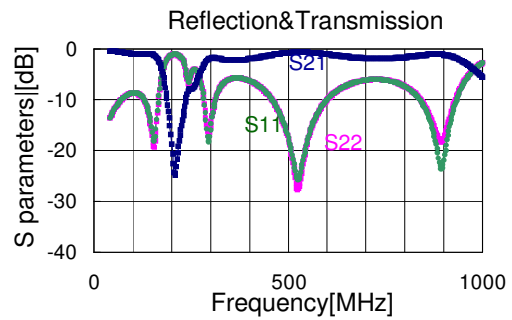
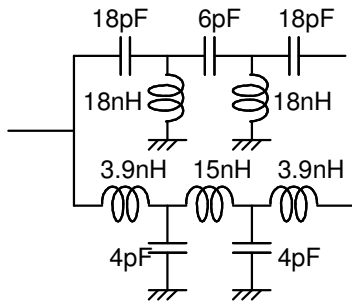
$$L_{nLP2} = L_{nLP2} / M_{LP} * K = 13.6 \text{ nH}$$

$$C_{nLP1} = C_{nLP1} / M_{LP} / K = 4.40 \text{ pF}$$

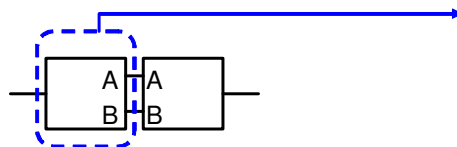


Measured S parameters of LC Balun, 50Ω-50Ω

Circuit

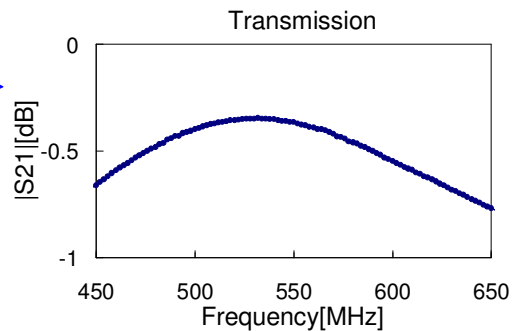


S params were measured by back to back configuration.



Transmission loss/Balun was presented.

Measured loss: 0.4dB at 550 MHz



Memo

LC lumped elements have discrete values.
Thus, the adjustment is needed by ADS.

Also, loss is not included in the design.
The experimental adjustment is needed.
It is done by a back to back configuration as I sent.

When impedance transform from 200Ω to 50Ω gives wide bandwidth.
The bandwidth decreases with decreasing impedance.

Design of balun

Example

Frequency: $f_D = 550 \text{ MHz}$

Impedance: $Z_u = 50 \Omega$, $Z_b = 150 \Omega$

HPF:

$$C_{nHP1} = C_{nHP1} / M_{HP} / K = 11.5 \text{ pF}$$

$$C_{nHP2} = C_{nHP2} / M_{HP} / K = 3.6 \text{ pF}$$

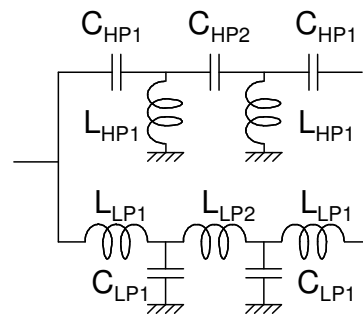
$$L_{nHP1} = L_{nHP1} / M_{HP} * K = 32.9 \text{ nH}$$

LPF:

$$L_{nLP1} = L_{nLP1} / M_{LP} * K = 7.3 \text{ nH}$$

$$L_{nLP2} = L_{nLP2} / M_{LP} * K = 23.6 \text{ nH}$$

$$C_{nLP1} = C_{nLP1} / M_{LP} / K = 2.5 \text{ pF}$$



References

- [1] E. Weber and F. Nebeker, "The Evolution of Electrical Engineering," presented at IEEE Press, Piscataway, New Jersey USA, 1994.
- [2] Heaviside and Oliver, "Electromagnetic Theory," *American Mathematical Society*, 1970.
- [3] Grant, I.S., Phillips, and W.R., *Electromagnetism 2nd ed*: John Wiley.
- [4] Ulaby and F.T., *Fundamentals of Applied Electromagnetics*, Media ed: Prentice Hall, 2004.
- [5] Steinmetz and C. Proteus, "The Natural Period of a Transmission Line and the Frequency of lightning Discharge Therefrom," *The Electrical world*, pp. 203 - 205, August 27, 1898.
- [6] *Radiocommunication handbook*: RSGB, chapter 17, page 20.
- [7] Naredo, J.L., A. C. Soudack, and J. R. Marti, "Simulation of transients on transmission lines with corona via the method of characteristics. Generation, Transmission and Distribution," presented at IEE Proceedings, Inst. de Investigaciones Electr., Morelos, Jan 1995.
- [8] D. M. Pozar, *Microwave Engineering*, 2nd ed: John Wiley & Sons, Inc, 1998.
- [9] "CST Microwave Studio Tutorials," *Computer Simulation Technology*, www.cst.de, vol. Version 4, July 2002.
- [10] C. A. Balanis, *Antenna Theory: Analysis and Design*, 3rd ed: Wiley-Interscience, 2005.
- [11] J. McLean, R. Sutton, and R. Hoffman, "TDK RF Solutions_Interpreting Antenna Performance Parameters for EMC Applications, Part 1: Radiation Efficiency and Input Impedance Match."

- [12] T. Weiland, "A discretization method for the solution of Maxwell's equations for six-component fields," *Electronics and Communications AEÜ*, vol. 31, pp. 116-120, 1977.
- [13] M. Clemens and T. Weiland, "Discrete Electromagnetism with The Finite Integration Technique," *Progress in Electromagnetics Research*, vol. 32, pp. 65-87, 2001.
- [14] "Advanced topics," *CST Microwave Studio menu, Version 5*, 2004.

PUBLICATIONS

1. Qing Liu, Peter S Hall, Alejandro L. Borja, "Dipole with left handed loading with optimised efficiency" for European Conference on Antennas and Propagation, EuCAP 2007, Edinburgh, UK.

Chairman's Commendation Award

2. Alejandro L. Borja, Peter S Hall, Qing Liu, Hideo Iizuka, "Omnidirectional Loop Antenna with Left-Handed Loading" for IEEE Antennas and Wireless Propagation Letter, AWPL 2007.

CST short paper Award 2008

3. Peter S Hall, Qing Liu, "Dipoles and loop antennas with left handed loading" for IEEE Loughborough Antennas and Propagation Conference LAPC 2008, Loughborough, UK.
4. Peter S Hall, Qing Liu, "Dual mode reconfigurable loop antenna with left handed loading" for 2nd International Congress on Advanced Electromagnetic Materials in Microwaves and Optics, Pamplona, Spain, Sep. 2008.
5. Qing Liu, Peter S Hall, "Varactor-loaded left handed loop antenna with reconfigurable radiation patterns" for IEEE International Symposium on Antennas and Propagation Conference, Charleston, SC USA, June 2009.
6. Herraiz-Martinez F. J., Hall P. S., Qing Liu, Segovia-Vargas D., "Tunable left-handed monopole and loop antennas" for IEEE Antennas and Propagation Society International Symposium, APSURSI'09, Pages:1-4, 1-5 June 2009.
7. Qing Liu, Peter S Hall, Alejandro L. Borja, "Efficiency of Electrically Small Dipole Antennas Loaded with Left Handed Transmission Lines" for IEEE Transactions on Antennas and Propagation, Vol. 57, No. 10, Oct. 2009 .